IIT RESEARCH INSTITUTE
Fluid Dynamics Section
Chicago, Illinois 60616

STUDY OF VIBRATIONS INDUCED IN THIN-WALLED PIPES UNDER VARYING FLOW CONDITIONS

by

J. M. Clinch

FINAL REPORT

CONTRACT NO. NAS8-20325
CONTROL NO. DCN 1-6-53-01095

June 1967

This report was prepared by IIT Research Institute under Contract No. NAS8-20325, "Study of Vibrations Induced in Thin-Walled Pipes Under Varying Flow Conditions," for the George C. Marshall Space Flight Center of the National Aeronautics and Space Administration. The work was administered under the technical direction of Propulsion and Vehicle Engineering Laboratory, George C. Marshall Space Flight Center with Mr. R. Jewell acting as project manager.

FOREWORD

This report describes the work performed by the IIT Research Institute for the National Aeronautics and Space Adm., George C. Marshall Space Flight Center, Huntsville, Alabama under Contracts NAS8-11248 and NAS8-20325. The work reported herein covers the period of research activities from June 26, 1964 to September 26, 1965 and also from May 15, 1966 to May 15, 1967. A final report summarizing the work on Contract NAS8-11248 was submitted to the Marshall Space Flight Center on September 24, 1965. The present report, however, contains a description of the past work on Contract NAS8-11248 and as a result supersedes the former report.

The author wishes to acknowledge the assistance of the following personnel who contributed to the foregoing projects: Dr. M. J. Fisher, Mr. P. A. Bauer, Mr. C. S. Caccavari, and Mr. S. J. Pernic.

Respectfully submitted,

IIT RESEARCH INSTITUTE

J. M. Clinch
Research Engineer

APPROVED BY:

M. J. Fisher
Senior Engineer
Group Leader

/njn

ABSTRACT

This research study involved an experimental and theoretical investigation of the vibrations induced in thin-walled cylindrical pipes by the passage of internal turbulent water flow.

A theoretical analysis based on the application of random vibration theory was developed for predicting the vibrational response of thin-walled pipes to the turbulent wall pressure field at high mode orders and frequencies.

A continuously operating water flow facility capable of producing Reynolds numbers of 2×10^6 was designed and constructed for this investigation. The noise levels in this facility were reduced to values commensurate with the measurement of the turbulent wall pressure fluctuations in a long cylindrical pipe section.

Wall-mounted miniature pressure transducers were fabricated to record the wall pressure fluctuations in turbulent pipe flow. The statistical properties of the wall pressure field determined from these recordings included the power spectral density and the space-time and spatial correlations of the wall pressures in 1/3-octave frequency bands. The data obtained from these measurements and also from determining the pipe damping factor were used in calculating the pipe wall response to turbulent flow excitation.

Measurements of the vibrational response to fully-developed turbulent flow of a thin-walled pipe in 1/3-octave bands showed very good agreement with the predicted values of the response over a wide range of flow speeds and exciting frequencies. The results obtained from measuring the pipe wall response at various positions downstream of a rigid pipe bend and orifice plate were essentially identical to those for fully-developed

flow conditions. It was found that the power spectral density of the pipe wall displacement could be expressed as a function of the Strouhal number. The results indicated that the displacement power spectral density of the pipe wall vibrations decreased at the rate of 15 dB/octave at low Strouhal numbers and 18 dB/octave at high Strouhal numbers.

TABLE OF CONTENTS

TABLE OF CONTENTS (Cont'd)

LIST OF ILLUSTRATIONS

LIST OF ILLUSTRATIONS (Cont'd)

LIST OF ILLUSTRATIONS (Cont'd)

I. INTRODUCTION

This report describes the work carried out for the Marshall Space Flight Center on Contracts NAS8-11248 and NAS8-20325. The work performed on the former contract was concerned with an experimental and theoretical investigation of the vibrations induced in thin-walled pipes by the passage of fully-developed turbulent water flow. A final report[1] describing the results and conclusions of this work was submitted to the Marshall Space Flight Center in September 1965.

The current Contract NAS8-20325 was an extension of the above investigation to study the effect of varying flow conditions on the vibrational response of thin-walled pipes. These conditions included the influence of pipe bends and constrictions on the response of thin-walled pipes coupled to them. The overall aim of these programs was to develop methods for predicting the response of thin-walled pipes to varying flow conditions.

The approach used in these investigations was essentially as follows. First, to develop an analysis based on random vibration theory that could be used to predict the response of a pipe to varying flow conditions. Second, to measure those statistical properties of the wall pressure fields that excite the pipe into vibration. Third, to employ the data obtained from these measurements to calculate the pipe wall response and to compare the predicted response with that determined experimentally.

Previous work[2,3] on structural excitation by turbulent flows has been primarily concerned with the response at low mode orders and frequencies. In this case, the response is generally dominated by widely separated resonances. To calculate the response under these conditions requires a knowledge of the frequencies and mode shapes. This complicates both the measurement and calculation since the response is governed by the structural

end conditions which are difficult to simulate experimentally. In the present program the pipe vibrations are investigated at high frequencies and mode orders. This permits the average response over a finite number of modes to be determined using the concept of modal density.

In the multi-modal approach the pipe wall displacements of particular points at particular instants are of no real concern, instead the average response is that averaged over the pipe surface both in space and time. Generally it is possible to calculate for a given structure the average number of resonances in a given frequency band. The average response is given by the product of the average response per resonant mode and the average number of modes in a frequency band. This process can be repeated for different bandwidths and the overall response computed. Such an approach can only be carried out where there are a finite number of individual resonances in a frequency band as would be the case at high mode orders and frequencies where a large number of modes are excited by a broad band of exciting frequencies. This has been assumed to be true for the case of turbulent flow excited pipe wall vibrations since the areas over which the pressures are correlated are small compared with the surface area and the excitation of each mode at high frequencies can be regarded as being independent ot the mode shape.

It has been shown in the final report[1] on Contract NAS8-11248, that by application of the above principles, the displacement power spectral density of a thin-walled pipe to fully-developed flow can be calculated. The response is characterized in terms of the average displacement over the surface of the pipe at high mode orders.

The theoretical approach outlined in Section II follows the general development used in Ref. 1. However, a correction factor that was omitted in the former analysis is included to

account for the virtual mass of the water-filled pipe. Furthermore, the modal density has been calculated from existing theory instead of solving for the natural frequencies of vibration of the pipe which tends to complicate the calculation. In Section III a description is given of the modified water flow loop facility. The instrumentation that was used for determining the statistical properties of the wall pressure field in turbulent flow is also described as well as the equipment used for measuring the pipe wall response. Section IV discusses the statistical data obtained from analyzing the recordings made of the wall pressure fluctuations that were subsequently used for calculating the response. In Section V the method employed for computing the response is described. A computational flow chart is included to show the steps in the calculation procedure and how the response can be predicted from a knowledge of the basic flow and structural variables. Section VI describes the results obtained from measurements of the wall displacement spectra of a long cylindrical pipe to the following flow conditions: (1) fully-developed turbulence, (2) flow generated by a 90° pipe bend, and (3) flow generated by an orifice plate. The response data obtained from these varying flow conditions are compared with the prediction calculated for fully-developed turbulent pipe flow.

It is shown that very good agreement between the measured and predicted values of the response were obtained for fully-developed turbulent flow. The experimental data for the response of a thin-walled pipe coupled to the pipe bend and orifice plate were found to be essentially of the same magnitude as that measured and predicted for fully-developed turbulence. This result implied that although the basic structure of the turbulence in pipe flow was altered by the presence of the pipe bends and the orifice, the actual wall pressure field and hence the response was unaffected by the varying flow conditions for the same mean

flow speeds and frequencies. An interesting exception occurred when the flow downstream of the orifice plate was partially cavitating. In this case the mean square displacement response was found to increase by about 3 dB above that measured for a non-cavitating flow. This indicated that cavitation is an important source of pipe excitation and must be accounted for in the design of piping systems delivering liquid flows. It is recommended that further work be carried out to investigate the response of thin-walled pipes at high frequencies to fluid cavitation.

II. THEORETICAL CONSIDERATIONS

2.1 ANALYSIS

In this section it is proposed to give an outline of the theory used for predicting the response of a thin-walled cylindrical pipe to the wall pressure field arising from the passage of fully-developed turbulent flow. The approach used basically follows that previously described by the writer in Ref. 1 using the concept of joint acceptance introduced by Powell[4].

It will be assumed that the thin-walled pipe can be approximated by a long uniform isotropic cylindrical shell. The random vibrations of the shell wall will be produced by random fluctuations in the pressures over the inside surface of the shell due to fully-developed turbulent water flow. The wall pressure field will be considered statistically stationary and spatially homogeneous over the inner shell wall.

The following assumptions will be made regarding the response of the shell wall to the forcing pressure fluctuations:

1. The fluctuating fluid pressures in turbulent flow give rise to small radial vibrations of the shell wall.
2. The forcing pressure field has a wide frequency spectrum and excites a large number of natural modes of vibration.
3. Axial and circumferential standing waves are induced in the shell wall.
4. The low order modes of vibration, which may exhibit individual widely spaced resonant peaks, are neglected.
5. At higher frequencies and mode orders, the natural frequencies are assumed to be bunched

sufficiently close together to approach a condition of continuous resonant response. In other words, the response is not dominated by several discrete frequencies, but is essentially a smooth continuous function.

6. The areas over which the pressures are correlated are small compared with the dimensions of the cylinder.
7. The average response is not affected by the cylinder end conditions.
8. A finite number of resonances are contained in each selected narrow frequency band.

Consider the coordinates $(x_1 y_1)$ and $(x_2 y_2)$ on the surface of a cylindrical shell of length L, radius a, and wall thickness h, shown in Fig. 1. Let the x-axis be the longitudinal axis of the cylinder, that is, the flow direction, and the y-direction the cylinder circumference.

If m and n are the mode numbers in the longitudinal x-direction and circumferential y-direction, the mode shapes at points $(x_1 y_1)$ and $(x_2 y_2)$ for small radial displacements are given by

$$\left.\begin{aligned} \alpha_{mn}(x_1 y_1) &= \sin \frac{m\pi x_1}{L} \cos \frac{n y_1}{a} \\ \alpha_{mn}(x_2 y_2) &= \sin \frac{m\pi x_2}{L} \cos \frac{n y_2}{a} \end{aligned}\right\} \qquad (2.1)$$

The space average value of the power spectral density $[\phi_d(\omega)]_{av}$ of the surface displacement of the pipe wall is given by[1]

$$[\phi_d(\omega)]_{av} = \sum_{m,n} \frac{[\alpha_{mn}^2(x,y)]_{av}\ \phi_p(\omega)\ A^2 j^2(\omega)}{|Z_{mn}(\omega)|^2} \qquad (2.2)$$

where

$$j^2(\omega) = \frac{1}{A^2}\iiiint R_f(x_1,y_1;x_2y_2;\omega)\alpha_{mn}(x_1y_1)\alpha_{mn}(x_2y_2)dx_1dy_1dx_2dy_2 \tag{2.3}$$

$\phi_p(\omega)$ is the power spectral density of the wall pressure field, A is the surface area of the pipe and $R_f(x_1y_1;x_2y_2;\omega)$ represents the spatial correlation between the pressures at points (x_1y_1) and (x_2y_2) in a narrow band $\Delta\omega$, and $j^2(\omega)$ is the joint acceptance, a pure number. The joint acceptance is a measure of the effectiveness of the pressure field in driving a particular mode of vibration in a given frequency band. The mechanical impedance, $Z_{mn}(\omega)$, of the mn^{th} mode is

$$|Z_{mn}(\omega)|^2 = M_{mn}^2\left[(\omega_{mn}^2 - \omega^2)^2 + \frac{\omega_{mn}^2\omega^2}{Q_{mn}^2}\right] \tag{2.4}$$

M_{mn} is the generalized mass for the mn^{th} mode, Q_{mn} is the damping factor, and ω_{mn} is the natural frequency of the mn^{th} mode.

Suppose W(x,y;t) is the radial displacement of the shell wall due to the fluctuating pressure p(x,y;t) at time t and at point (x,y) on the surface of the shell. The overall mean square displacement of the shell wall may be obtained from the power spectral density of the displacement, that is

$$[\langle W^2\rangle]_{av} = \int_0^\infty [\phi_d(\omega)]_{av}\, d\omega \tag{2.5}$$

where the integration is performed over all frequencies.

Thus, from Eq. (2.2), the overall mean square displacement $[\langle W^2\rangle]_{av}$ is given by

$$[\langle W^2\rangle]_{av} = \sum_{m,n}[\alpha^2(x,y)]_{av}\, A^2 \int_0^\infty \frac{\phi_p(\omega)j^2(\omega)}{|Z_{mn}(\omega)|^2}\, d\omega \tag{2.6}$$

For a simply supported cylinder having orthogonal modes m and n,

$$[\alpha_{mn}^2(x,y)]_{av} = \frac{1}{2\pi aL}\int_0^L\int_0^{2\pi a} \alpha_{mn}^2(x,y)\,dxdy$$

$$= \frac{1}{2\pi aL}\int_0^L\int_0^{2\pi a} \sin^2\frac{m\pi}{L}x\,\cos^2\frac{n}{a}y\,dxdy = \frac{1}{4} \qquad (2.7)$$

Substituting Eq. (2.7) into (2.6) gives

$$[\langle W^2\rangle]_{av} = \frac{A^2}{4}\sum_{m,n}\int_0^\infty \frac{\phi_p(\omega)j^2(\omega)}{|Z_{mn}(\omega)|^2}\,d\omega \qquad (2.8)$$

The power spectral density $\phi_p(\omega)$ is a function of frequency ω, and the joint acceptance, $j^2(\omega)$ is a function of both frequency and bandwidth. It will be assumed that for resonant response conditions, the above quantities are essentially constant over the narrow bandwidth $\Delta\omega_{mn}$ of the mn mode. The value of the integral of $1/|Z_{mn}(\omega)|^2$ is obtained by integrating across the resonant bandwidth.

Equation (2.8) can, therefore, be approximated by the following expression

$$[\langle W^2\rangle]_{av} = \frac{A^2}{4}\sum_{m,n}\phi_p(\omega)j^2(\omega)\int_0^\infty \frac{d\omega}{|Z_{mn}(\omega)|^2} \qquad (2.9)$$

It may be shown[5] that the value of the integral in Eq. (2.9) is given by

$$\int_0^\infty \frac{d\omega}{|Z_{mn}(\omega)|^2} = \frac{\pi}{2}\,\frac{1}{M_{mn}^2}\,\frac{Q_{mn}}{\omega_{mn}^3} \qquad (2.10)$$

The generalized mass, M_{mn}, is related to the effective mass of the cylinder, M_e, by the equation

$$M_{mn} = \rho_e h \int_0^L \int_0^{2\pi a} \alpha_{mn}^2(x,y)\, dxdy = \frac{A\rho_e h}{4} = \frac{M_e}{4} \qquad (2.11)$$

where ρ_e is the effective density of the cylindrical shell.

Combining Eqs. (2.10) and (2.11) and substituting into Eq. (2.9) gives

$$[\langle W^2 \rangle]_{av} = \frac{2\pi}{\rho_e^2 h^2} \sum_{m,n} \frac{\phi_p(\omega) j^2(\omega) Q_{mn}}{\omega_{mn}^3} \qquad (2.12)$$

Consider a typical narrow band, $\Delta\omega$, having upper and lower frequency limits given by $\omega + \Delta\omega/2$ and $\omega - \Delta\omega/2$ respectively, where ω is the center band frequency. In this bandwidth are contained a finite number of closely packed resonances. It will be assumed that the bandwidth is sufficiently narrow so that the quantities $\phi_p(\omega)$, $j^2(\omega)$, and Q_{mn} are constant over the bandwidth. The space average value of the mean square response in this bandwidth will be

$$[\langle W^2(\omega) \rangle]_{av} = \frac{2\pi}{\rho_e^2 h^2} \phi_p(\omega) j^2(\omega) Q \sum_{m,n} \frac{1}{\omega_{mn}^3} \qquad (2.13)$$

If there exist ΔN resonant frequencies of the form, ω_{mn}, in bandwidth $\Delta\omega$, that is, the modal density (see Fig. 2), then the summation in Eq. (2.13) can be replaced by the integral equation

$$[\langle W^2(\omega) \rangle]_{av} = \frac{2\pi Q}{\rho_e^2 h^2} \phi_p(\omega) j^2(\omega) \frac{\Delta N}{\Delta\omega} \int_{\omega-\Delta\omega/2}^{\omega+\Delta\omega/2} \frac{d\omega}{\omega_{mn}^3} \qquad (2.14)$$

On integration, Eq. (2.14) becomes

$$[\phi_d(\omega)]_{av} = \frac{[\langle W^2(\omega) \rangle]_{av}}{\Delta\omega} = \frac{2\pi Q}{\rho_e^2 h^2} \phi_p(\omega) j^2(\omega) \frac{\Delta N}{\Delta\omega} \frac{1}{\omega^3} \qquad (2.15)$$

Equation (2.15) represents the space-average, power spectral density of the radial displacement of the cylindrical shell wall to a random, spatially homogeneous pressure field. To obtain a solution to Eq. (2.15) for the wall pressure field applied by uniform turbulent water flow, it is necessary to calculate the joint acceptance function, $j^2(\omega)$.

The joint acceptance function, $j^2(\omega)$, is given by the integral equation (2.3), that is,

$$j^2(\omega) = \frac{1}{A^2}\iiiint R_f(x_1y_1;x_2y_2;\omega)\alpha_{mn}(x_1y_1)\alpha_{mn}(x_2y_2)dx_1dy_1dx_2dy_2 \tag{2.3}$$

To evaluate the joint acceptance for turbulent flow excitation of the inner cylindrical shell wall, requires a knowledge of the narrow band spatial correlation functions of the turbulent wall pressure field in both the longitudinal and circumferential directions.

It has been shown experimentally[6,7] that for a convected turbulent wall pressure field in the longitudinal flow direction, the narrow band space-time cross-correlation function at frequency ω can be expressed as

$$R_f(x_1,x_2;\tau;\omega) = A_f \cos \omega \left(\tau - \frac{|x_1-x_2|}{U_c}\right) \tag{2.16}$$

In other words, each correlation curve rises to a maximum at a value of the time delay, τ, given by

$$\tau = \frac{|x_1 - x_2|}{U_c} \tag{2.17}$$

where U_c is the convection speed of the turbulent eddies in a selected narrow band, and $|x_1-x_2|$ is the spatial separation between points along the wall. The amplitude A_f of the cosine function represents the envelope of the peaks of the correlation curves.

Harrison[8] and Bull and Willis[6] have indicated that the amplitude, A_f, of the correlation curves is a unique function of the Strouhal number, $(\omega|x_1-x_2|)/U_c$. However, it was subsequently pointed out by Bull[9] and Fisher and Davies[10] that a Strouhal number dependence leads to anomalous results for the correlations at low frequencies.

In the present analysis, it will be assumed that the amplitude of the longitudinal correlation function is of the form suggested by Dyer[11], that is

$$A_f = \exp \frac{-|x_1-x_2|}{U_c\tau_o} \tag{2.18}$$

where τ_o is a measure of the eddy lifetime in a given narrow band. The eddy lifetime, τ_o, can be determined experimentally from the value the moving-axis time envelope falls to a correlation coefficient of 1/e or 0.37. The product of the eddy lifetime and convection speed in Eq. (2.18) can be used to define the longitudinal correlation length, L_x

$$L_x = U_c\tau_o \tag{2.19}$$

The form of the narrow band spatial correlation at zero time delay in the longitudinal x-direction can, therefore, be represented by the damped cosine function

$$R_f(x_1,x_2;\omega) = \exp \frac{-|x_1-x_2|}{L_x} \cos \frac{\omega(x_1-x_2)}{U_c} \tag{2.20}$$

In the circumferential y-direction, there is no convection process. Thus a convenient form for the narrow band spatial correlation is

$$R_f(y_1,y_2;\omega) = \exp \frac{-|y_1-y_2|}{L_y} \tag{2.21}$$

For incompressible flow the circumferential correlation length, L_y, is independent of the convection speed, U_c. However, both L_x and L_y are functions of frequency. Assuming that the narrow band spatial correlations of the pressure field and mode shapes over the cylinder surface are separable functions, then the joint acceptance can be represented by the product of joint acceptances in the longitudinal and circumferential directions

$$j^2(\omega) = j_x^2(\omega)\, j_y^2(\omega) \tag{2.22}$$

Thus, substituting Eqs. (2.1), (2.20), and (2.21) into Eq. (2.3) leads to

$$j_x^2(\omega) = \frac{1}{L^2}\iint \exp\frac{-|x_1-x_2|}{L_x}\cos\frac{\omega(x_1-x_2)}{U_c}\sin\frac{m\pi x_1}{L}\sin\frac{m\pi x_2}{L}\,dx_1dx_2 \tag{2.23}$$

$$j_y^2(\omega) = \frac{1}{4\pi^2a^2}\iint \exp\frac{-|y_1-y_2|}{L_y}\cos\frac{ny_1}{a}\cos\frac{ny_2}{a}\,dy_1dy_2 \tag{2.24}$$

Equation (2.23) can be evaluated over the cylinder length, L. However, the form of the exponential function will depend on whether x_1 is greater than or less than x_2. Splitting Eq. (2.23) into two parts:

(a) when $x_2 > x_1$, the integration limits are from L to x_1

(b) when $x_2 < x_1$, the integration limits are from x_1 to 0

Thus, $j_x^2(\omega)$ may be written as

$$j_x^2(\omega) = \frac{1}{L^2}\left[\int_0^L \sin px_1dx_1\int_0^{x_1}\exp[-\alpha(x_1-x_2)]\cos q(x_1-x_2)\sin px_2dx_2 + \int_{x_1}^L \exp[-\alpha(x_2-x_1)]\cos q(x_2-x_1)\sin px_2dx_2\right] \tag{2.25}$$

where $p = m\pi/L$, $q = \omega/U_c$, and $\alpha = 1/L_x$.

A similar argument is applicable for Eq. (2.24). In this case, however, the integration is over the cylinder circumference, $2\pi a$. Thus, $j_y^2(\omega)$ can be expressed as

$$j_y^2(\omega) = \frac{1}{4\pi^2 a^2}\int_0^{2\pi a}\cos\frac{ny_1}{a}\,dy_1\left[\int_0^{y_1}\exp[-\beta(y_1-y_2)]\cos\frac{ny_2}{a}\,dy_2 + \int_{y_1}^{2\pi a}\exp[-\beta(y_2-y_1)]\cos\frac{ny_2}{a}\,dy_2\right] \tag{2.26}$$

where $\beta = 1/L_y$.

The solution for Eq. (2.25) is

$$j_x^2(\omega) = \frac{\alpha(\alpha^2+p^2+q^2)}{L[(\alpha^2+p^2+q^2)^2 - 4p^2q^2]} + \frac{2p^2/L^2}{[(\alpha^2+p^2-q^2)^2 - 4\alpha^2q^2]^2 + 16\alpha^2q^2(\alpha^2+p^2-q^2)^2} \cdot \left\{[(\alpha^2+p^2-q^2)^2 - 4\alpha^2q^2][1 - (-1)^m \exp(-\alpha L)\cos qL] + 4\alpha q(\alpha^2+p^2-q^2)\cdot(-1)^m \exp(-\alpha L)\sin qL\right\} \tag{2.27}$$

Also, the solution for Eq. (2.26) is

$$j_y^2(\omega) = \frac{\beta a}{2\pi(n^2+\beta^2a^2)}\left\{1 - \frac{\beta a}{\pi(n^2+\beta^2a^2)}[1 - \exp(-\beta 2\pi a)]\right\} \tag{2.28}$$

It is seen from Eq. (2.27) that the joint acceptance in the longitudinal flow direction is a function of the following variables

$$j_x^2(\omega) = F(p,q,\alpha,L)$$

where $p = m\pi/L$ is the longitudinal or axial mode wave number for elastic waves in the cylinder wall; $q = \omega/U_c$ is the wave number associated with turbulent eddies of frequency ω, being convected at a speed, U_c; and α is the reciprocal of the longitudinal correlation length, L_x, defined by Eq. (2.19).

In general, α will be large, since the correlation length will be very small compared with the cylinder length, L. Furthermore, it can be shown that for the range of frequencies, flow speeds, and cylinder lengths investigated experimentally, the turbulence wave number, q, is much greater than the longitudinal elastic mode wave number, p. Under these conditions, Eq. (2.27) becomes independent of the mode number, m, and reduces to the following expression

$$j_x^2(\omega) \simeq \frac{\alpha}{L(\alpha^2+q^2)} \tag{2.29}$$

This simplified form of the longitudinal joint acceptance function, $j_x^2(\omega)$, is shown plotted in Fig. 3 against qL for typical values of αL. Thus, from a knowledge of the turbulence wave number, q, and correlation length, L_x, which will be determined experimentally from the narrow band space-time correlations of the turbulent wall pressures, the joint acceptance function $j_x^2(\omega)$ can be calculated.

A similar argument is valid for the circumferential joint acceptance function, $j_y^2(\omega)$ given by Eq. (2.28). However, in this case $j_y^2(\omega)$ is not quite independent of the circumferential mode number, n, at small values of βa. The symbol β is the reciprocal of the circumferential correlation length, L_y, defined by Eq. (2.21). It may be shown that provided β is large compared to the cylinder radius, a

$$j_y^2(\omega) = \frac{\beta a}{2\pi(\beta^2a^2+n^2)}\left[1 - \frac{\beta a}{\pi(\beta^2a^2+n^2)}\right] \tag{2.30}$$

The circumferential joint acceptance, $j_y^2(\omega)$, given by Eq. (2.30), is shown plotted in Fig. 4 as a function of βa for several low order circumferential mode numbers, n. It is seen that for values of $\beta a < 50$, $j_y^2(\omega)$ depends on the mode number, n. However, for $\beta a > 50$, an accurate estimate of $j_y^2(\omega)$ can be calculated without any knowledge of the mode number, provided β is known from narrow band correlation measurements in turbulent flow. In view of the foregoing considerations, the power spectral density of the cylinder wall displacement given by Eq. (2.15) can be written as

$$[\phi_d(\omega)]_{av} = \frac{2\pi Q}{\rho_e^2 h^2} \phi_p(\omega)\, j_x^2(\omega)\, j_y^2(\omega) \frac{\Delta N}{\Delta\omega} \frac{1}{\omega^3} \qquad (2.31)$$

where $j_x^2(\omega)$ and $j_y^2(\omega)$ are defined by Eqs. (2.29) and (2.30).

Equation (2.31), therefore, represents the narrow band space-average, mean square displacement response of a thin-walled cylindrical pipe to turbulent flow excitation. It is seen that the response obeys a resonance type mass law whose amplitude is Q-dependent and inversely proportional to the square of the effective mass per unit area of the cylinder. The overall response may be obtained by integrating the narrow band response over all the exciting frequencies.

2.2 DISCUSSION OF THEORY

It is apparent from the above theory that to predict the response of a thin-walled cylindrical pipe containing turbulent water flow, it is necessary to have a knowledge of the joint acceptance functions, $j_x^2(\omega)$ and $j_y^2(\omega)$, the power spectral density of the wall pressure fluctuations $\phi_p(\omega)$, the damping factor, Q, the modal density, $\Delta N/\Delta\omega$, and the effective density of the water-loaded cylinder, ρ_e.

The joint acceptance functions can be calculated when the narrow frequency band wall pressure correlations have been measured for turbulent water flow inside the cylinder or pipe. The power spectral density of the wall pressures, $\phi_p(\omega)$, may also be determined experimentally. It is shown in Section IV that $\phi_p(\omega)$ can be expressed in terms of the frequency, flow velocity, pipe diameter, and fluid density.

The damping factor, Q, for the water-loaded cylindrical pipe can be determined experimentally by exciting one of the natural frequencies and measuring the amplitude decay as a function of time. In Section VI, measurements of the damping were made at several widely separated resonances to verify the theoretical assumption that Q is independent of frequency.

Finally, the modal density, $\Delta N/\Delta\omega$, of the cylinder resonances, and the effective density, ρ_e, of the water-loaded cylinder are calculated from established theories. Heckl[12] derived an expression for the modal density of a cylindrical shell in terms of the physical constants and dimensions of the shell. This expression, corrected for the water loading, is used in Section V for determining the modal density. It is well known[13,14] that the effect of liquid on the vibrations of a cylinder not only increases the number of resonances, but also gives rise to added surface mass to the vibrational response of the shell wall. In view of the water loading, correction factors are introduced in the calculation procedure outlined in Section V to account for the increased modal density and additional mass per unit area of the vibrating cylinder wall.

Although a knowledge of the actual resonant frequencies of the water-filled cylinder is not required in the response calculation, an outline is given in Appendix A to show how the frequencies could be computed for a given cylindrical shell. The equations derived for the natural frequencies are used in

obtaining an approximate expression for the effective density of the shell wall, ρ_e, due to water loading.

In summarizing, therefore, a method of calculation that may be used for predicting the response of a thin walled cylindrical pipe to turbulent water flow excitation has been developed. It is shown that to calculate the response, a knowledge of certain of the statistical properties of the wall pressure field in turbulent flow and the vibration characteristics of the water-loaded cylinder is required.

III. EXPERIMENTAL EQUIPMENT

The experimental work performed during the investigations carried out under Contracts NAS8-11248 and 20325 could be divided into three categories. First, the design and construction of a water loop facility to produce fully-developed turbulent flow in a long section of thin-walled pipe at Reynolds numbers up to a maximum of 2×10^6. A description of this flow loop has been given in Ref. 1. For the work on Contract NAS8-20325, the flow loop was modified in order to study the vibrations induced in a thin-walled pipe coupled to pipe bends and orifice plates. The second category concerned the development of instrumentation for determining the properties of the wall pressure field in turbulent pipe flow. Thirdly, the use of instrumentation for measuring the displacements of the thin-walled pipe to varying flow conditions over a wide range of flow speeds.

3.1 MODIFIED WATER FLOW LOOP FACILITY

A diagram of the modified water flow loop is shown in Fig. 5.

The equipment comprising the flow loop consisted of two centrifugal pumps operated in series to obtain the maximum available pressure head, and capable of delivering 2,500 gallons of water per minute. The pumps were driven by a pair of variable speed internal combustion engines. Thus, differing flow rates could be achieved without the necessity of throttling the flow. The engines were located outside the laboratory building and anchored to a large concrete base to minimize structural vibrations and airborne noise. A 6,000 gallon open reservoir was located adjacent to the pump inlets. The purpose of the reservoir was to provide water storage capacity and to raise the pressure at the pump inlets to prevent cavitation.

Flow from the pumps passed through a 25 ft. length of 6 in. diameter nylon-reinforced rubber hose to provide some attenuation of the unwanted pump noise. The flow was then directed into a closed 2,000 gallon pressure vessel. The pressure vessel-rubber hose combination was designed to operate as a high pass acoustic filter to suppress the pump noise. After passing through two 90° elbows, the flow entered a straight run of pipe. The working section for the fully-developed flow tests was located about 180 pipe diameters downstream of the elbows.

Two working sections were used in the experimental work. The rigid section used in determining the properties of the wall pressure field was a smooth inner-walled 20 ft. long, steel pipe of 6 in. inside diameter and 7 in. outside diameter fitted with end flanges. The instrument plug, containing the assembly of miniature transducers for recording the wall pressure fluctuations, was mounted flush with the inside wall about 6 in. from the downstream end of the working section.

The thin-walled cylindrical pipe working section was also 20 ft. long and 6 in. inside diameter, but had a wall thickness of 0.025 in. Thus both the rigid and thin-walled sections were interchangeable units. The cylinder was fitted with end flanges welded to short lengths of pipe sleeve of 0.5 in. wall thickness. The pipe sleeves were silver soldered to the cylinder ends. The thin-walled pipe section was made by rolling a stainless steel sheet into a cylindrical tube. A wall thickness of 0.025 in. corresponded to the thinnest metal sheet of 20 ft. length that the tubing manufacturer could roll, and guarantee that the surface was uniform and free from irregularities. This precluded the possibility of investigating the flow-induced vibrations of thinner walled steel cylinders. Long lengths of tubing were employed to ensure that the end supports of the cylinder did not affect the vibrational response when subjected to the forcing pressure field in turbulent flow.

Flow leaving the working section entered a rigid 90° pipe bend which was connected to another working section for investigating the response of a thin-walled pipe to the flow generated by the bend. It might be pointed out that for the pipe constriction experiments an orifice plate was positioned at the upstream end of the first working section. Also, a pitot-static tube assembly was employed for measuring the flow velocity downstream of the second working section. After passing through a series of interconnecting pipes and elbows the flow finally was fed to the open reservoir and pump inlets, thus completing the flow loop.

With the flow loop facility, it was possible to produce fully-developed turbulent flow in the 6 in. diameter working sections, and obtain maximum flow velocities of about 500 in/sec. The corresponding Reynolds number based on the pipe diameter was about 2×10^6. Consequently, both the wall pressure field in turbulent water flow and the vibrational response of the thin-walled pipe to this field could be investigated over a wide range of flow velocities.

3.2 PRESSURE TRANSDUCERS

Measurements of the wall pressure fluctuations in turbulent flow were made using miniature piezoelectric transducers set flush with the internal surface of the rigid thick-walled pipe working section. The transducer elements were lead zirconate titanate discs (trade name PZT-5H) of diameter 0.020 in. and 0.010 in. thickness with silvered electrodes and polarized in the thickness direction.

The inner surface of the rigid steel pipe was chemically treated to remove all the oxides and mineral deposits, and subsequently honed to a smooth-wall finish having a tolerance of $\pm$ 0.001 in. Extreme care was exercised to ensure that there

were no protrusions greater than the tolerance limit when the plug containing the transducers was mounted flush with the inner surface of the pipe. Nineteen of the miniature transducers were mounted in the T-shaped slot of a brass plug adaptor which could be inserted in a 1.5 in. diameter hole drilled through the wall of the rigid pipe working section.

A description of the method of mounting the transducers in the instrument plug has been reported by the writer, Clinch[15] and in Ref. 1. The distances between alternate pairs of transducers in the axial and circumferential directions of the cylindrical pipe varied from 0.03 in. for the closest separation to 0.90 in. for the maximum separation. This permitted the wall pressure cross-correlations to be measured over a wide range of transducer separations. Figure 6 shows the completed transducer assembly.

Electrical leads from each transducer were taken out to an array of Microdot connectors positioned around the periphery of the plug. Two 3 in. lengths of Microdot cable were connected to the input of a pair of phase-matched low noise cathode follower-preamplifiers. A circuit diagram of the cathode follower-preamplifier is shown in Fig. 7. Thus, the signals from any given pair of transducers could be fed to the preamplifiers for pressure spectrum and cross-correlation measurements. The input impedance of the preamplifier was about 300 Megohms, and the capacitance of a transducer and cable connector about 70×10^{-12} farads.

The low frequency response of the transducer-amplifier combination, defined by the reciprocal of the product of the capacitance and resistance, was about 10 cps. The preamplifier gain was about 50:1, and the signal-to-noise ratio about 40 dB. The frequency response was flat to 100 Kcps, and the preamplifiers, which were battery powered, were stable throughout the whole investigation.

In practice, it was found necessary to provide further amplification of the signals from the preamplifiers using two matched plug-in Tektronix oscilloscope amplifiers (Type L) with a variable gain unit. This permitted the signals from the transducers to be amplified to a level sufficient for recording and analysis. The technique used for calibrating the pressure transducers has been described in Ref. 1.

Unfortunately, not all of the transducers were found to be operative. This was partly due to errors in the mounting technique caused by stray contact resistances and electrical shorting. However, sufficient transducers were operational to permit a detailed examination of the wall pressure field in turbulent pipe flow.

3.3 SPECTRUM ANALYZER AND AUXILIARY EQUIPMENT

For direct spectral analysis of the signals from the transducer-preamplifier combination, a Bruel and Kjaer 1/3-octave audio-frequency spectrometer (Type 2112) was used. Signal averaging in 1/3-octave band frequencies was determined by reading a calibrated root-mean-square (RMS) voltmeter. In this way the RMS and mean square values of the wall pressure fluctuations at various frequencies could be readily determined from a prior knowledge of the transducer sensitivities.

A two-channel Tektronix oscilloscope (Type 502) was employed for monitoring the amplitude-time history of the wall pressure fluctuations from given pairs of transducers during an experiment. However, in order to eliminate the extraneous low frequency noise detected by the transducers, it was necessary to incorporate Krohn-Hite variable band pass filters (Type 330N) in the recording system. The band pass filter was set for a lower cut-off frequency of 50 cps; and an upper frequency of 20 Kcps.

For the cross-correlation experiments, the signals from alternate pairs of transducers were recorded directly onto magnetic tape for a period of about 60 sec for subsequent analysis using the analog correlation equipment. An FM tape recorder (Ampex Model FR-1300) was used; the transducer signals being recorded on two separate channels of the magnetic tape running at a speed of 60 in/sec. This provided a frequency response from DC to 20 Kcps. Another channel on the tape recorder was used for voice recording to identify the transducers under investigation. A block diagram showing the arrangement of the recording and analyzing equipment is given in Fig. 8.

3.4 ELECTRONIC ANALOG CORRELATOR

The cross-correlation or covariance, $C_{12}(\tau)$, for two randomly varying signals $v_1(t)$ and $v_2(t)$ is defined by

$$C_{12}(\tau) = \frac{1}{T} \int_{-T/2}^{T/2} v_1(t)\, v_2(t+\tau)\, dt \qquad (3.1)$$

where T is the averaging time, and τ is the delay time used in displacing signal $v_2(t)$ with respect to $v_1(t)$.

The auto-correlation, $C_{11}(\tau)$, on the other hand, is performed by delaying a given signal with itself

$$C_{11}(\tau) = \frac{1}{T} \int_{-T/2}^{T/2} v_1(t)\, v_1(t+\tau)\, dt \qquad (3.2)$$

An electronic analog correlator (Honeywell Model 9410) with a variable multi-channel time delay unit was used for determining the wall pressure correlations in turbulent pipe flow.

A block diagram showing the operating principles of the correlator is given in Fig. 9. By means of the variable time delay unit, each input signal to the correlator can be delayed

with respect to the other. One signal then modulates the height and the other the width of a pulse, which is subsequently averaged over a preselected time by an R-C network. The output from the integrating network, which is read on a DC millivoltmeter, gives the covariance between the signals. By repeating this process over a selected range of time delays, the covariance or cross-correlation between the input signals can be determined as a function of the time delay.

In practice, it was found that an averaging time of 5 sec was sufficiently long to obtain statistically stationary values. Care was taken to maintain peak-to-peak signal amplitudes less than 2 volts to avoid over-loading the correlator. The frequency response of the correlator was flat from 50 cps to 250 Kcps, and three decade time delay ranges were provided which could be varied from 0 to 17 millisecs.

The cross-correlation coefficient, $R(\tau)$, was obtained by normalizing the covariance by dividing by the RMS amplitude of each signal.

$$R_{12}(\tau) = \frac{\langle v_1(t)\, v_2(t+\tau) \rangle}{\sqrt{\langle v_1^2(t) \rangle} \cdot \sqrt{\langle v_2^2(t) \rangle}} \qquad (3.3)$$

The RMS amplitudes were determined from the mean square values of the signals, that is, the auto-correlations for zero time delay.

The correlator was primarily used for determining the space-time correlations of the wall pressure fluctuations in turbulent pipe flow. Narrow frequency band correlations were obtained by replaying the magnetic tape recordings of the turbulent wall pressures from various transducer pairs through two phase matched 1/3-octave filters (Bruel and Kjaer Type 2112) to the input terminals of the correlator. Space correlations between

the signals were simply determined with the delay unit set at zero time. The overall accuracy of the correlator was of the order of $\pm$ 1 percent.

Figure 10 shows the instrumentation used for processing the tape recorded signals from the transducers to obtain the wall pressure cross-correlations in turbulent flow.

3.5 VIBRATION MEASURING EQUIPMENT

The instrument used for detecting the vibrations of the thin-walled cylindrical pipes was a Dressen-Barnes ultramicrometer (Omega Model 155). The ultramicrometer is basically a non-contacting frequency modulated capacitance device that may be used for measuring small displacement amplitudes of vibrating surfaces.

The Dressen-Barnes instrument utilized a capacitance type sensor probe in conjunction with a converter/power supply unit. The converter employed a Foster-Seeley phase discriminator circuit. The probe face was a 0.125 in. diameter circular disc surrounded by an annular guard ring of 0.5 in. outside diameter. A calibrated micrometer thimble having a 150 μinch per turn sensitivity was mechanically coupled to the probe.

Variations in capacity produced by small changes in the probe-object separation produced frequency modulation in the discriminator. This circuit was energized by a 25 Mcps crystal-controlled oscillator. Any capacitance variation causes the discriminator characteristics to shift with respect to the 25 Mcps carrier, resulting in a DC output. Figure 11 gives a block diagram of the converter unit. The ultramicrometer was capable of measuring vibrational amplitudes as low as 0.2 μinch over a frequency range from DC to 1 Mcps to an accuracy of about 10 percent. Below 0.5 μinch, however, the errors were possibly greater than 20 percent.

The procedure used in calibrating the ultramicrometer was to set the probe face in a plane parallel to a flat metallic reference surface at a distance of 0.002 in. This clearance corresponded to the center point of balance in the discriminator circuit. The micrometer thimble was then turned to change the gap clearance by known amounts on each side of the balance point, and the resultant voltage deflections noted on a DC coupled oscilloscope.

The ultramicrometer calibration curve is shown in Fig. 12 It is seen that the discriminator curve is linear to 150 μinch on either side of the constant gap setting of 0.002 in., corresponding to zero on the curve. The sensitivity of 60 μinch per volt is determined from the slope of the discriminator curve.

IV. TURBULENT WALL PRESSURE FIELD MEASUREMENTS

It has been shown in the theoretical approach that in order to calculate the response of a thin-walled cylindrical pipe section to turbulent flow excitation, it is necessary to have information on the statistical properties of the wall pressure field. In particular, a knowledge of the power spectral density and the narrow band correlation functions of the wall pressures in the longitudinal and circumferential pipe wall directions is required.

This section describes the measurements of these statistical properties for fully-developed flow. The results obtained are compared wherever possible with existing empirical representations of the properties of the turbulent wall pressure field.

It was recognized that the presence of extraneous background noise in the working section would be detected by the wall-mounted pressure transducers. Because of this, it was necessary to investigate to what extent the background noise contributed to the total signal output from the transducers in various frequency bands. Comparison was, therefore, made between the measured values of the root-mean-square pressure fluctuations and those values already established for local boundary layer turbulence.

4.1 ROOT-MEAN-SQUARE PRESSURE FLUCTUATIONS

Measurements of the wall pressure fluctuations were made for various centerline pipe flow velocities, extending from 193 in/sec to 520 in/sec. The corresponding range of Reynolds numbers varied from 6.5×10^5 to 1.8×10^6. This variation in flow speeds and Reynolds numbers was commensurate with the pumping capabilities in the water flow loop.

An initial series of experiments were performed to measure the overall RMS wall pressures as a function of the Reynolds number. The overall pressures were obtained by summation of the mean square pressure in each 1/3-octave band from given wall-mounted transducers. However, because the background noise at low frequencies showed definite interference with the noise produced by local boundary layer turbulence, it was necessary to establish the lower limiting frequency above which measurements could be made of the turbulent wall pressure field.

Apart from the unavoidable background noise, other extraneous contributions to the output signal from a transducer included the spurious signals caused by transducer vibrations and the electronic noise in the amplification system.

Preliminary tests with a transducer shielded from the flow indicated that its output signal was about 1 percent of that obtained with the transducer exposed to the flow. It was therefore concluded that the vibration signal was negligible in comparison with the overall pressure signal. Also the electronic noise in the amplifiers was less than 0.5 percent of the mean square pressure and its effect on the spectral density measurements was negligible. These tests clearly established that the main source of interference was the background noise in the working section.

It was apparent from the power spectral density measurements that background noise was detectable at frequencies less than 160 cps. Recordings of the mean square pressure in 1/3-octave bands were therefore made above this lower limiting frequency to obtain the overall RMS signal arising only from the turbulent boundary layer pressure fluctuations. The range of frequencies over which these measurements were made extended from 160 cps to 1600 cps.

In Fig. 13, the ratio of the measured overall RMS pressure, $\sqrt{\langle p^2 \rangle}$, to the mean flow dynamic pressure, $1/2\ \rho_L U_\infty^2$, is plotted against the Reynolds number. It is seen from these results that the pressure coefficient is independent of the Reynolds number and is given by the relationship

$$\frac{\sqrt{\langle p^2 \rangle}}{1/2\ \rho_L U_\infty^2} \simeq 0.007 \qquad (4.1)$$

This value for the pressure coefficient is consistent with that reported by other investigators[16,3] from measurements of the turbulent pressure fluctuations on rigid walls in subsonic airflows. It was found that no significant variation in the overall RMS pressure was detectable between widely separated transducers. This implied that the wall pressure field was probably homogeneous, which, of course, was an assumption made in the theory.

4.2 POWER SPECTRAL DENSITY OF THE WALL PRESSURE FIELD

The power spectral density of the wall pressure fluctuations was obtained from measurements of the mean square pressure in each 1/3-octave band over a wide range of frequencies and flow velocities. The experimental results are shown in Fig. 14 in which the normalized power spectral density, S_p, is plotted as a function of the Strouhal number.

$$S_p = \frac{\phi_p(f)}{\rho_L^2 U_\infty^3 d} = F\left(\frac{fd}{U_\infty}\right) \qquad (4.2)$$

where $\phi_p(f)$ is the power spectral density, that is, the mean square pressure per unit bandwidth, U_∞ is the centerline pipe flow velocity, ρ_L is the fluid density, d is the pipe diameter, and f is the center frequency of a 1/3-octave band. This is a

conventional method of presenting spectral data, and provides a useful scaling law for the power spectral density in terms of the frequency, pipe diameter, and flow velocity.

A comparison between the present results and the averaged wall pressure spectra measured by Bakewell[16] for subsonic airflow in a smooth-walled pipe is also shown in Fig. 14. The general features and magnitude of the spectral density curves are seen to be similar in both cases. It is noted, however, that some scatter between the experimental points occurs at low Strouhal numbers. This is primarily due to the effects of extraneous noise, which increased the measured power spectral density. A lower cut-off frequency of 63 cps was used for these measurements. However, at frequencies above 160 cps the extraneous noise had a negligible influence on the spectral density.

In the higher Strouhal number range, the present data show slightly increased spectral levels. This behavior is probably caused by differences in transducer size. Bakewell used larger diameter transducers (0.070 in.) than in the present work and, as a result, greater attenuation of the high frequency pressure fluctuations over the transducer face would have occurred.

To account for this loss of resolution at high frequencies, Corcos[17] introduced a correction factor for the power spectral density in terms of the transducer diameter and turbulence wave number. However, Willmarth and Roos[18] pointed out that Corcos overestimated the correction factor when the transducer diameter is less than the boundary layer thickness. Because this condition is valid for the spectral data shown in Fig. 14, no attempt was made to correct the results for the attenuation effect at high frequencies.

4.3 BROAD-BAND CORRELATIONS OF THE WALL PRESSURE FIELD

Measurements of the broad-band space-time correlations were obtained by playing back the tape recorded signals from given transducer pairs through the variable time delay unit of the analog correlator. A description of the equipment used for recording and analyzing the transducer signals has been given in Section 3.3.

Broad-band space-time correlations of the wall pressure field in the longitudinal flow direction are presented for two flow speeds in Fig. 15. The cross-correlation coefficient is shown plotted as a function of the time delay, τ, where each correlation curve represents a different separation distance, Δx, between transducers. It is seen that for a given separation, the correlation curve rises to a maximum at a certain value of the time delay, τ_m, and the amplitude of these maxima decrease rapidly with increasing transducer separation. The amplitude decay of the correlations can be attributed to the presence of shear stresses across the turbulent boundary layer of the pipe, which cause the pressure fluctuations to lose their coherence as the convection pattern proceeds downstream. The rate at which the turbulent pressure field is convected is established by plotting the transducer separation against the time delay, τ_m, at which the correlation curves reach a maximum value, i.e.,

$$U_c = \Delta x/\tau_m \qquad (4.3)$$

The slope of the plot gives the convection speed of the pressure field moving past the transducers.

For an observer moving with the convection speed, U_c, the auto-correlation is the envelope of the peaks of the correlation curves. If it is assumed that the moving-axis auto-correlation curve decays exponentially with time, τ, then the

eddy lifetime, τ_o, is the value of the time delay when the correlation coefficient falls to 1/e or 0.37 (see Section II). Thus, the longitudinal correlation length, L_x, may be obtained from the product of the convection speed, U_c, and eddy lifetime, τ_o.

Referring to Fig. 15 it is also seen that the ratio of the convection speed to the centerline pipe flow velocity, U_c/U_∞ is consistent with that reported by other investigators from broad-band pressure field measurements in turbulent boundary layers[9, 16]. It is also apparent that the estimated value of the correlation length, L_x, is independent of the flow velocity, being approximately 0.18 in. at both selected flow speeds. This suggests that with increased flow speed, the eddy lifetime decreases in the same proportion as the convection speed increases.

Measurements of the broad-band circumferential space-time correlations showed that there was no convection process occurring. Because of this, it was necessary to measure only spatial correlations in the circumferential direction. The results from measurements of the broad-band space correlations, i.e., in a fixed frame of reference, are shown in Fig. 16.

The longitudinal scale, λ_x, is defined by

$$\lambda_x = \int_0^\infty R(\Delta x,0;0)\, d(\Delta x) \qquad (4.4)$$

and the circumferential scale, λ_y, is

$$\lambda_y = \int_0^\infty R(0,\Delta y;0)\, d(\Delta y) \qquad (4.5)$$

The space correlation curves at small separations are seen to decay almost exponentially. Thus, the integral scales are simply the distances the correlation coefficients fall to a

value of 1/e or 0.37. For the experimental data shown in Fig. 16 the longitudinal scale, λ_x, is larger by a factor of 1.5 than the circumferential scale, λ_y. This estimate is in fair agreement with the ratio of the longitudinal to lateral scales in turbulent boundary layers reported by Bakewell et al[16] and Maestrello[3]

It is of interest to note that the ratio of the correlation length, L_x, to the integral scale length, λ_x, is about 4:1. Thus, whereas to an observer at a fixed point the pressure field would be coherent for only short distances, to an observer who moved with the convection speed, the pressure fluctuations would appear coherent over much greater distances.

4.4 NARROW-BAND CORRELATIONS OF THE WALL PRESSURE FIELD

The aim of these experiments was to determine the longitudinal and circumferential correlation lengths and convection speeds of the wall pressure fluctuations in narrow frequency bands. This information was necessary in order to evaluate the joint acceptance functions used in calculating the response of the thin-walled pipe to the turbulent wall pressure field.

The instrumentation used for measuring the narrow-band cross-correlations of the pressure signals from transducer pairs has been described in Section III. For these experiments, two phase matched, 1/3-octave band pass filters were employed, and the cross-correlations between spatially separated transducers determined at center band frequencies of 250, 500, 1000, and 1600 cps. The selection of these frequencies was dictated by the presence of extraneous noise in the transducer output signals for frequencies outside this range.

The results from measurements of the longitudinal narrow-band space-time correlations at two flow speeds are shown in Figs. 17 and 18. It is seen that the general features of the

correlation curves are similar to broad-band correlations presented in Fig. 15. However, whereas the broad-band correlation curves exhibit broader, flatter peaks with increasing transducer separation, the shape of each narrow-band correlation curve is governed only by the frequency. In particular, the high frequency correlations are characterized in terms of sharp narrow curves, and the low frequencies by broader correlation curves.

Referring to Figs. 17 and 18 it is seen that both the eddy lifetime, τ_o, and convection speed, U_c, decrease with increasing frequency. The longitudinal correlation length, L_x, determined from the product of the eddy lifetime and convection speed appears to be a function only of the frequency and independent of the flow velocity, U_∞.

Figure 19 shows the result of plotting the measured ratio of the convection speed, U_c, to the centerline pipe flow velocity, U_∞, against the center frequency of the 1/3-octave bands. It is apparent that the ratio U_c/U_∞ decreases slightly from 0.7 at 250 cps to less than 0.6 at 1600 cps. The present variation of U_c/U_∞ with frequency is in good agreement with the results of other investigators, notably Bakewell et al[16]. This suggests that larger turbulent eddies associated with lower frequencies would exist nearer the center of the pipe and, as a result, be convected at speeds comparable with the mean flow velocity, whereas the smaller scale, high frequency eddies would be swept along closer to the wall at slower speeds.

Figure 20 shows the results from measurements of the narrow band space correlations in the circumferential direction. It is seen that the correlation amplitude decays almost exponentially with increasing transducer separation, and that the rate of decay is greater at higher frequencies. The circumferential correlation distance, L_y, defined by the distance the correlation coefficient falls to 1/e, again appears to be a

function of only the frequency and not of the flow velocity. This dependence of the circumferential correlation function on the frequency supports the form of the narrow band circumferential correlation function proposed in the theory (Section II).

From the above measurements of the narrow band correlation functions in the longitudinal and circumferential directions, the variation of the correlation lengths L_x and L_y with frequency for the two flow speeds are shown in Figs. 21 and 22 It is noted that the ratio of L_x/L_y is about 6:1 and independent of the frequency. This suggests that a typical pressure producing eddy is coherent over much greater distances in the flow direction than in the circumferential direction.

Finally, the important statistical parameters that have been determined from the narrow band wall pressure correlations are given in Table I.

TABLE I

Frequency f (cps)	U_∞ = 193 in/sec				U_∞ = 330 in/sec			
	U_c/U_∞	L_x (in)	L_y (in)	L_x/L_y	U_c/U_∞	L_x (in)	L_y (in)	L_x/L_y
250	0.66	0.280	0.047	5.95	0.69	0.300	0.055	5.45
500	0.62	0.190	0.033	5.75	0.62	0.220	0.040	5.50
1000	0.59	0.137	0.024	5.70	0.59	0.154	0.027	5.70
1600	0.59	0.120	0.020	6.00	0.59	0.116	0.022	5.30

V. CALCULATION OF THE PIPE WALL RESPONSE TO TURBULENT FLOW EXCITATION

5.1 INTRODUCTION

In this section a method is outlined for calculating the response of a thin-walled pipe to the wall pressure field applied by fully-developed turbulent water flow. An equation has been derived in Section II for the displacement power spectral density of a thin-walled pipe in terms of the turbulent pressure field which forces it into vibration, and the vibrational characteristics of the pipe itself. It was assumed that the response spectrum is essentially a smooth continuous function. Furthermore, a large number of individual pipe wall resonances are excited by turbulent pressure fluctuations having wave numbers much larger than the flexural wave numbers in the surface of the pipe.

Under these conditions, the power spectral density of the displacement response becomes independent of the mode number and is given by Eq. (2.31), that is,

$$\phi_d(\omega) = \frac{2\pi Q}{\rho_e^2 h^2} \phi_p(\omega)\, j_x^2(\omega)\, j_y^2(\omega) \frac{\Delta N}{\Delta\omega} \cdot \frac{1}{\omega^3} \qquad (5.1)$$

where the symbols in this equation have been defined in Section II and Appendix B. For the purpose of calculating the response from Eq. (5.1), it is necessary to consider each term independently.

5.1.1 Power Spectral Density, $\phi_p(\omega)$

From the wall pressure spectrum measurements, described in Section IV, it has been shown that the normalized power spectral density, S_p, can be expressed as a function of the pipe Strouhal number, i.e.,

$$S_p = \frac{\phi_p(f)}{\rho_L{}^2 U_\infty{}^3 d} = F\left(\frac{fd}{U_\infty}\right) \tag{5.2}$$

Thus, for a given Strouhal number, fd/U_∞, the power spectral density, $\phi_p(f)$, is

$$\phi_p(f) = \rho_L{}^2 U_\infty{}^3 d\, S_p \tag{5.3}$$

Consequently, if the Strouhal number is calculated, the normalized power spectral density can be determined from Fig. 14, and the corresponding power spectral density computed for a given flow velocity, fluid density and pipe diameter from Eq. (5.3).

5.1.2 Joint Acceptance Functions, $j_x{}^2(\omega)$ and $j_y{}^2(\omega)$

The longitudinal joint acceptance, $j_x{}^2(\omega)$, is defined by Eq. (2.29), that is,

$$j_x{}^2(\omega) \simeq \frac{\alpha}{L(\alpha^2+q^2)} \tag{5.4}$$

where $\alpha = 1/L_x$ and $q = \omega/U_c = 2\pi f/U_c$. Equation (5.4) can be written as

$$j_x{}^2(\omega) \simeq \frac{1}{L_x q^2 L}\left[1 + \left(\frac{1}{qL_x}\right)^2\right]^{-1} \tag{5.5}$$

In order to evaluate $j_x{}^2(\omega)$ for a given pipe section of length L, containing turbulent flow, a knowledge of the variation of L_x and q with frequency is required. The value of q can be calculated from the frequency and convection speed, U_c, where the variation of U_c/U_∞ with frequency is presented in Fig. 19 The longitudinal correlation length, L_x, as a function of the frequency is shown in Fig. 21. By substituting these values

in Eq. (5.5) the longitudinal joint acceptance, $j_x^2(\omega)$, can be computed.

The circumferential joint acceptance function, $j_y^2(\omega)$, is given by Eq. (2.30), that is,

$$j_y^2(\omega) = \frac{\beta a}{2\pi(\beta^2 a^2+n^2)}\left[1 - \frac{\beta a}{\pi(\beta^2 a^2+n^2)}\right] \qquad (5.6)$$

where $\beta = 1/L_y$, a is the pipe radius, and n is the circumferential mode number. The variation of L_y with frequency is shown in Fig. 22.

It has been assumed that βa is large compared with the mode number n, and as a result the mode number can be neglected in Eq. (5.6). Consequently, Eq. (5.6) can be written

$$j_y^2(\omega) \simeq \frac{1}{2\pi\beta a}\left[1 - \frac{1}{\pi\beta a}\right] \qquad (5.7)$$

Since $\beta a \gg 1$, then

$$j_y^2(\omega) \simeq \frac{L_y}{2\pi a} \qquad (5.8)$$

Under these conditions the circumferential joint acceptance, $j_y^2(\omega)$, becomes a measure of the ratio between the correlation length and pipe circumference. Equation (5.8) can, therefore, be used to calculate $j_y^2(\omega)$ from the known values of L_y.

5.1.3 Effective Density of Shell Wall, ρ_e

It has been mentioned in the theoretical approach that liquid loading has an important influence on the vibrations of thin-walled cylinders. Generally, there are additional forces exerted on the surface of a vibrating structure by the surrounding fluid. These forces consist of two parts; one proportional to the fluid velocity and the other proportional to the fluid

acceleration. The former generates a damping force due to the sound radiation from the vibrating surface, while the latter causes an increase in the mass of the structure. This increase in mass arises from the vibrating mass of fluid or virtual mass adjacent to the surface of the structure. If the surrounding fluid is air, the above effects are quite small, but for liquid loading the virtual mass and acoustic damping play an important role and therefore cannot be neglected.

Theoretical studies[13,14] have shown that liquid coupling, apart from increasing the effective mass or density of a structure, can influence the vibrational response in several ways. First, the added mass tends to reduce the amplitude of vibration. Second, the resonant frequencies of the structure are decreased, and therefore the number of resonances or modal density are increased.

In Appendix A, a method is outlined that might be employed to determine the virtual mass from the natural frequencies of an empty and water-filled cylindrical shell. However, in order to calculate numerically the natural frequencies and virtual mass, an extensive digital computer program would be required. In view of the complexity of the problem due to water loading, it was decided to use a simpler approach.

It has been shown by Berry and Reissner[13] that the correction factor for the virtual mass, B, for an infinitely long cylindrical shell containing fluid is given by

$$B = \frac{1}{\lambda_L} \frac{I_n(\lambda_L)}{I_n'(\lambda_L)} \tag{5.9}$$

where I_n is the modified Bessel function of the first kind of order n, and the prime denotes the derivative of I_n with respect to the argument λ_L, and where λ_L is given by

$$\lambda_L = \frac{\omega a}{c_L} \tag{5.10}$$

where ω is the angular frequency, c_L is the sound velocity of the fluid, and a is the shell radius. Dyer[19] showed that for lower frequencies, $\lambda_L < 1$, the virtual mass factor is nearly independent of λ_L and varies with the circumferential mode number, n.

The effective density of the shell wall, ρ_e, due to the virtual mass is

$$\rho_e = \rho_s (1 + \mu B) \tag{5.11}$$

where ρ_s is the density of the shell wall, and μ is given by

$$\mu = \frac{a\rho_L}{\rho_s h} = \frac{a\rho_L}{m_s} \tag{5.12}$$

where h is the wall thickness and m_s is the mass per unit area of the shell. From Eqs. (5.9), (5.11), and (5.12) the virtual mass of the liquid, m_L, is

$$m_L = \frac{a\rho_L}{\lambda_L} \frac{I_n(\lambda_L)}{I_n'(\lambda_L)} \tag{5.13}$$

Thus the effective mass per unit area of the shell is given by

$$\rho_e h = m_s + m_L \tag{5.14}$$

It is shown in Appendix A, that if the shell wall is regarded as a flat plate of thickness h, the virtual mass factor, μB, can be approximated by

$$\mu B \simeq \frac{\rho_L}{\rho_s} \left(\frac{c_s}{4\pi\sqrt{3} f h} \right)^{1/2} \tag{5.15}$$

where c_s is the speed of compressional waves in the shell wall, and ρ_L is the fluid density. Equation (5.15) corresponds to

the virtual mass factor derived by Dyer[11] for a vibrating plate radiating sound into a water-filled enclosure.

The correction factor $(1 + \mu B)$ calculated from the above equation for the dimensions and physical constants of the water-loaded cylindrical shell under investigation is shown plotted as a function of frequency, f, in Fig. 23. It is seen that the effective mass of the shell is significantly increased by the water loading. However, the correction factor appears to decrease with increasing frequency. This correction factor due to the water loading has been used in the procedure outlined in Section 5.2 for calculating the pipe wall response to turbulent water flow excitation.

5.1.4 Modal Density, $\Delta N/\Delta\omega$

The number of resonant frequencies, ΔN, contained in a narrow frequency band of width, $\Delta\omega$, for a simply supported cylindrical shell of length, L, has been calculated by Heckl[12]. The approach used to determine the modal density was based on a solution of the simplified shell equations[13] for the natural frequencies of vibration. The theoretical result for the modal density may be expressed as

$$\frac{\Delta N}{\Delta\omega} = \frac{\sqrt{3}aL}{2\pi c_s h}\left(\pi/2 - \sin^{-1}\left[1 - (2\omega a/c_s)\right]\right) \qquad (5.16)$$

Equation (5.16) is valid for the range of frequencies where $\omega a/c_s < 1$. Heckl made measurements over this range using a simply supported thin-walled cylinder and found good agreement between the predicted and measured modal density. It may be noted that the actual cylinder end conditions are important only for the lower mode vibrations. When the frequency associated with the low order modes is exceeded, the mode is mainly governed by the vibrations away from the cylinder ends.

Equation (5.16) does not account for the liquid loading, which increases the modal density. Due to the increase in the mass of the shell wall caused by liquid loading, the sound velocity for compressional waves in the wall, c_s, will be reduced by

$$c_s' = \frac{c_s}{(1 + \mu B)^{1/2}} \tag{5.17}$$

where c_s' is the corrected sound velocity in the material of the wall.

The value of the correction factor $(1 + \mu B)$ in Eq. (5.17) can be obtained from Fig. 23. Thus, Eq. (5.16) becomes

$$\frac{\Delta N}{\Delta \omega} = \frac{\sqrt{3}aL}{2\pi c_s' h} \left\{ \frac{\pi}{2} - \sin^{-1} \left[1 - \left(\frac{2\omega a}{c_s'} \right) \right] \right\} \tag{5.18}$$

In Fig. 24, the modal density is shown plotted against the frequency, f, using the dimensions and physical constants of the thin-walled cylinder under investigation.

It is seen that the modal density increases with frequency, indicating fewer modes in the low frequency region. At higher frequencies the modal density does not vary appreciably between successive bandwidths. This would suggest that at very high frequencies the modal density would be essentially constant and independent of the frequency.

5.1.5 Damping Factor, Q

The damping of the thin-walled cylinder vibrations will consist of two parts, one structural and the other acoustic. The structural damping generally predominates, and results from internal hysteresis in the cylinder material and from energy dissipation at the cylinder joints. The hysteresis effect is usually small compared with the damping at the joints, especially as in the present case, where the joints are heavily

loaded by the cylinder end flanges. Acoustic or radiation damping is due to the sound radiated from the cylinder vibrations and the resulting energy dissipation.

It has been assumed in the theory that the overall damping factor Q is independent of frequency. In general, this is an oversimplification since the acoustic damping is known[20] to vary with frequency. Measurements of the overall damping factor for the water-loaded cylindrical shell are described in Section VI. Attempts were also made to investigate the assumption that the damping was independent of the frequency.

5.2 CALCULATION PROCEDURE

A method for calculating the displacement response of the thin-walled cylindrical pipe to the wall pressure field applied by fully-developed turbulent water flow is outlined in this section. The method used is considered in general terms with the aid of a computational chart to indicate as clearly as possible each step in the calculation. A numerical example is then given to illustrate the calculation procedure.

Equation (5.1) for the power spectral density of the pipe wall displacement can be expressed in terms of the frequency, f, as

$$\phi_d(f) = \frac{\langle W^2 \rangle}{\Delta f} = 4.03 \times 10^{-3} \frac{Q}{\rho_e^2 h^2} \phi_p(f) j_x^2(f) j_y^2(f) \frac{\Delta N}{\Delta f} \frac{1}{f^3} \quad (5.19)$$

This equation is obtained by replacing the circular frequency, ω, by $\omega = 2\pi f$ and $\Delta\omega = 2\pi\Delta f$. $\langle W^2 \rangle$ represents the time averaged value of the mean square radial displacement of the pipe wall in the frequency band Δf, averaged over the surface of the pipe. The relations for $\phi_p(f)$ and ρ_e are defined by Eqs. (5.3) and (5.11). Substituting these expressions into Eq. (5.19) yields,

$$\phi_d(f) = \frac{4.03 \times 10^{-3}\, Q}{h^2(1+\mu B)^2} \left(\frac{\rho_L}{\rho_s}\right)^2 S_p \left(\frac{U_\infty}{f}\right)^3 dj_x^{\,2}(f) j_y^{\,2}(f) \frac{\Delta N}{\Delta f} \qquad (5.20)$$

where $j_x^{\,2}(f)$, $j_y^{\,2}(f)$ and $\Delta N/\Delta f$ are given by Eqs. (5.5), (5.8), and (5.18) respectively.

The computational procedure that is employed in evaluating Eq. (5.20) is outlined in Fig. 25. This chart gives a step-by-step procedure and shows in block diagram form how each term in Eq. (5.20) is obtained from a knowledge of the basic flow and structural variables.

To illustrate the method of calculation, a numerical example is given below based on a typical flow velocity and frequency for turbulent flow excitation of the thin-walled cylindrical pipe (see Chapter VI).

Consider the response of a long, uniform thin-walled cylindrical pipe to the wall pressure field arising from fully-developed turbulent water flow in a narrow 1/3-octave frequency band:

	Pipe		
Stainless Steel			
Length	L	=	240 in.
Diameter	d	=	6 in.
Radius	a	=	3 in.
Wall Thickness	h	=	0.025 in.
Mass Density	ρ_s	=	1.295 lb. sec^2/in^4
Sound Velocity	c_s	=	2.14×10^5 in/sec
	Flow		
Water			
Flow Velocity	U_∞	=	520 in/sec
Mass Density	ρ_L	=	0.162 lb. sec^2/in^4
Sound Velocity	c_L	=	5.68×10^4 in/sec

Frequency

1/3-Octave Band

Center Frequency	f	= 200 cps
Bandwidth	Δf	= 46 cps

Referring to Fig. 25, the following procedure is adopted where each number is listed on the chart.

1. Compute $fd/U_\infty = 2.31$
2. Read $S_p = 1.25 \times 10^{-6}$ (Fig. 14)
3. Compute $S_p \rho_L^2 U_\infty^3 d = \phi_p(f) = 27.6$ lb^2 sec/in^4
4. Read $U_c/U_\infty = 0.70$ (Fig. 19)
5. Compute $U_c = 364$ in/sec
6. Compute $q = 2\pi f/U_c = 3.45$ in^{-1}
7. Read $L_x = 0.330$ in. (Fig. 21)
8. Compute $j_x^2(f) = 6.0 \times 10^{-4}$ (Eq. 5.5)
9. Read $L_y = 0.056$ (Fig. 22)
10. Compute $j_y^2(f) = 2.97 \times 10^{-3}$ (Eq. 5.8)
11. Compute $\phi_p(f) j_x^2(f) j_y^2(f) = 4.9 \times 10^{-5}$ lb^2 sec/in^4
12. Measure damping factor $Q = 25$ (Section 6.2)
13. Read or Compute $(1 + \mu B) = 6.6$ (Fig. 23, Eq. 5.15)

14. Compute $(1 + \mu B)^2 = 43.6$

15. Compute $c_s' = 8.32 \times 10^4$ in/sec

(Eq. 5.17)

16. Read or Compute $\Delta N/\Delta f = 0.256$ sec

(Fig. 24, Eq. 5.18)

17. Compute $Q/(1 + \mu B)^2 \cdot \Delta N/\Delta f = 0.147$ sec

18. Compute

$$\frac{4.03 \times 10^{-3}}{\rho_s{}^2 h^2} \cdot \frac{1}{f^3} = 4.81 \times 10^{-7} \text{ in}^6/\text{lb}^2 \text{ sec}$$

19. Compute $\phi_d(f) =$

$$\phi_p(f) j_x{}^2(f) j_y{}^2(f) \frac{Q}{(1+\mu B)^2} \frac{\Delta N}{\Delta f} \cdot \frac{4.03 \times 10^{-3}}{\rho_s{}^2 h^2} \cdot \frac{1}{f^3} =$$

34.6×10^{-13} in^2 sec

(Eq. 5.20)

20. Compute $\langle W^2(f) \rangle = \phi_d(f)\Delta f = 159 \times 10^{-12}$ in^2

(Eq. 5.19)

21. Compute $\sqrt{\langle W^2(f) \rangle} = 12.6 \times 10^{-6}$ in.

By repeating the above steps for other 1/3-octave frequencies ranging from 100 cps to 1600 cps, the power spectral density and RMS displacement of the pipe wall to turbulent flow excitation can be evaluated. The results obtained from such a calculation procedure are summarized below in Table II.

TABLE II

Frequency f (cps)	Flow Speed, U_∞ = 520 in/sec	
	Power Spectral Density $\phi_d(f)$ in^2 sec	RMS Displacement $\sqrt{\langle W^2(f) \rangle}$ in.
100	83.0×10^{-12}	43.6×10^{-6}
125	33.7×10^{-12}	31.2×10^{-6}
160	85.5×10^{-13}	17.8×10^{-6}
200	34.5×10^{-13}	12.6×10^{-6}
250	12.2×10^{-13}	8.4×10^{-6}
315	39.0×10^{-14}	5.4×10^{-6}
400	11.8×10^{-14}	3.3×10^{-6}
500	37.7×10^{-15}	2.1×10^{-6}
630	10.5×10^{-15}	1.25×10^{-6}
800	22.5×10^{-16}	0.64×10^{-6}
1000	68.6×10^{-17}	0.40×10^{-6}
1250	16.3×10^{-17}	0.22×10^{-6}
1600	29.3×10^{-18}	0.10×10^{-6}

The above calculations can be performed for other flow speeds and pipe sizes by reference to the computational chart (Fig. 25). In this way it was possible to compute the displacement response of a given thin-walled pipe to a wide range of frequencies and flow speeds.

A discussion of the theoretical prediction for the pipe wall response is reserved until a comparison can be made with the experimental results.

5.3 DISCUSSION OF CALCULATION METHOD

It has been shown that the displacement response of a thin-walled cylindrical pipe to the wall pressure field applied by turbulent water flow can be readily calculated from a knowledge of the statistical flow properties and vibration characteristics of the pipe. The method employed is quite general but is subject to certain limitations.

It was assumed in the theory that the pressure correlation lengths are very small compared with the pipe dimensions. This assumption was borne out by the experimental data for the longitudinal and circumferential correlation lengths. In this case the joint acceptance functions will be independent of the mode numbers.

The empirical scaling law developed for the power spectral density of the wall pressure field indicated that the spectra can be scaled with flow velocity and frequency as shown by the method of plotting the normalized spectral density against the pipe Strouhal number. The scaling of the spectra with pipe diameter was not investigated. However, it was felt that in view of the agreement between independent spectral data using pipes of differing diameter; the Strouhal number dependence was valid.

The major problem regarding the power spectral density calculation was the low frequency extraneous noise whose spectral level is a function of the noise transmission in the flow system. Because of this the method of extrapolating the spectrum to low frequencies or Strouhal numbers is subject to errors.

The effect of water loading has been shown to complicate the calculation of the pipe wall response. Approximations were made to estimate the apparent increase in the mass of the pipe and modal density due to the water loading. It was emphasized, however, that further work was necessary to investigate the natural frequencies of pipe wall vibrations with and without the presence of water. However, such work is felt beyond the scope of the present investigation.

One significant result from the calculation procedure is that the response appears to be independent of the pipe length. This arises from the fact that the longitudinal joint acceptance term varies inversely with the pipe length while the modal density is directly proportional to the length. The product of these two terms in the response equation leads to the conclusion that the response is not affected by the pipe length. On the other hand, the pipe wall response is dependent on the pipe diameter because the power spectral density of the pressure fluctuations varies with the pipe diameter and Strouhal number.

VI. MEASUREMENTS OF THE PIPE WALL RESPONSE AND COMPARISONS BETWEEN THEORY AND EXPERIMENT

This section contains the results of measurements of the vibrations of a thin-walled cylindrical pipe due to the wall pressure field generated by the passage of turbulent water flow. The aim of this work was to measure the displacement amplitude of the pipe wall as a function of both the frequency and mean flow velocity and to compare the data obtained with the theoretical predictions. Measurements were also made of the vibrations induced in the thin-walled cylindrical pipe coupled to the downstream end of a rigid 90° bend and to an orifice plate of diameter 4.75 in. These tests were carried out to meet the objectives of the research program under Contract NAS8-20325, to study the effect of environmental influences on the pipe wall response.

The thin-walled cylinder used in the experimental work was a 20 ft. long stainless steel pipe section of 6 in. diameter and 0.025 in. wall thickness. A traversing mechanism was designed and constructed for moving two ultramicrometer vibration sensors over the pipe wall to detect the flow-induced vibrations. By means of the ultramicrometer probes, it was possible not only to determine the wall displacements at various positions over the pipe surface, but also to perform space correlations to identify any predominant modes that may be excited into vibration. The vibrations induced in the thin-walled pipe by the wall pressure field (in turbulent pipe flow) generated by the pipe bend and orifice plate were also detected and measured using a calibrated accelerometer pickup and compared with the ultramicrometer data.

An initial series of measurements were carried out to determine the overall damping factor of the water-filled thin-walled pipe. The main body of the experimental work, however,

was concerned with measurements of the pipe wall vibrations resulting from turbulent flow excitation. Comparisons were made between the power spectral density of the pipe wall displacements as predicted from the theory for fully-developed flow and that determined experimentally for various flow conditions (e.g., pipe bends and orifices).

6.1 METHOD OF MOUNTING ULTRAMICROMETERS AND ACCELEROMETERS

In order to detect the pipe wall vibrations, it was necessary to design and construct a traversing mechanism for moving the ultramicrometer probes over the pipe surface in the longitudinal and circumferential directions. It was decided to use two ultramicrometers to perform space correlation measurements. Because of this, the mounting system was constructed in such a way that the ultramicrometers could be moved relative to each other in the required direction. For this purpose two steel straps were rigidly attached to the pipe sleeves at the ends of the thin-walled cylinder. A hexagonal rod which was used as a traversing track was suspended from the end straps by means of a bracket. In this way it was possible to traverse the full length of the thin-walled cylindrical working section.

The ultramicrometers and their holders were mounted on two aluminum rings that were attached to the hexagonal rod and mounted concentric with the axis of the cylindrical pipe. The traversing system was arranged so that the ultramicrometer probes could either be mounted on one concentric ring to perform circumferential correlations or alternatively mounted on separate rings so that the pipe could be scanned longitudinally. To maintain the correct symmetry between the probe face and pipe wall, the concentric rings could also be adjusted in the vertical as well as the horizontal plane. A view showing the ultramicrometer probes and their mounting system is shown in Fig. 26.

The ultramicrometer holders were positioned so that the probe could first be coarsely adjusted to the approximate clearance between the probe face and pipe wall for the calibration procedure, and then, by fine micrometer adjustment, to obtain the correct gap setting of 0.002 in. for balance in the discriminator circuit (see Section III). This procedure had to be completed for every measuring position over the surface of the pipe since the ultramicrometer was inaccurate unless the proper clearance between the probe face and pipe wall was maintained.

The accelerometer pickup used in several of the tests was a small lightweight Kistler force gage accelerometer (Model 808) having a sensitivity of 50 mV/g. The reason for using the accelerometer was twofold. First, as has been pointed out above it was necessary to adjust the ultramicrometer probe for balance over the linear range in the discriminator circuit for each measuring position. This procedure was very time consuming since the pipe wall displacement had to be measured for thirty-five positions (Section 6.3) in order to obtain the space average value of the pipe wall response. Second, the use of an accelerometer provided the means of establishing the validity of the ultramicrometer data when the measured accelerations were converted into displacement amplitudes. The accelerometer was rigidly attached to the pipe wall by means of a thin metal strap which could be tensioned by a thumb screw around the pipe circumference. In mounting the accelerometer, care was taken to insure good contact between the pickup face and the surface of the pipe.

6.2 DETERMINATION OF THE DAMPING FACTOR

It has been shown in the theory outlined in Section II, that a knowledge of the damping of the flow-induced pipe wall vibrations is required in the response calculation (see Section V).

It was recognized that the overall damping would not only depend on the structural and acoustic damping associated with the water-filled cylindrical pipe working section itself, but would also include the effect of other variables in the interconnecting pipes joining the working section to the water flow loop.

These variables would include pipe support brackets, the flanges at each end of the working section, and the water columns in the interconnecting pipes. In view of the combined effect of these unknown variables on the overall damping, it was necessary to perform in situ measurements of the damping factor.

For determining the damping factor the pipe wall was subjected to an impulse from a hammer blow and the resulting vibrational amplitude signal detected by an ultramicrometer was fed to an oscilloscope. Both the resonant frequency and exponential amplitude decay of the signal were determined from the oscilloscope trace. The damping factor, Q, was found from the relation[21]

$$Q = \pi f T \tag{6.1}$$

where f is the resonant frequency excited, and T is the time the amplitude decays to 1/e of its initial value. Figure 27 shows the resonant frequency and the amplitude decay curve taken from the oscilloscope display.

It was found using the impulse technique that only one predominant mode of vibration at a frequency of about 85 cps was excited. This made it impossible to verify the assumption made in the theory that the damping factor Q was constant over the range of frequencies investigated. It was therefore decided to attempt to excite higher frequencies using an alternative approach. The method adopted was to use a loudspeaker driven by an oscillator through a 75 watt amplifier. The

loudspeaker was moved to various positions close to the pipe wall in an attempt to force the pipe into vibration. Unfortunately this method was found to be incapable of coupling sufficient energy into the pipe system to induce resonant vibrations.

It was next decided to remove the thin-walled pipe from the flow loop and repeat the above method of exciting the pipe without the influence of the interconnecting pipes and structural supports. For this experiment the end flanges of the thin-walled pipe were fitted with steel blanking plates and the pipe was completely filled with water.

In this case it was possible to induce resonant vibrations of the pipe using the loudspeaker system. The signals detected by the ultramicrometer were fed through a narrow band pass filter and displayed on a two-channel oscilloscope. To investigate the frequencies, the loudspeaker was placed about midway along the pipe axis close to the wall and the exciting frequency slowly increased by means of the oscillator. On passing through a resonant frequency, the pipe responded and the oscillator and band pass filter were finely adjusted until the output signal from the ultramicrometer had maximum amplitude. The oscillator was then switched off, and the amplitude decay of the signal determined from the resulting oscilloscope trace.

The results of these measurements for frequencies varying from about 200 cps to 1300 cps are shown in Fig. 28. It is seen that the damping factor measured using acoustic excitation is independent of the frequency which verifies the assumption made in the theoretical approach. However, the average value of the damping factor ($Q \simeq 315$) for the water-filled cylinder alone is about an order of magnitude higher than that obtained from the in situ measurement using the impulse technique. This would suggest that the vibrational energy that is

normally dissipated in the interconnecting water columns joining the thin-walled cylinder to the flow loop would be prevented from occurring by reflection of standing waves from the blanking plates at the cylinder ends.

The significance of this result is immediately apparent for it indicates that environmental influences play an important role in determining the magnitude of the damping, and clearly emphasizes the importance of performing in situ measurements of the damping. Consequently, the measured in situ value of the damping factor (Q = 25) was taken as being characteristic of the actual system damping.

It is apparent from the calculation procedure outlined in Section V that the pipe wall response to turbulent flow excitation is proportional to the damping factor Q (see Eq. (5.20)). The value of the damping factor used therefore determines directly the magnitude of the predicted response. If the higher value obtained by performing damping measurements with the pipe alone had been used, the predicted response would have been much higher than that measured experimentally (see Section 6.5).

6.3 MEASUREMENTS OF THE PIPE WALL DISPLACEMENTS

The displacement amplitudes of the pipe wall vibrations were mostly measured using a single ultramicrometer probe. However, some subsequent measurements were made using the accelerometer pickup affixed to the pipe wall at preselected points. For the ultramicrometer tests the probe was moved to selected positions over the surface of the thin-walled pipe and recordings made of the wall displacements. This was necessary in order to obtain values of the displacement response averaged over the pipe surface so as to compare the measured displacements with those predicted from the theory.

The signal resulting from the pipe wall vibrations due to the passage of turbulent flow was detected in the discriminator-amplifier circuit of the ultramicrometer and also the accelerometer when it was used, and fed to a Bruel and Kjaer 1/3-octave frequency analyzer (Type 2112). The output signal from the analyzer was then applied to the input of a Bruel and Kjaer graphic level recorder (Type 2305). The level recorder is basically a self-adjusting potentiometer with an electromechanical drive system for displaying the voltage signals graphically on moving chart paper as a function of frequency.

This procedure permitted direct plotting of the voltage levels in 1/3-octave frequency bands by sampling the levels consecutively at a linear rate from the analyzer. A calibration voltage, whose level was measured on a true RMS meter, was applied to the analyzer and recorder to give a reference voltage on the recorder. Once the level had been established, the voltage on the dB scale of the chart paper could be related to the amplitude displacement of the pipe wall from the known sensitivity of the ultramicrometer or accelerometer by conversion into displacements. In this way a continuous record of the RMS vibration displacements of the pipe wall averaged over various 1/3-octave frequency bands could be displayed on the recorder chart paper for each measuring position over the pipe surface. A block diagram of the analyzing and recording system is shown in Fig. 29.

The first series of measurements were carried out to determine the background noise detected by the ultramicrometer. For this purpose the pumps were operated at full speed but with the flow outlet valves closed. Under these conditions flow was prevented from reaching the working section. The purpose of these tests was to insure that the signal-to-noise ratio was sufficiently high over the frequency range investigated so that

no correction was required for the noise contribution to the wall displacement spectra due to the passage of turbulent flow. A typical chart record of the background noise spectrum is shown in Fig. 30. It is seen that three major peaks occur in the spectrum at frequencies of about 25, 50, and 100 cps. These may be attributed to structural and airborne disturbances which contain harmonics of a fundamental frequency. The source of these disturbances probably originated from the engines used to drive the pumps.

It was found from subsequent measurements of the spectra of the flow-induced pipe wall vibrations, that the background noise level was at least 15 dB below the total vibration signal detected in the frequency range 100 to 1,000 cps. At higher frequencies the major problem was the inherent electronic noise in the ultramicrometer detection system, which in some cases was only a few dB below the signal level. Because of this, no attempt was made to analyze the recorded signals at frequencies greater than 1000 cps. At frequencies below 100 cps, considerable uncertainty existed as to the contribution the background noise made to the total vibration signal. In particular, the wall pressure spectrum measurements, discussed in Section IV, have indicated that at low frequencies the extraneous flow noise emanating from the pumps in the water flow loop was sufficiently large to cause interference with the turbulent wall pressure fluctuations. Consequently, the vibration signals recorded at frequencies below 100 cps were excluded from the analysis of the pipe wall displacement spectra.

Measurements of the pipe wall vibrations to turbulent flow excitation were carried out at flow speeds ranging from 248 in/sec to 520 in/sec. For each flow speed recordings of the spectra were made at 30° intervals spanning half the pipe circumference at five longitudinal stations. These stations were situated at the mid-point of the pipe section and at two

positions 2 ft. apart on both sides of the mid-point. Measurements closer to the ends of the 20 ft. pipe section were not attempted because of the restraining influence of the pipe sleeves and flanges. Thus, a continuous chart recording at a given flow speed contained thirty-five records of the wall displacement spectra corresponding to the above measuring positions over the pipe surface. The space average value of the RMS displacement amplitude in a given 1/3-octave frequency band was obtained from the arithmetic mean of the wall displacements at the thirty-five measuring positions.

Although considerable scatter between the measured wall displacements at various positions was apparent, it was difficult using a single point measuring technique to determine whether any preferential modes were excited. Variations in the RMS displacement over the pipe surface by factors of two or more were noted in the low frequency range. However, at higher frequencies the differences between the space average and local point displacements were no more than 30 percent. Subsequent measurements of the space correlations using two ultramicrometers revealed that some predominant modes were excited at frequencies below 160 cps. Figure 31 shows typical chart records of the displacement spectra of the pipe wall vibrations at several flow speeds. It may be seen that at frequencies below 100 cps several pronounced peaks occur each of which may be associated with a particular low order mode of vibration. In the higher frequency range, however, the almost continuous response indicates that a large number of resonances are excited. This observation verifies the assumption of continuous resonant response at high frequencies that was made in the theory used for predicting the pipe wall response to turbulent flow excitation.

A general feature of these records is that in spite of the averaging effect of the 1/3-octave band pass filters, the spectra at high frequencies are characterized by a multitude of minor peaks and valleys. It is recognized, however, that had a slower writing speed been used much smoother response spectra would have been recorded. A mean line was therefore drawn through these spectra in order to determine the average vibration amplitude in each 1/3-octave band.

The amplitude decay of the spectra shown in Fig. 31 is seen to vary with frequency and flow speed. For the lowest flow speeds the decay rate is about 12 dB/octave. On the other hand, at the highest flow speed shown, the amplitude decay is only 9 dB/octave at frequencies ranging from 100 cps to 400 cps. For the higher frequencies, however, the amplitude again falls off at 12 dB/octave.

Finally, it was observed during one experiment that the pipe wall vibration level appeared to increase by at least 3 dB in the high frequency range. The reason for this occurrence was not immediately apparent. However, it was subsequently revealed that the water in the reservoir had fallen below the level of the entry pipe, causing air to be entrained in the water (see Section III). It was concluded that the small air bubbles in the water flow acted as additional disturbances in the wall pressure field, causing the pipe wall response to increase at high frequencies. However, before any definite conclusions can be drawn further investigations of this phenomena are required.

The data obtained from the above measurements to determine the space average values of the pipe wall displacements as a function of frequency and flow speed are presented and discussed in Section 6.5, where comparisons are made between the measured and theoretically predicted values.

6.4 SPACE CORRELATIONS OF PIPE WALL VIBRATIONS

Measurements of the displacement spectra of the pipe wall vibrations for fully-developed flow have indicated wide variations between the displacements at selected positions over the pipe surface. This was particularly apparent in low frequency bands where the presence of pronounced resonant peaks was seen to occur at frequencies in the neighborhood of 100 cps.

In principle it should be possible to identify the predominant modes by performing space correlations in narrow frequency bands. For this purpose two ultramicrometer probes were used which could be traversed relative to each other in the circumferential and longitudinal directions (see Section 6.1).

With the pipe wall excited into vibration by turbulent flow, the signal outputs from the probes were passed through two phase-matched Bruel and Kjaer 1/3-octave band pass filters (Type 2112) and fed into the input terminals of the electronic analog correlator. The operating principles of the correlator have been described previously in Section III.

The shape of the modes excited into vibration was determined from the variation in the correlation coefficient or phase change that occurred as one probe was moved relative to the other over the pipe surface. The results obtained from spatial correlations in the circumferential direction are shown in Fig. 32. It is seen that in the 1/3-octave bands centered on frequencies of 80 and 100 cps, two circumferential standing waves (n=2) are excited. Because the filter bandwidth was relatively wide, it was impossible by this method to determine the exact resonant frequency. However, the mode shape at 80 cps is more highly correlated than at 100 cps suggesting a possible intermodal coupling or interaction process at frequencies centered about 80 cps.

In order to identify the longitudinal mode, m, that was associated with the circumferential mode (n=2), one probe was positioned at one end of the 20 ft. pipe section, while the other probe was moved away from its along the pipe axis. It was found from the observed variation in the correlation coefficient that a phase change of about 180° occurred between the probes at the opposite ends of the pipe section. This indicated the presence of one half wavelength (m=1) between the pipe supports.

The existence of an acoustic standing wave in the water column of fundamental frequency 80 cps whose nodes were situated at the pipe supports was considered. However, in this case the distance corresponding to one half wavelength would be about 30 ft. as calculated from the free field sound velocity in water. While this distance exceeded the length of the pipe section, it was felt that acoustic disturbances accounted for a significant proportion of excitation field at low frequencies due mainly to the transmission of pump noise in the flow system.

Finally, the results of narrow band circumferential space correlation measurements at frequencies of 160 cps and 200 cps are shown in Fig. 33. It is seen that the correlation is virtually zero over the pipe circumference indicating that at higher frequencies many resonances are contained within the selected bandwidths. The fact that no predominant modes are excited is supported by the results obtained from measurements of the wall vibration spectra (see Fig. 31).

6.5 COMPARISON OF MEASUREMENTS WITH THEORETICAL PREDICTION

It has been shown in Section V that the displacement response of the thin-walled pipe to fully-developed turbulent flow can be calculated as a function of the frequency and flow

speed. In this section comparisons are made between the predicted and measured values of the displacement response for the following flow conditions: (1) fully-developed pipe flow, (2) flow downstream of a 90° pipe bend at various axial and longitudinal locations of the thin-walled pipe coupled to the bend, and (3) flow generated by a 4.75 in. diameter orifice plate installed at the upstream end of the 6 in. diameter thin-walled pipe. The measurement of the wall displacement under these conditions were similarly taken at various positions along the pipe section downstream of the orifice plate.

6.5.1 Fully-Developed Turbulent Flow

Measurements of the wall displacements averaged over the surface of the pipe have been described in Section 6.4. The predicted values for fully-developed flow were calculated using the procedure outlined in Section V (see Table II).

Figure 34 shows the result of plotting the average RMS pipe wall displacement for fully-developed flow against the frequency for two flow speeds. It is seen that the agreement between the theoretically predicted values and the experimental results is remarkably good. At the highest flow speed (U_∞ = 520 in/sec), the experimental points are slightly below the predicted values in the lower frequency range. However, at the lower flow speed (U_∞ = 248 in/sec) the agreement is excellent over the whole frequency range. It may also be noted that the absolute values of the pipe wall displacements are very small. For example, at the higher flow speed, the RMS displacement decreases from 30 microinches at about 100 cps to a fraction of a microinch at 1000 cps.

In Fig. 35, the power spectral density of the pipe wall displacement, $\phi_d(f)$, is shown plotted against the Strouhal number, fd/U_∞. The theoretical prediction shown represents

the best-fit curve drawn through the calculated values for the highest and lowest flow speeds investigated (see Fig. 34). The variation between these calculated values and the mean line drawn through them was very small and amounted to less than the scatter between the experimental points at lower Strouhal numbers.

It is seen from Fig. 35 that the agreement between theory and experiment for fully-developed turbulence is very good, particularly in the intermediate Strouhal number range. At lower Strouhal numbers, however, the theoretically predicted values for the power spectral density are slightly in excess of the measured values. The converse appears to be the case at higher Strouhal numbers. This disparity could be caused by errors in measuring extremely small pipe wall displacements at high frequencies. In this region the vibration signals are only a few dB above the noise levels in the ultramicrometer measuring system.

It is apparent from the theoretical prediction that the power spectral density of the pipe wall displacement appears to follow two separate scaling laws. At lower Strouhal numbers the spectral level decreases at the rate of 15 dB/octave, changing to 18 dB/octave at higher Strouhal numbers. The change in slope would seem to occur at a Strouhal number of about six ($fd/U_\infty \simeq 6$). The measured values for the power spectral density also indicate a rate of decay of 15 dB/octave in the lower Strouhal number range. However, because of the scatter between the experimental points at higher Strouhal numbers, it is uncertain whether the spectral level follows a -18 dB/octave Strouhal number dependence. It might be pointed out that it is possible on the basis of the experimental results alone to suggest that the spectral level decays at the rate of 15 dB/octave over the whole range of Strouhal numbers. However, the errors involved in measuring very small pipe wall displacements

at high frequencies could account for the apparent increase in spectral levels above the theoretically predicted values at higher Strouhal numbers.

6.5.2 Varying Flow Conditions

The data obtained from measuring the response of the thin-walled pipe coupled to the 90° rigid pipe bend using the ultramicrometer pickup is shown in Fig. 36 for the maximum flow speed (U_∞ = 520 in/sec). In Fig. 36, the average RMS wall displacement is plotted as a function of the frequency at various positions downstream of the 90° bend. The wall displacements at three axial stations are shown and represent the average of seven circumferential readings of the response taken over the wall relative to pipe bend. Deviations in the wall displacement by factors of two or more were noted. However, it appeared that no preferential modes were excited at any particular location over the pipe surface.

The experimental data for the response of the thin-walled pipe for fully-developed flow is also shown in Fig. 36. It is noted that the displacements for the various axial stations downstream of the 90° bend show general agreement with the response for fully-developed flow. This result indicated that the large flow velocity gradient known to exist across the pipe section in the secondary-swirling flow downstream of the 90° bend has no detectable affect on the response at any particular location. It would seem therefore that the high mode order response of a thin-walled pipe is unaffected by the flow conditions downstream of a pipe bend. It must be emphasized, however, that it is possible the response of the pipe at low frequencies and mode orders could, in fact, be drastically altered by the swirling flow generated by the pipe bend. However, investigations of the response of the first few pipe modes were beyond the scope of the present research program.

In order to check the ultramicrometer data a number of the above measurements were repeated using the accelerometer pickup. The accelerometer data are shown in Fig. 37 in which the power spectral density of the wall displacement is plotted against the Strouhal number. The accelerations were, of course, recorded as usual in 1/3-octave bands on the logarithmic chart paper and then converted into displacements using the center frequency of each 1/3-octave band.

Because it was felt that the response of the thin-walled pipe coupled to a 45° bend would be essentially no different from that of the tests on the 90° bend, it was decided to abandon the response tests using the 45° bend that were originally planned in the scope of work. The remaining experimental work was therefore confined to studying the response of the thin-walled pipe to the flow generated by a 4.75 in. sharp-edged orifice plate, installed upstream of the 6 in. diameter pipe section, to a wide range of flow speeds.

Also shown in Fig. 37 are the data obtained from measuring the response of the thin-walled pipe coupled to the orifice plate. Measurements were made at axial distances of two, four and eight pipe diameters downstream of the orifice plate. Although not shown in Fig. 37, the measured wall displacements were, within the limits of experimental error, comparable in magnitude at each measuring position.

At the lowest flow speed (U_∞ = 248 in/sec), the space average displacement response is virtually identical to that measured and predicted for fully-developed turbulence and also compares with the data measured downstream of the 90° pipe bend. However, for the higher flow speed (U_∞ = 520 in/sec), the flow downstream of the orifice was cavitating. The data indicated that on the average the power spectral density of the displacement response was at least 3 dB greater than that for fully

developed turbulence. The dotted curve drawn through the experimental points for cavitating flow shown in Fig. 37 would indicate that the response decreases at the rate of 15 dB/octave over the whole range of Strouhal numbers. Obviously further work covering a wider range of cavitating flow conditions is required to establish the validity of this result.

Finally, it might be pointed out that during one of the preliminary tests when the flow was suddenly stopped by shutting off the pumps, the resistance offered by the orifice plate caused a vacuum in the thin-walled pipe section which resulted in the collapse of the pipe wall. Because of this, it was recognized that extreme care must be exercised when shutting off the pumps. In other words, the flow must be gradually reduced by slowly decreasing the speed of the engines driving the pumps and not suddenly stopping the flow as in this particular case.

VII. CONCLUSIONS AND RECOMMENDATIONS FOR FURTHER WORK

The object of the work described in this report was to predict the vibrational response of thin-walled pipes to the wall pressure field arising from the passage of turbulent fluid flow. The approach used for calculating the response was essentially different to previous investigations of structural excitation by random pressure fields which were primarily concerned with the low order modal response. In the present work attention has been directed towards the analysis and measurement of the response of thin-walled pipes to a wide variety of turbulent flow conditions at high mode numbers and frequencies.

Two basic assumptions were made in the theoretical analysis for fully-developed turbulent flow that were subsequently verified experimentally. First, it was assumed that the turbulent wall pressure fluctuations were correlated over areas that were small compared with the surface area of the pipe. In this case the excitation of each high order mode could be regarded as being independent of the mode shape. Secondly, at high frequencies a region of high modal density existed such that the response over a finite frequency band embracing many modes could be represented by a smoothed spectrum function. This permitted the average response over a wide range of finite frequency bands to be investigated, and is in contrast to the succession of well-separated predominant resonant peaks that would be associated with the low order modal response of a structure.

On the basis of the above-mentioned assumptions, a response equation was derived for the displacement power spectral density of the pipe wall. The pipe wall response was expressed in terms of the damping factor, the effective mass per unit area of the pipe, the modal density, and certain of the statistical properties of the wall pressure field in fully-developed

turbulent pipe flow. Consequently, in order to predict the response it was necessary to measure these statistical properties and also the pipe damping factor. However, the modal density and virtual mass of the water-loaded pipe could be calculated from existing theories.

The experimental approach therefore consisted of determining the statistical properties of the turbulent wall pressure fluctuations so that a comparison could be made between the predicted response of the thin-walled pipe with that measured experimentally over a wide range of flow speeds and exciting frequencies. Measurements of the power spectral density of the wall pressure fluctuations showed very good agreement with the results from independent investigations. The data obtained for the wall pressure correlation lengths in narrow frequency bands verified the assumed form of the space correlation functions used in the theory for predicting the response of the thin-walled pipe.

It was concluded from the results of measuring the wall pressure fluctuations in fully-developed turbulent pipe flow that while the exciting frequencies varied with the flow speed, the correlation lengths were essentially independent of the flow speed.

Measurements of the damping factor emphasized the importance of performing in situ measurements, that is, with the thin-walled pipe connected to the water flow loop facility. The results indicated that the environment in which the damping factor is measured determines its magnitude. For example, when the damping of the water-filled pipe section alone was measured, the damping factor obtained was at least an order of magnitude greater than that determined with the pipe in situ. As a result of the data obtained from these foregoing measurements, a procedure was developed for calculating the response of a

thin-walled pipe to a wide range of exciting frequencies and flow speeds for fully-developed turbulence. The computational procedure adopted showed that the response could be predicted from a knowledge of certain of the flow and structural variables.

Measurements of the pipe wall displacement response to a wide range of flow conditions were carried out on a long uniform cylindrical pipe of given wall thickness and diameter. The experimental data obtained from measuring the pipe wall response to fully-developed turbulent flow over a wide range of Strouhal numbers showed very good agreement with the predicted response. At low Strouhal numbers it was found that the power spectral density of the response varied inversely with the fifth power of the Strouhal number, while at higher Strouhal numbers the results indicated a sixth power relationship. It was concluded from these data that the method used for calculating the response was capable of accurately predicting the response of a thin-walled pipe to fully-developed turbulent flow excitation over a wide range of Strouhal numbers.

Experimental data for the response of the thin-walled pipe to the wall pressure fields generated by pipe bends and orifice plates showed that for non-cavitating flow conditions the pipe wall response was of the same magnitude as that measured and predicted for fully-developed turbulence. This implied that the method used for calculating the high frequency response to fully-developed flow can also be employed to predict the response of a straight section of thin-walled pipe situated downstream of an orifice plate and pipe bend. On the other hand, for cavitating flow conditions preliminary results indicated that, on the average, the mean square value pipe wall response increases by about 3 dB. However, the response appeared to decrease at the rate of 15 dB/octave as was the case for fully-developed flow.

The results obtained from the present investigation suggested several possibilities for further work. Although variations in the dimensions of the thin-walled pipe were not investigated experimentally, the theory developed for calculating the response indicated that the power spectral density of the pipe wall displacement varies inversely with the square of the wall thickness while the pipe diameter can be expressed in terms of the Strouhal number. Consequently, an experimental study to investigate the effect of varying the pipe dimensions on the response would be a useful extension to the present work.

Other experimental investigations for future work might include the effect of different flows on the pipe wall response. For example, one experiment indicated that the presence of air bubbles in the water increased the magnitude of the high frequency response. This could be investigated further by generating air-water mixtures under controlled conditions, and measuring both the wall pressure field and pipe wall response to two-phase flow excitation. A more general study, however, would be a more detailed examination of the effect of fluid cavitation on the response. Preliminary data for cavitating water flow downstream of the orifice plate indicated that the pipe wall response can be drastically altered by cavitating flows. The present water flow facility is particularly suitable for a continuing investigation since the internal pressure can be varied independently of the flow speed. In principle, this makes it possible to produce cavitation in given pipe sections by reducing the local static pressure below the water vapor pressure.

In concluding, it is felt that the work described in this report represents an important contribution to the subject of structural excitation by random pressure fields. The present investigation considered the particular case of the response

of thin-walled pipes to turbulent flows. The writer sees no reason, however, why the approach used in this research study cannot be applied to other problems associated with the structural response to the wall pressure fields generated by various unsteady flow conditions. This would require experimental investigations of the statistical properties of the wall pressure fluctuations in order to obtain the necessary empirical data to calculate the vibrational response of the structure.

APPENDIX A

METHODS FOR CALCULATING THE NATURAL FREQUENCIES AND VIRTUAL MASS OF A FLUID-LOADED CYLINDRICAL SHELL

The equations of motion and natural frequencies for small radial vibrations of a finite cylindrical shell with and without the presence of an internal fluid medium are well known[14,22]. A method is outlined in this section that could be used to calculate the natural frequencies and virtual mass of a water-filled cylindrical shell (Section V).

It has been shown by Berry and Reissner[13] that for a simply supported cylindrical shell containing internal fluid, the approximate frequency equation for small radial motions of the shell wall is

$$\Omega_{mn}^2 \simeq \frac{c_s^2}{a^2(1+\mu B)} \left[\frac{(1-\sigma^2)\beta_m^4}{(n^2+\beta_m^2)^2} + \frac{h^2}{12a^2}(n^2+\beta_m^2)^2 + \frac{(1-\sigma^2)p_L}{2Eh} a(2n^2+\beta_m^2) \right] \tag{A.1}$$

where $\beta_m = m\pi a/L$, Ω_{mn} is the natural frequency of the fluid-loaded shell for the m,n mode of vibration, and p_L is the internal fluid pressure. The remaining symbols in Eq. (A.1) are defined in Appendix B. The terms inside the closed bracket on the right-hand side of Eq. (A.1) represent the contributions to the frequency caused by the stretching of the shell, wall bending, and internal pressure respectively.

It might be pointed out that the experiments of Fung et al[23] and Mixson and Herr[24] indicated that the internal pressure had a significant influence on the natural frequencies for both empty and water-filled cylindrical shells. The effect of the internal pressure has been to increase the natural frequency, and therefore must be accounted for in the frequency calculations.

The frequency equation (A.1) is strictly valid only for a simply supported cylinder. This means that the cylinder ends must remain circular during radial vibrations. Such boundary conditions will not be satisfied for the thin-walled cylinder used in the present investigation as the ends are constrained by the pipe sleeve and flanges. The correction factor used by Arnold and Warburton[25] in accounting for clamped ends is to replace the longitudinal wavelength factor β_m in Eq. (A.1) by the modified expression

$$\beta_m' = (m + c)\,\pi a/L \qquad (A.2)$$

where c is the correction factor, which may vary between 0.2 and 0.6. This would suggest that at higher longitudinal mode numbers, m, the effect of the cylinder end conditions will be less important.

Referring to Eq. (A.1), the relation between the natural frequencies of the empty and fluid-loaded shell will be

$$\Omega_{mn} = \frac{\omega_{mn}}{(1+\mu B)^{1/2}} \qquad (A.3)$$

where ω_{mn} is the natural frequency of the empty shell and μB is the virtual mass factor given by Eqs. (5.9) and (5.12), Section V, that is

$$B = \frac{1}{\lambda_L}\,\frac{I_n(\lambda_L)}{I_n'(\lambda_L)} \qquad (A.4)$$

$$\mu B = \frac{a\rho_L}{\rho_s h}\,\frac{1}{\lambda_L}\,\frac{I_n(\lambda_L)}{I_n'(\lambda_L)} \qquad (A.5)$$

For a shell of finite length, L, Warburton[14] showed that

$$\lambda_L^2 = \left(\frac{\omega_{mn} a}{c_L}\right)^2 - \left(\frac{m\pi a}{L}\right)^2 \qquad (A.6)$$

Equation (A.6) reduces to Eq. (5.10), page 40, for an infinitely long shell. The natural frequencies of the empty shell can be evaluated numerically as a function of the longitudinal and circumferential mode numbers, m and n, from Eq. (A.1) for $\mu B = 0$. Having computed the frequencies, ω_{mn}, the argument λ_L can also be evaluated from Eq. (A.6) and the values of the Bessel function B in Eq. (A.4) determined for various circumferential mode orders, n. The procedure is quite complicated and would require numerical solutions using a digital computer. However, from a knowledge of the empty shell natural frequencies, ω_{mn}, and fluid-loading factor $(1+\mu B)$, the natural frequencies, Ω_{mn}, for the water-filled shell could be evaluated.

It has been shown[14], however, that for the radial vibrations of a long cylindrical shell at low frequencies, the value of λ_L is small, and

$$B \simeq 1/n \tag{A.7}$$

Physically, 1/n represents the flexural wavelength per unit circumferential distance, that is,

$$1/n = \lambda_f/2\pi a \tag{A.8}$$

The speed of flexural waves in a flat plate[11] of thickness h is given by

$$c_f^2 = \frac{\pi h c_s}{\sqrt{3}} f_b \tag{A.9}$$

where f_b is the plate bending frequency.

The flexural wavelength, λ_f, from Eq. (A.9) will be

$$\lambda_f = \frac{c_f}{f_b} = \frac{\pi h c_s}{\sqrt{3} f}^{1/2} \tag{A.10}$$

Assuming the shell circumference to be a flat plate loaded on one side by fluid, then from Eqs. (A.7) and (A.8)

$$B \simeq \frac{1}{a}\left(\frac{hc_s}{4\pi\sqrt{3}f}\right)^{1/2} \tag{A.11}$$

Consequently, the virtual mass factor, μB, can be expressed as

$$\mu B \simeq \frac{\rho_L}{\rho_s}\left(\frac{c_s}{4\pi\sqrt{3}fh}\right)^{1/2} \tag{A.12}$$

Equation (A.12) is equivalent to Eq. (5.15) used in Section V for calculating the variation of the water-loading correction factor $(1+\mu B)$ with frequency for the given thin-walled cylinder.

APPENDIX B

LIST OF SYMBOLS

The following symbols were used in the text except where otherwise stated.

a	pipe radius
A	surface area of pipe
A_f	amplitude of narrow band longitudinal correlation function (see Eq. 2.18)
B	correction factor for virtual mass (see Eq. 5.9)
c_f	speed of flexural waves in shell wall
c_L	sound velocity in fluid medium
c_s	longitudinal wave velocity in shell material, $c_s = \sqrt{\frac{E}{\rho_s(1-\sigma^2)}}$
c_s'	longitudinal wave velocity in shell material corrected for fluid-loading (see Eq. 5.17)
d	pipe diameter
E	Young's modulus
f	frequency
h	pipe wall thickness
I_n	Bessel function of the first kind of order n
$j^2(\omega)$	joint acceptance in narrow band $\Delta\omega$ centered on frequency ω
$j_x^2(\omega)$	joint acceptance in longitudinal x-direction
$j_y^2(\omega)$	joint acceptance in circumferential y-direction
L	length of pipe section

L_x	longitudinal pressure correlation length ($L_x = U_c \tau_o$)
L_y	circumferential pressure correlation length
m	longitudinal mode number in x-direction
m_s	mass per unit area of pipe ($m_s = \rho_s h$)
M_e	effective mass of pipe ($M_e = A\rho_e h$)
M_{mn}	generalized mass in m,n mode
n	circumferential mode number in y-direction
N_R	Reynolds number ($N_R = U_\infty d/\nu$)
N_S	Strouhal number ($N_S = fd/U_\infty$)
$\Delta N/\Delta f$	modal density (see Eq. 5.18)
p	longitudinal mode wave number ($p = m\pi/L$)
$p(\bar{x},t)$	fluctuating fluid pressure at position $\bar{x}$ and time t
$\sqrt{\langle p^2 \rangle}$	RMS value of wall pressure fluctuations
p_L	internal fluid static pressure
q	turbulence wave number ($q = \omega/U_c$)
Q	damping factor
R( )	correlation coefficient
S_p	normalized power spectral density of wall pressure fluctuations (see Eq. 5.2)
t	time
T	integration time
U_c	convection speed of turbulent eddies
U_∞	mean flow velocity at centerline of pipe
$W(\bar{x},t)$	wall displacement at position $\bar{x}$ and time t
$\langle W^2 \rangle$	overall mean square wall displacement

$\langle W^2(f) \rangle$	mean square displacement in narrow band Δf centered on frequency f
x,y	surface co-ordinates
Δx	transducer separation in longitudinal x-direction ($\Delta x = \lvert x_1 - x_2 \rvert$)
Δy	transducer separation in circumferential y-direction ($\Delta y = \lvert y_1 - y_2 \rvert$)
$Z_{mn}(\omega)$	mechanical impedance of the m,n mode of vibration (see Eq. 2.4)
α	inverse of longitudinal pressure correlation length ($\alpha = 1/L_x$)
β	inverse of circumferential pressure correlation length ($\beta = 1/L_y$)
β_m	dimensionless longitudinal mode wave number ($\beta_m = m\pi a/L$)
λ_f	wavelength of flexural waves
λ_L	dimensionless frequency ($\lambda_L = \omega a/c_L$)
λ_x	integral scale length of wall pressure fluctuations in longitudinal x-direction
λ_y	integral scale length of wall pressure fluctuations in circumferential y-direction
μ	dimensionless mass factor ($\mu = a\rho_L/\rho_s h$)
ν	kinematic viscosity of fluid
ρ_e	effective mass density of pipe
ρ_L	mass density of fluid
ρ_s	mass density of shell material
σ	Poisson's ratio
τ	time delay
τ_o	eddy lifetime

$\phi_d(f)$ power spectral density of pipe wall displacement (see Eq. 5.19)

$$\phi_d(f) = \frac{\langle W^2(f) \rangle}{\Delta f}$$

$\phi_p(f)$ power spectral density of wall pressure fluctuations

$$\phi_p(f) = \frac{\langle p^2(f) \rangle}{\Delta f}$$

ω angular frequency ($\omega = 2\pi f$)

ω_{mn} natural frequency of empty shell in m,n mode of vibration

Ω_{mn} natural frequency of fluid-filled shell in m,n mode of vibration (see Eq. A.1)

LIST OF REFERENCES

1. Clinch, J.M., Study of Vibrations Induced in Thin-Walled Pipes by Fluid Flow. IIT Research Institute, Report prepared for Nat. Aero. & Space Adm., Marshall Space Flight Center under Contract NAS8-11248 (Sept. 24, 1965).

2. Wilby, J.F. and Blackman, D.R., Response of Panels to Random Pressure Fields. University of Southampton, A.A.S.U. Report No. 243 Part II (1963).

3. Maestrello, L., Measurement and Analysis of the Response Field of Turbulent Boundary Layer Excited Panels. J. Sound Vib. 2 (3), 270 (1965).

4. Powell, A., On the Response of Structures to Random Pressures, Chapter 8, Random Vibrations, S. H. Crandall, Ed., Technology Press, Cambridge, Mass. (1958).

5. Crandall, S.H., Statistical Properties of Response to Random Vibration, Chapter 4, Random Vibrations, S. H. Crandall, Ed., Technology Press, Cambridge, Mass., p. 83 (1958).

6. Bull, M.K. and Willis, J. L., Some Results of Experimental Investigations of the Surface Pressure Field Due to a Turbulent Boundary Layer. University of Southampton, A.A.S.U. Report No. 199 (1961).

7. Corcos, G.M., Pressure Fluctuations in Shear Flows. University of California Inst. of Eng. Res. Report, Series 183, No. 2 (1962).

8. Harrison, M., Pressure Fluctuations on the Wall Adjacent to a Turbulent Boundary Layer. David Taylor Model Basin Report No. 1260 (1958).

9. Bull, M.K., Properties of the Fluctuating Wall-Pressure Field of a Turbulent Boundary Layer. University of Southampton, A.A.S.U. Report No. 234 (1963).

10. Fisher, M.J. and Davies, P.O.A.L., Correlation Measurements in a Non-Frozen Pattern of Turbulence. J. Fluid Mech. 18, 97 (1964).

11. Dyer, I., Sound Radiation into a Closed Space from Boundary Layer Turbulence. Bolt, Beranek and Newman Report No. 602, Cambridge, Mass. (1958).

12. Heckl, M., Vibrations of Point-Driven Cylindrical Shells. J. Acoust. Soc. Am. 34, 1553 (1962).

13. Berry, J.G. and Reissner, E., The Effect of an Internal Compressible Fluid Column on the Breathing Vibrations of a Thin Pressurized Cylindrical Shell. J. Aeronaut. Sci. 25, 288 (1958).

14. Warburton, G.B., Vibration of a Cylindrical Shell in an Acoustic Medium. J. Mech. Eng. Sci. 3, 69 (1961).

15. Clinch, J.M., Miniature Transducer Assembly for Measuring the Properties of the Wall-Pressure Field in Turbulent Flows. J. Acoust. Soc. Am. 40, 254 (1966).

16. Bakewell, H.P., Carey, G.F., Libuka, J.J., Schloemer, H.H. and Von Winkle, W.A., Wall Pressure Correlations in Turbulent Pipe Flow. U.S. Navy Underwater Sound Laboratory Report No. 559 (1962).

17. Corcos, G.M., On the Resolution of Pressure in Turbulence. J. Acoust. Soc. Am. 35, 192 (1963).

18. Willmarth, W.W. and Roos, F.W., Resolution and Structure of the Wall Pressure Field Beneath a Turbulent Boundary Layer. J. Fluid Mech. 22, 81 (1965).

19. Dyer, I., Estimation of Sound-Induced Missile Vibration, Chapter 9, Random Vibrations, S.H. Crandall, Ed., Technology Press, Cambridge, Mass., p. 264 (1958).

20. Junger, M.C., The Outgoing Wave in Cylindrical Coordinates. J. Acoust. Soc. Am. 25, 40 (1953).

21. Kinsler, L.E. and Frey, A.R., Fundamentals of Acoustics, John Wiley and Sons, New York, 2nd Ed., p. 18 (1950).

22. Timoshenko, S., Theory of Plates and Shells, McGraw-Hill Book Company, New York, Chapter 15 (1959).

23. Fung, Y.C., Sechler, E.E. and Kaplan, A., On the Vibration of Thin Cylindrical Shells under Internal Pressure. J. Aeronaut. Sci. 24, 650 (1957).

24. Mixson, J.S. and Herr, R.W., An Investigation of the Vibration Characteristics of Pressurized Thin-Walled Circular Cylinders Partly Filled with Liquid. Nat. Aeronaut. and Space Adm. Tech. Report R-145 (1962).

25. Arnold, R.N. and Warburton, G.B., The Flexural Vibrations of Thin Cylinders. J. and Proc. Inst. Mech. Eng. (London) 167, 62 (1953).

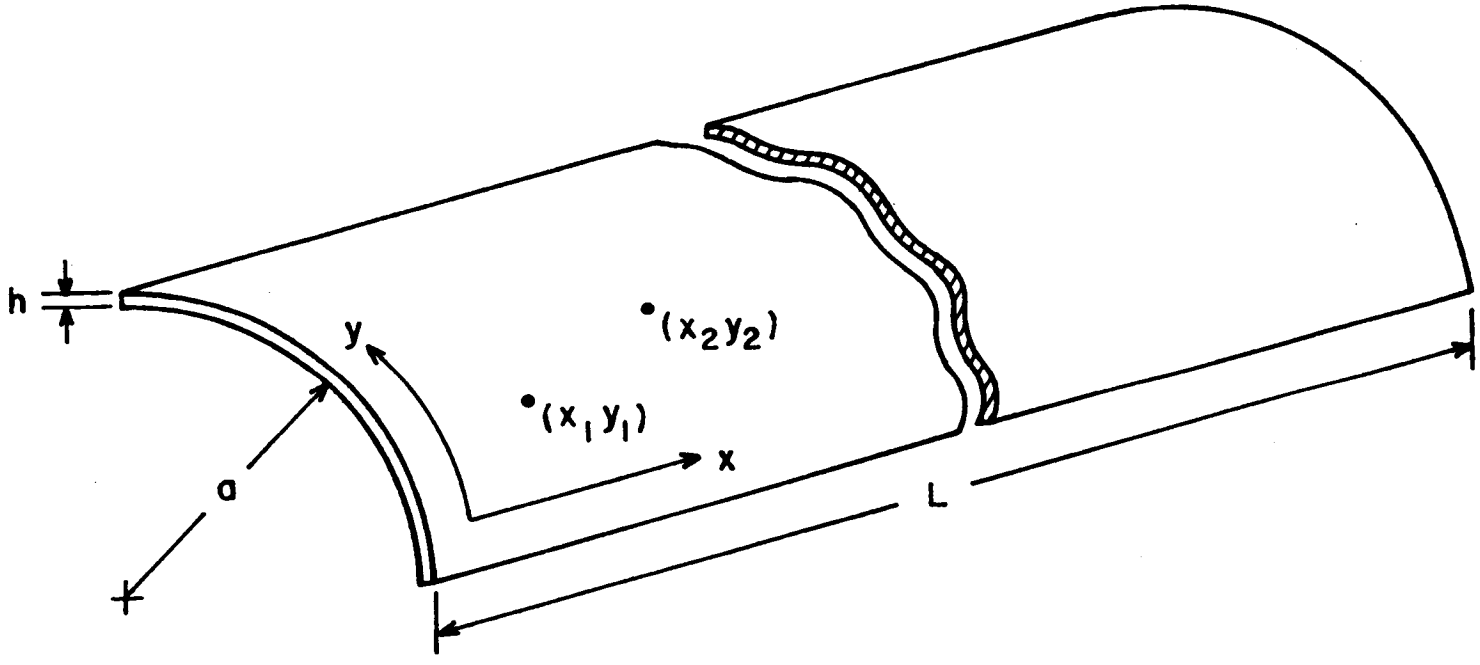

FIGURE 1. DIMENSIONS AND COORDINATES OF THIN-WALLED CYLINDRICAL SHELL.

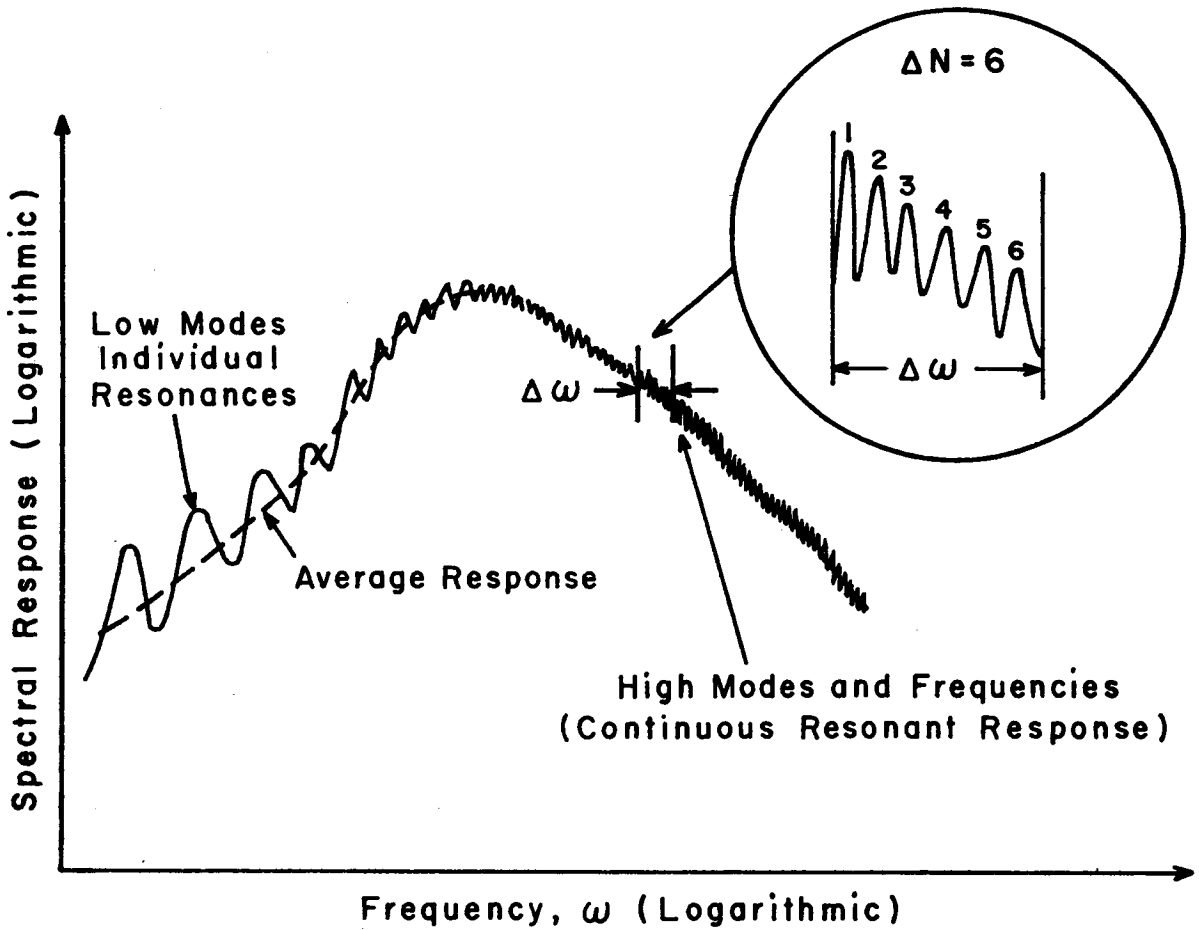

FIGURE 2. ILLUSTRATION OF MODAL DENSITY IN NARROW BAND $\Delta\omega$ FOR CONTINUOUS RESONANT RESPONSE OF A STRUCTURE EXCITED INTO RANDOM VIBRATION.

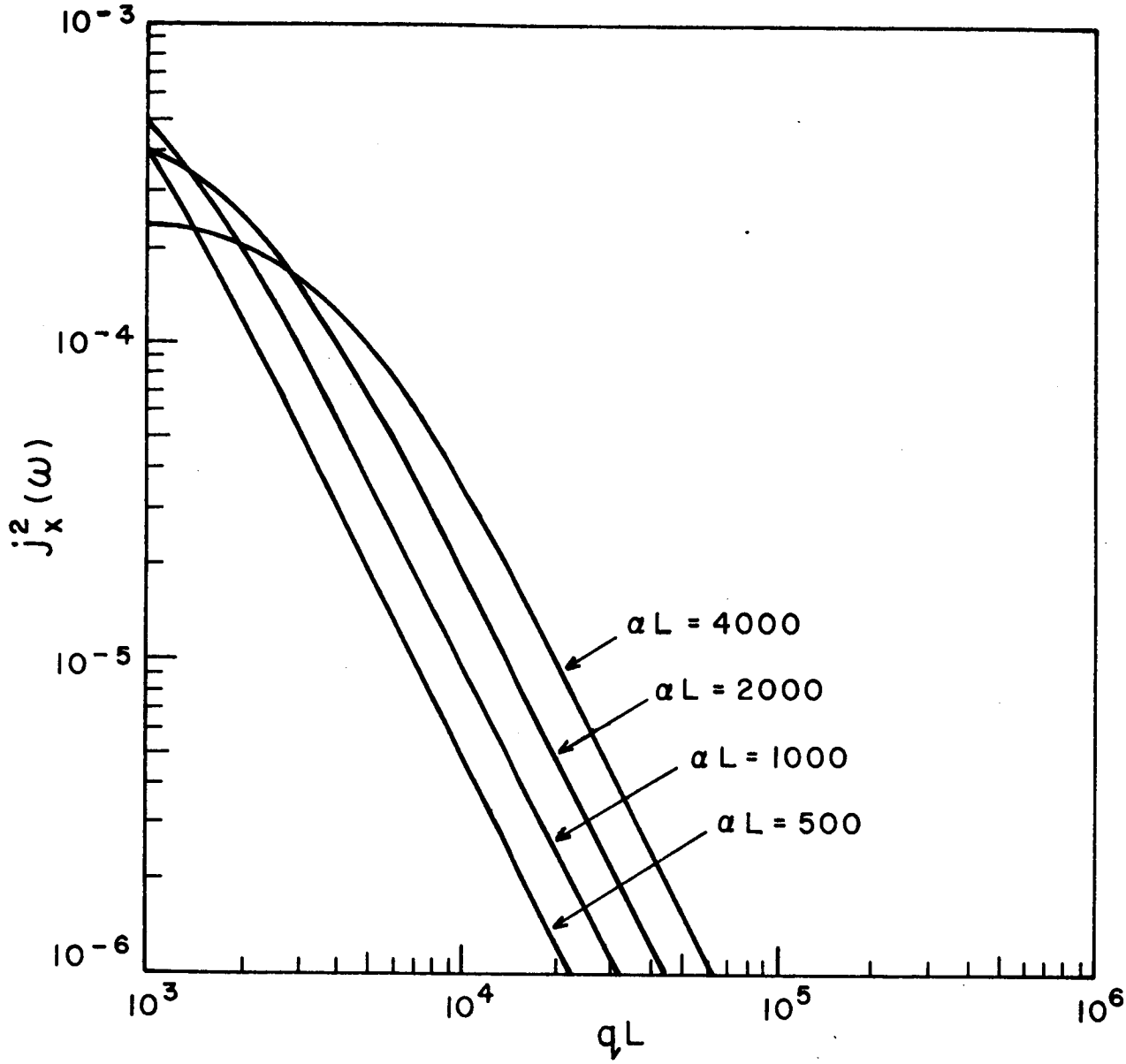

FIGURE 3. LONGITUDINAL JOINT ACCEPTANCE FUNCTION, $j_x^2(\omega)$.

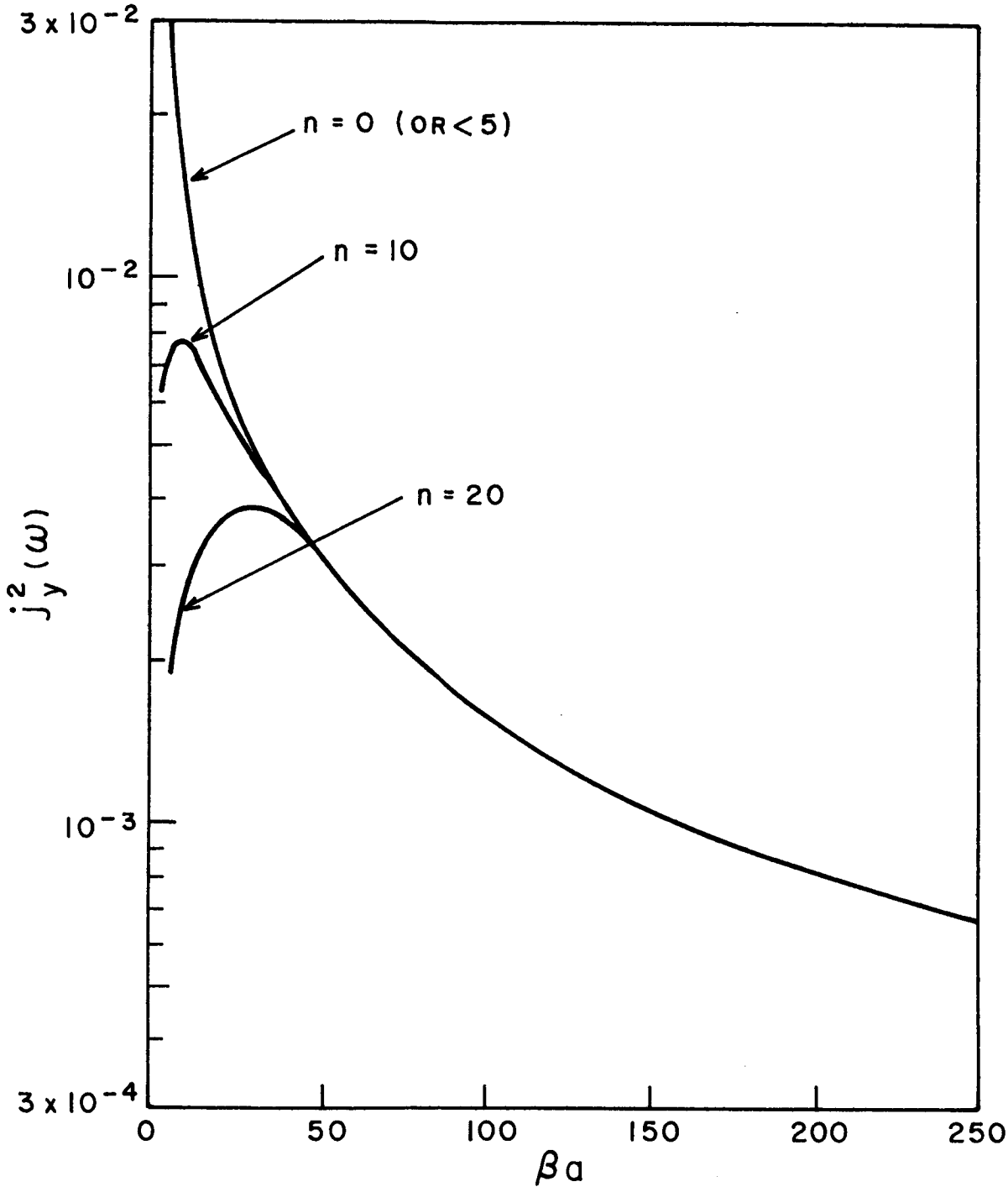

FIGURE 4. CIRCUMFERENTIAL JOINT ACCEPTANCE FUNCTION, $j_y^2(\omega)$.

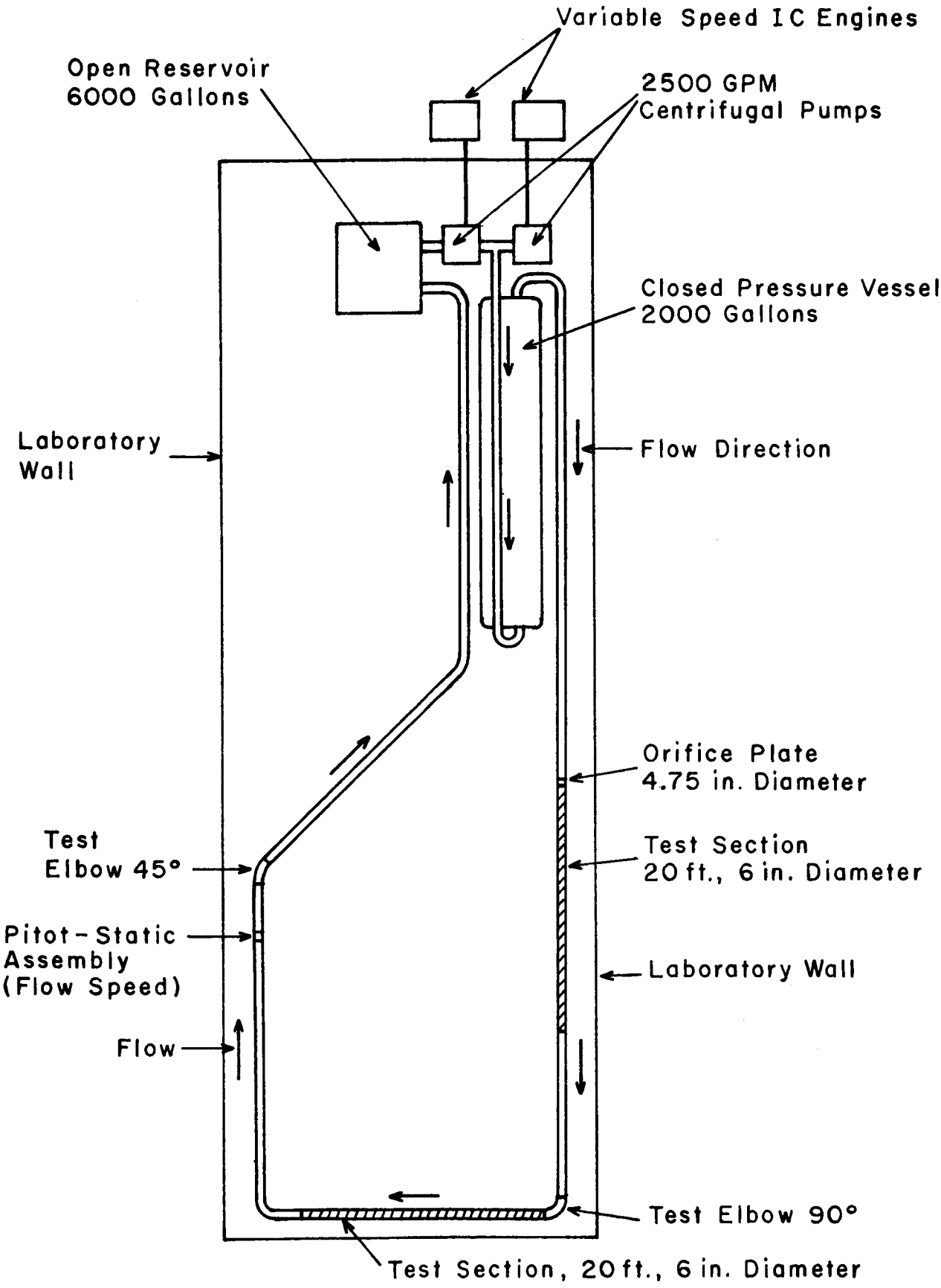

FIGURE 5. PLAN SHOWING LAYOUT OF MODIFIED WATER FLOW LOOP FACILITY.

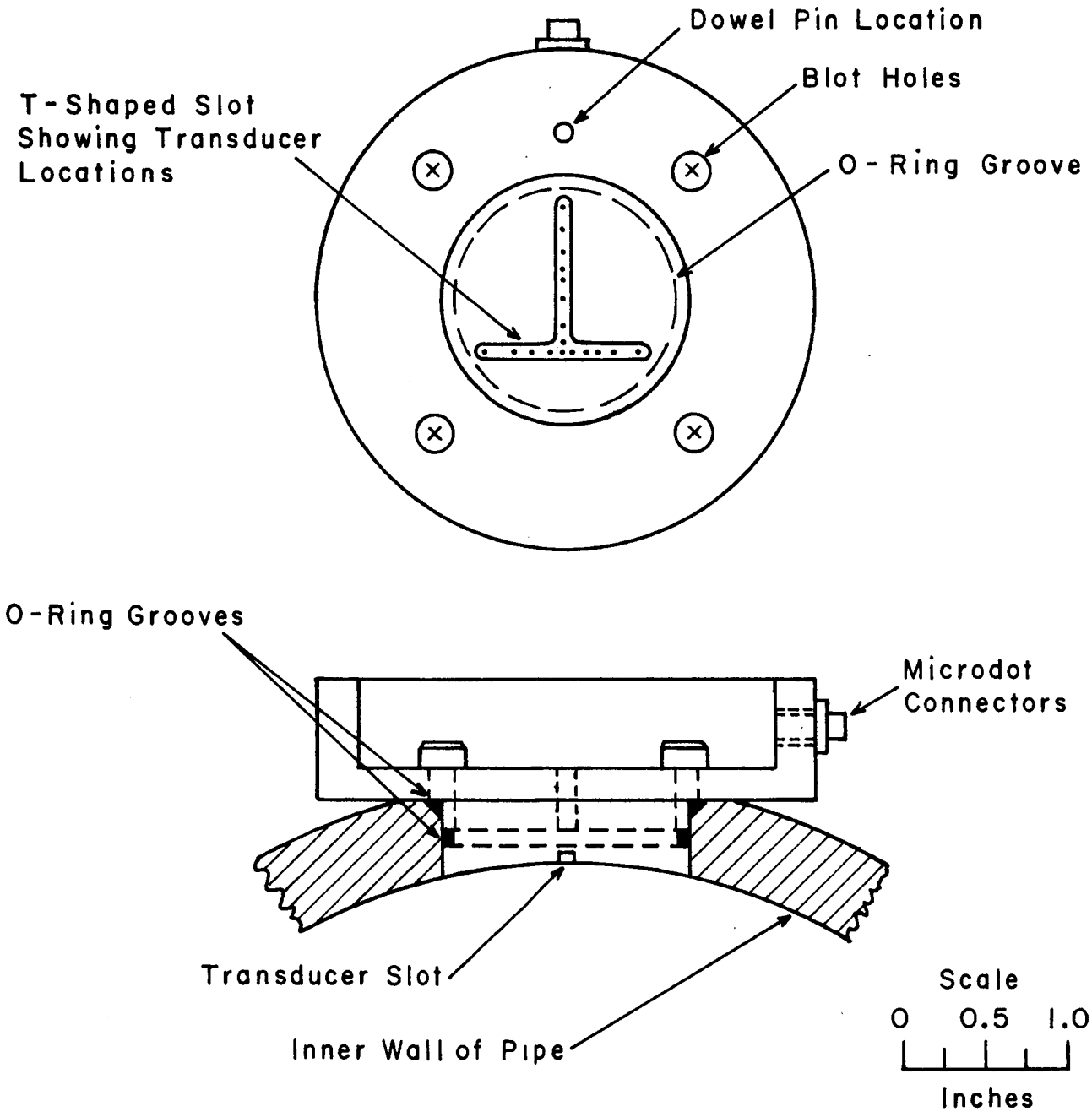

FIGURE 6. PRESSURE TRANSDUCER ASSEMBLY.

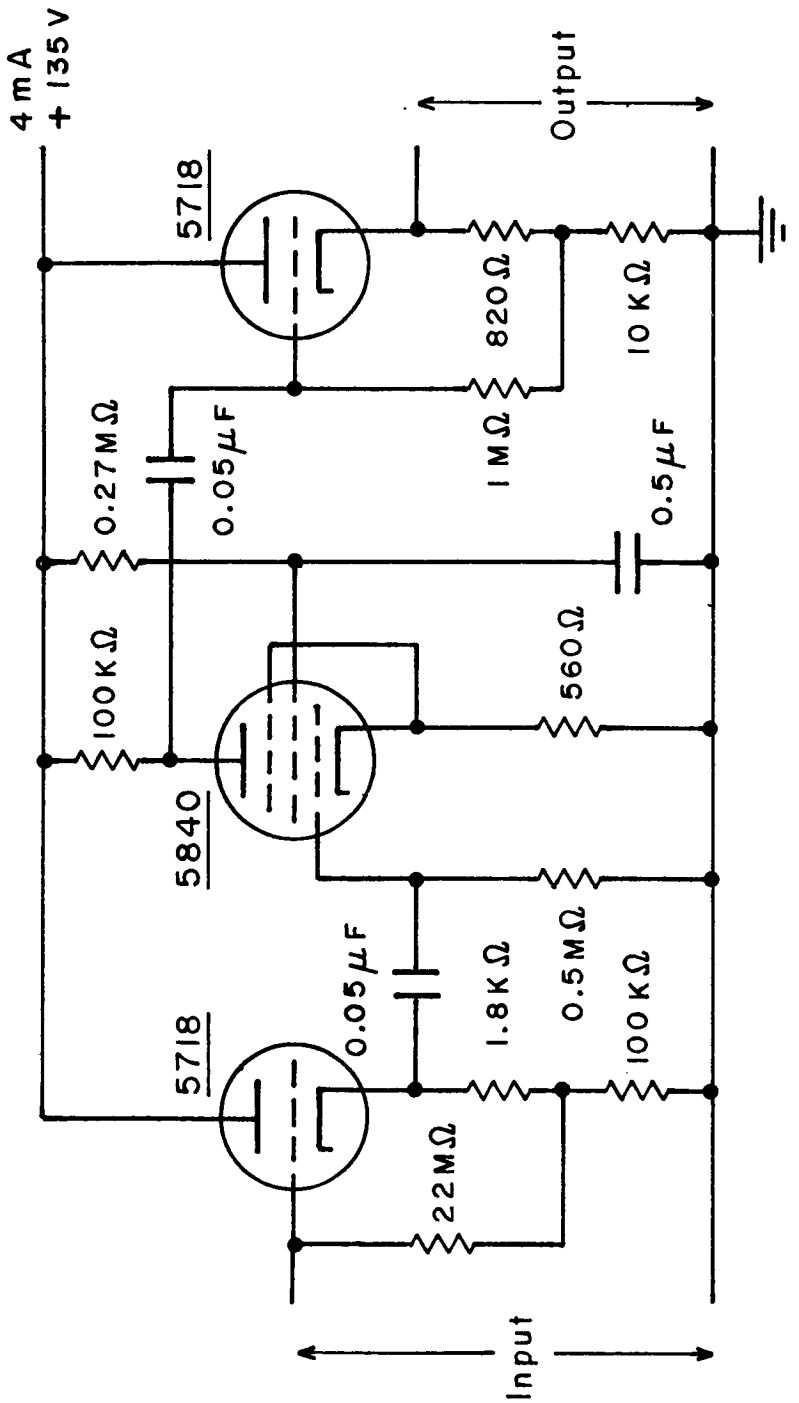

FIGURE 7. CATHODE FOLLOWER-PREAMPLIFIER CIRCUIT.

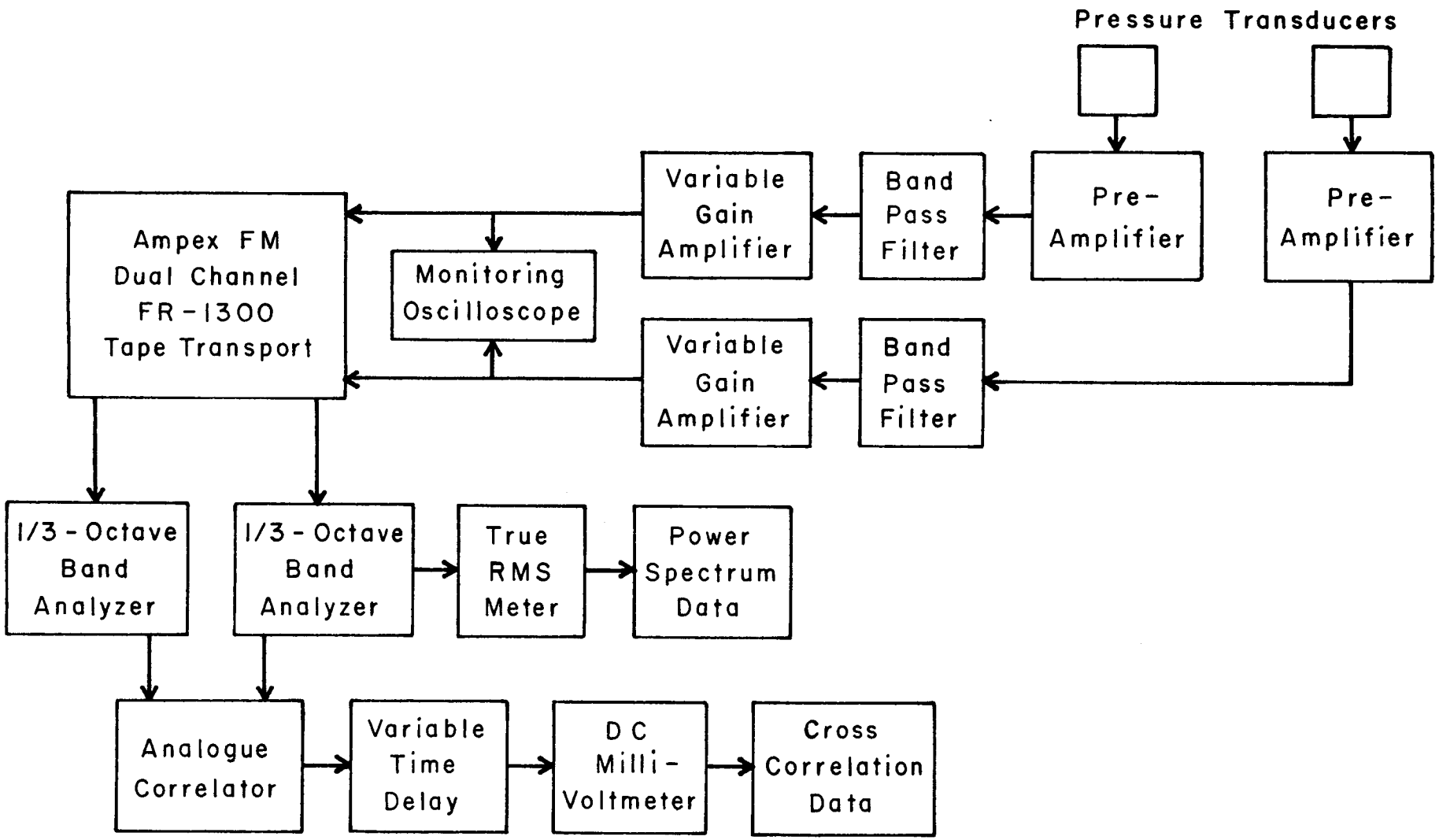

FIGURE 8. BLOCK DIAGRAM OF INSTRUMENTATION USED FOR RECORDING AND ANALYZING TURBULENT WALL PRESSURE FIELD.

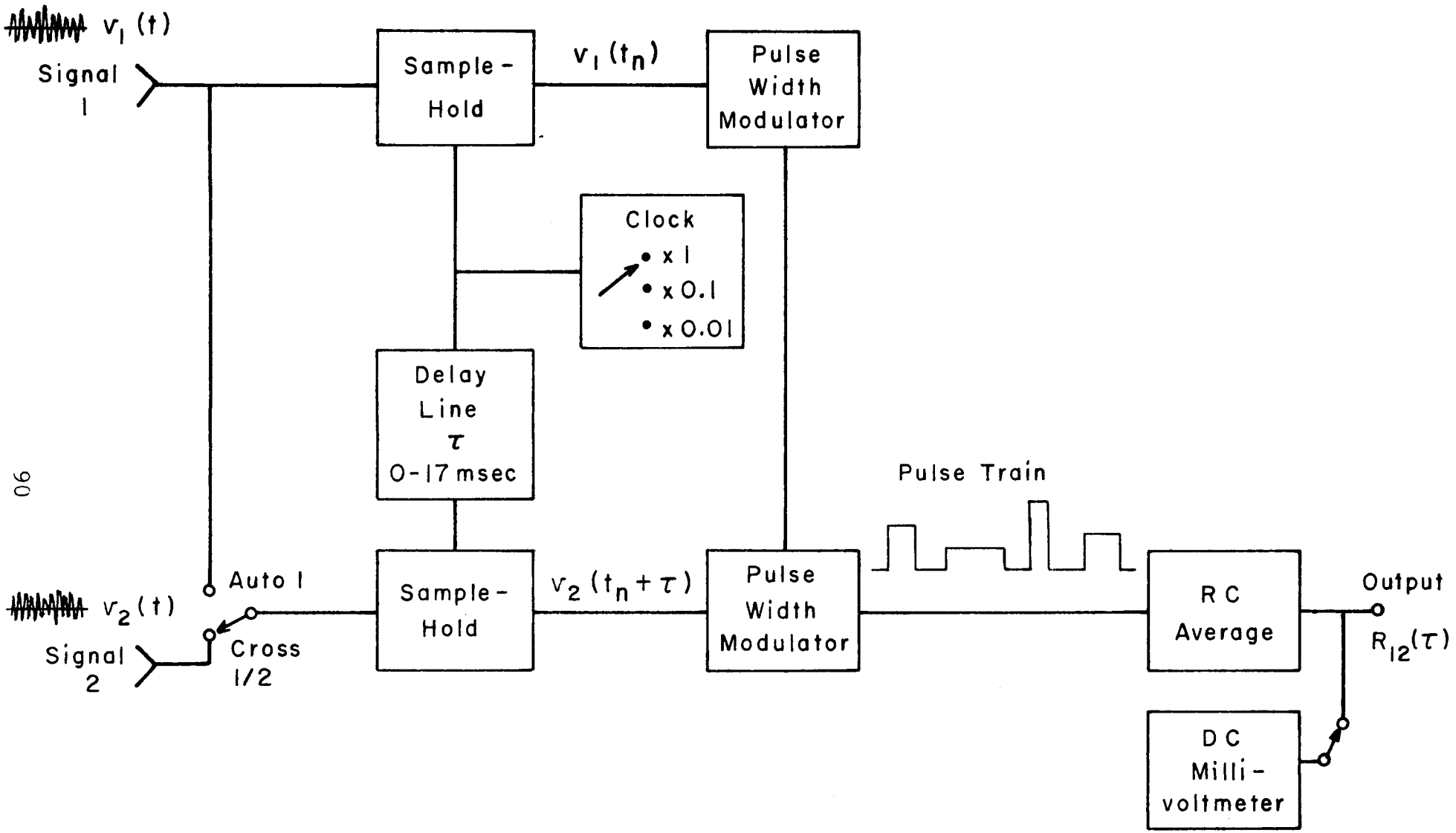

FIGURE 9. BLOCK DIAGRAM OF MODEL 9410 HONEYWELL TIME DELAY ELECTRONIC ANALOGUE CORRELATOR.

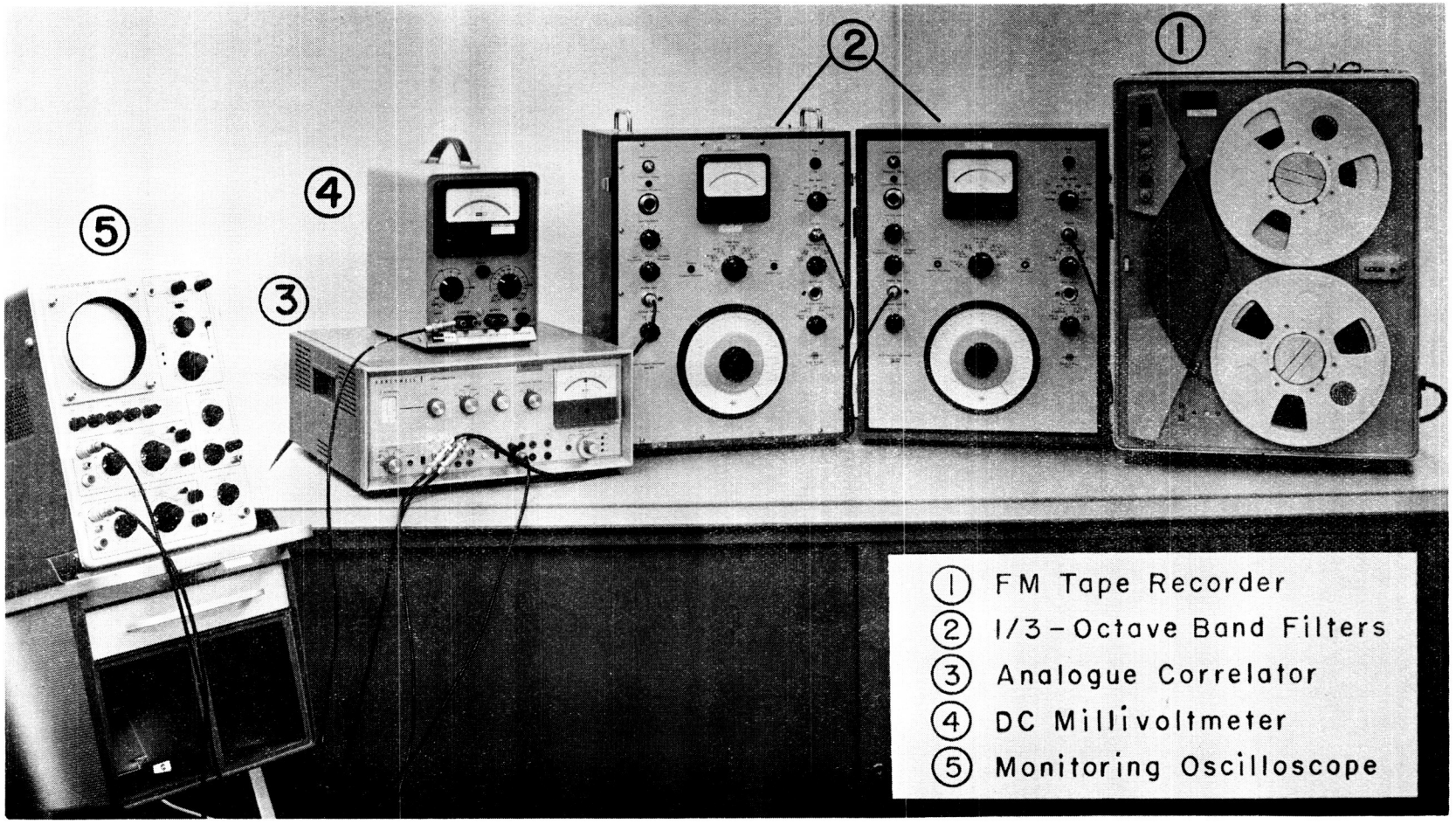

FIGURE 10. EQUIPMENT USED FOR ANALYZING RECORDINGS OF WALL PRESSURE FLUCTUATIONS.

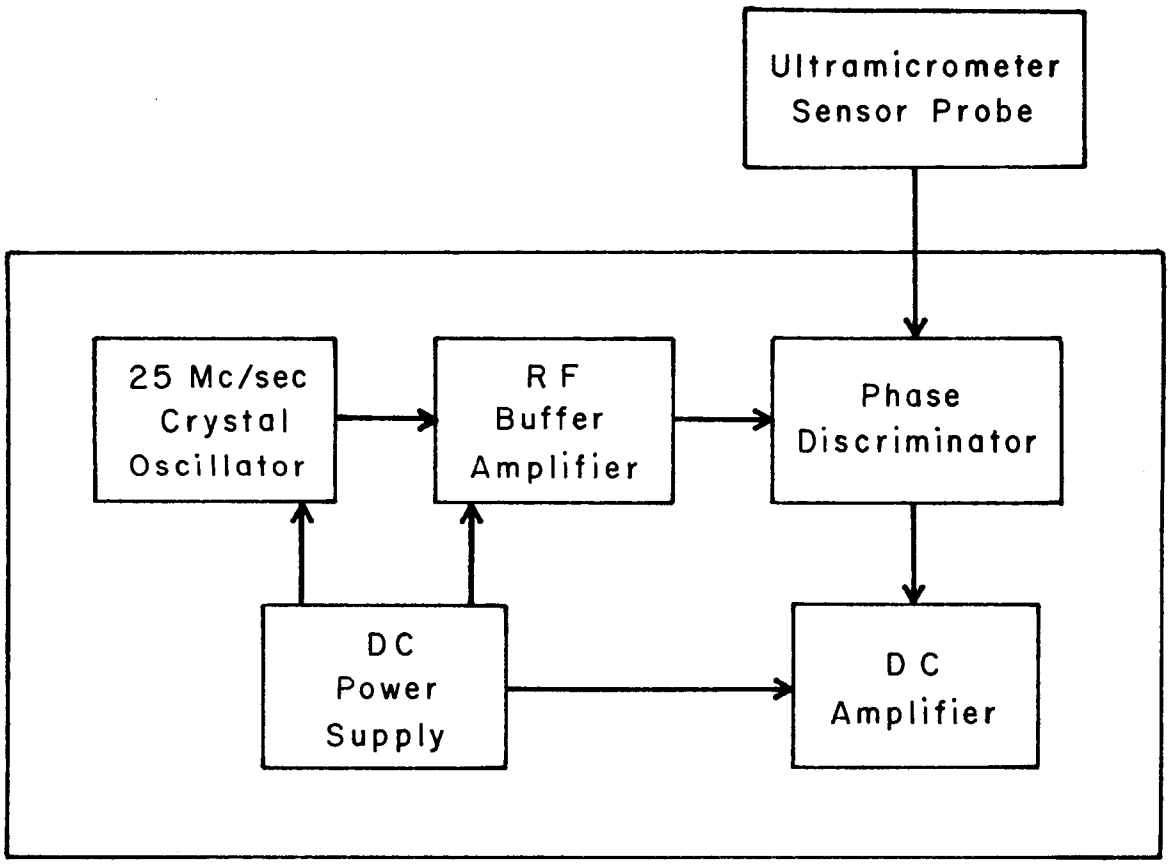

FIGURE 11. BLOCK DIAGRAM OF OMEGA MODEL 155 CONVERTER FOR ULTRAMICROMETER MEASUREMENTS.

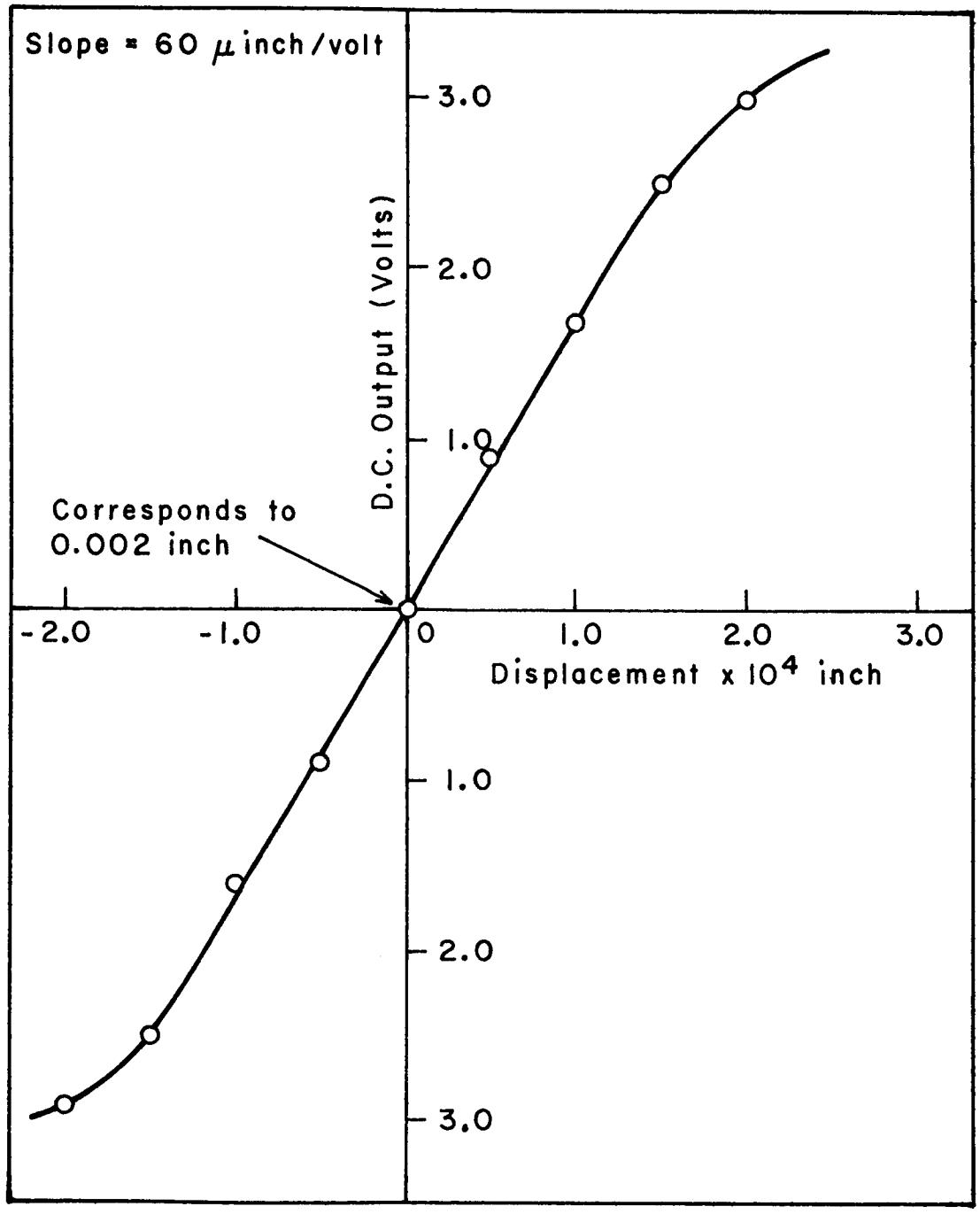

FIGURE 12. CALIBRATION CURVE OF ULTRAMICROMETER.

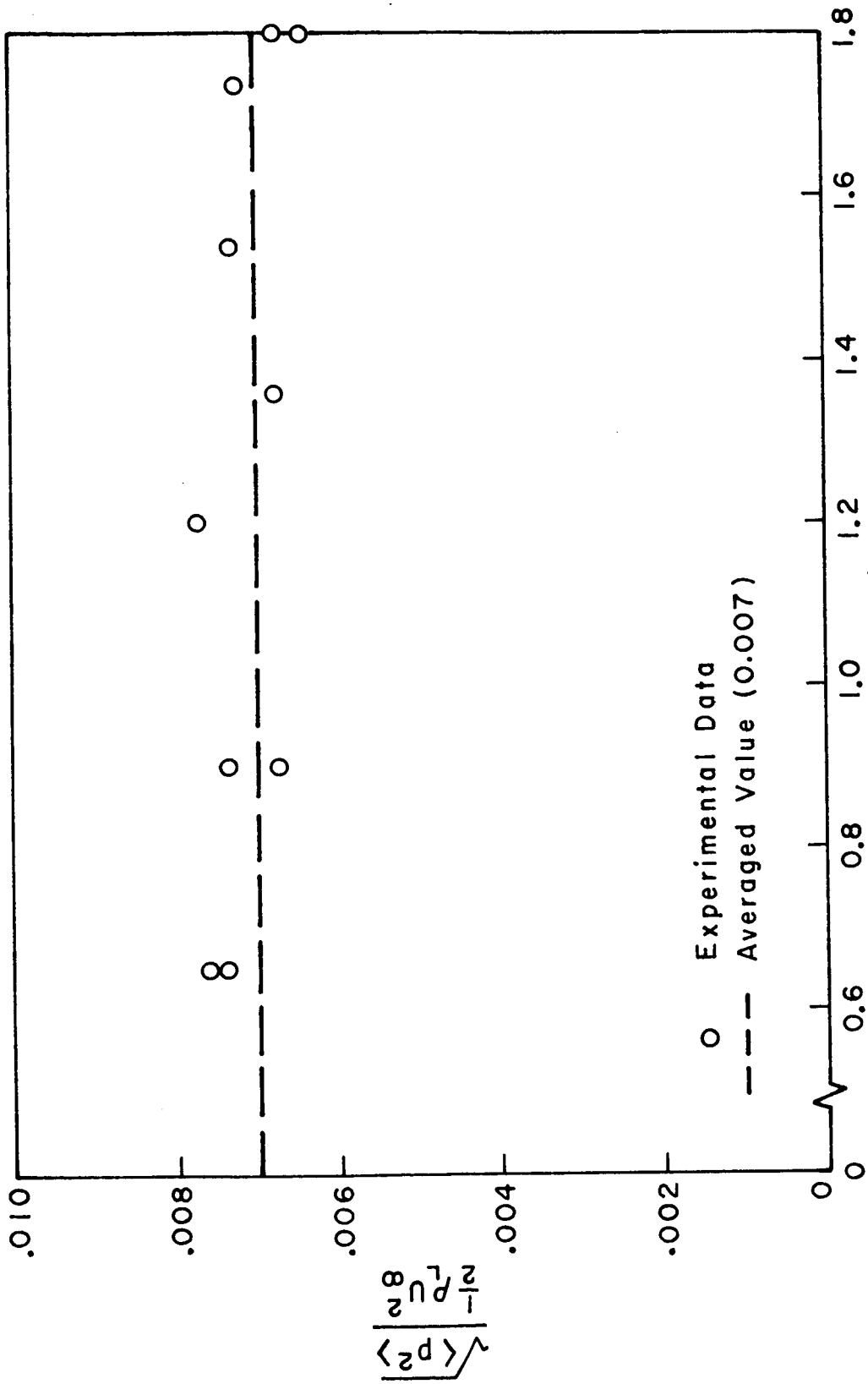

FIGURE 13. NORMALIZED OVERALL ROOT-MEAN-SQUARE PRESSURE AT THE WALL AS FUNCTION OF REYNOLDS NUMBER.

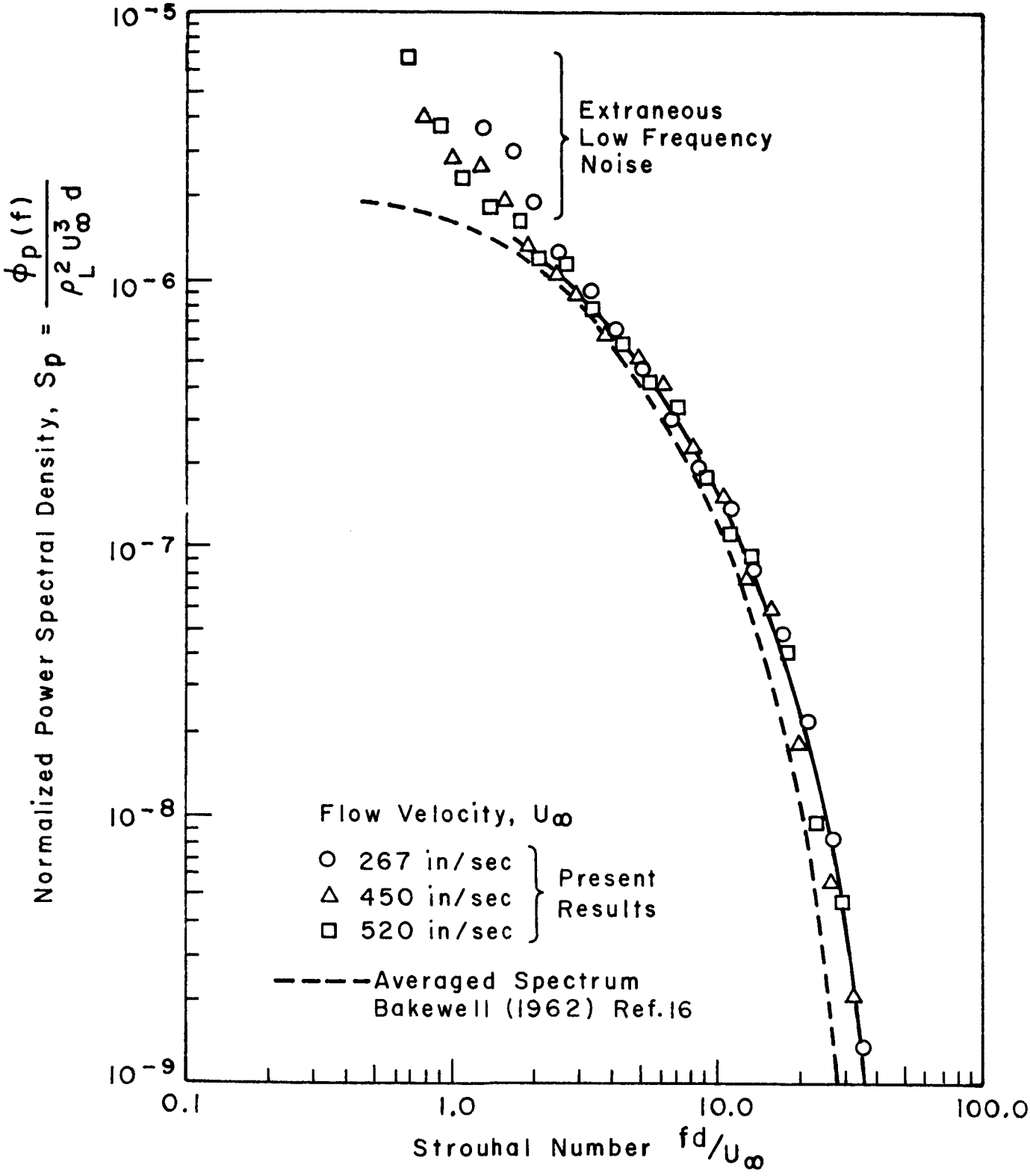

FIGURE 14. FREQUENCY SPECTRUM OF TURBULENT WALL PRESSURE FIELD.

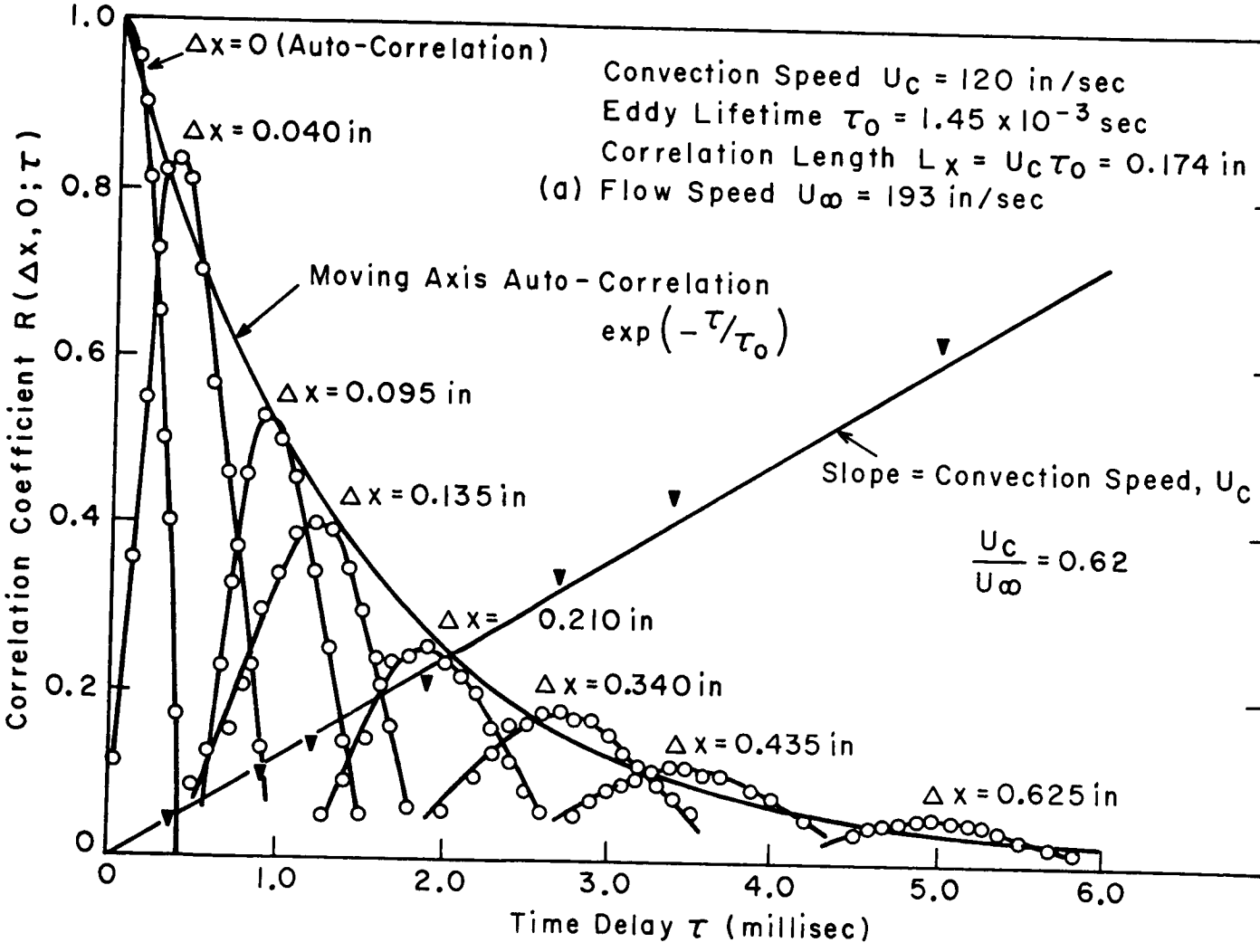

FIGURE 15. BROAD-BAND SPACE-TIME C

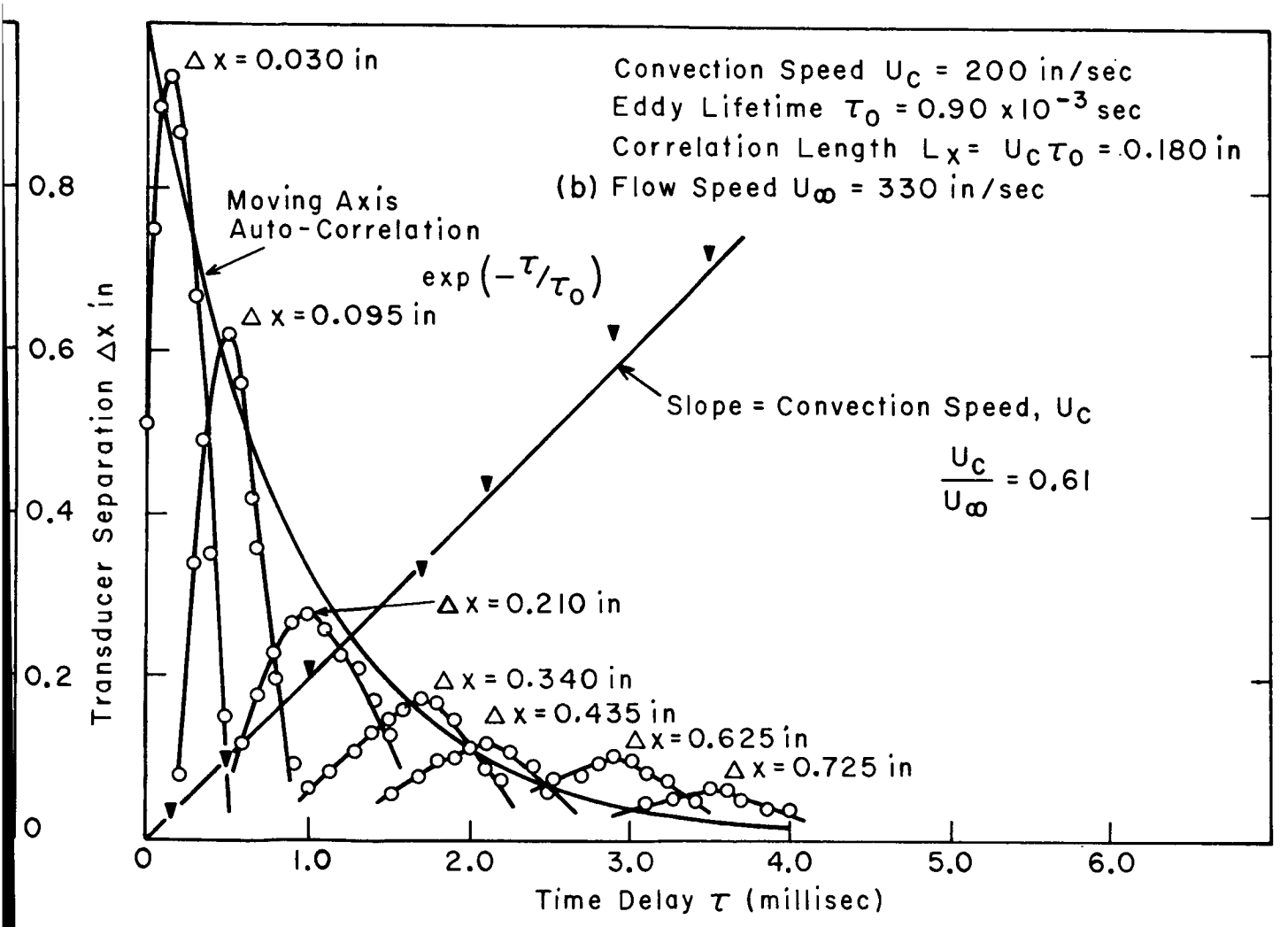

ORRELATIONS IN LONGITUDINAL FLOW DIRECTION.

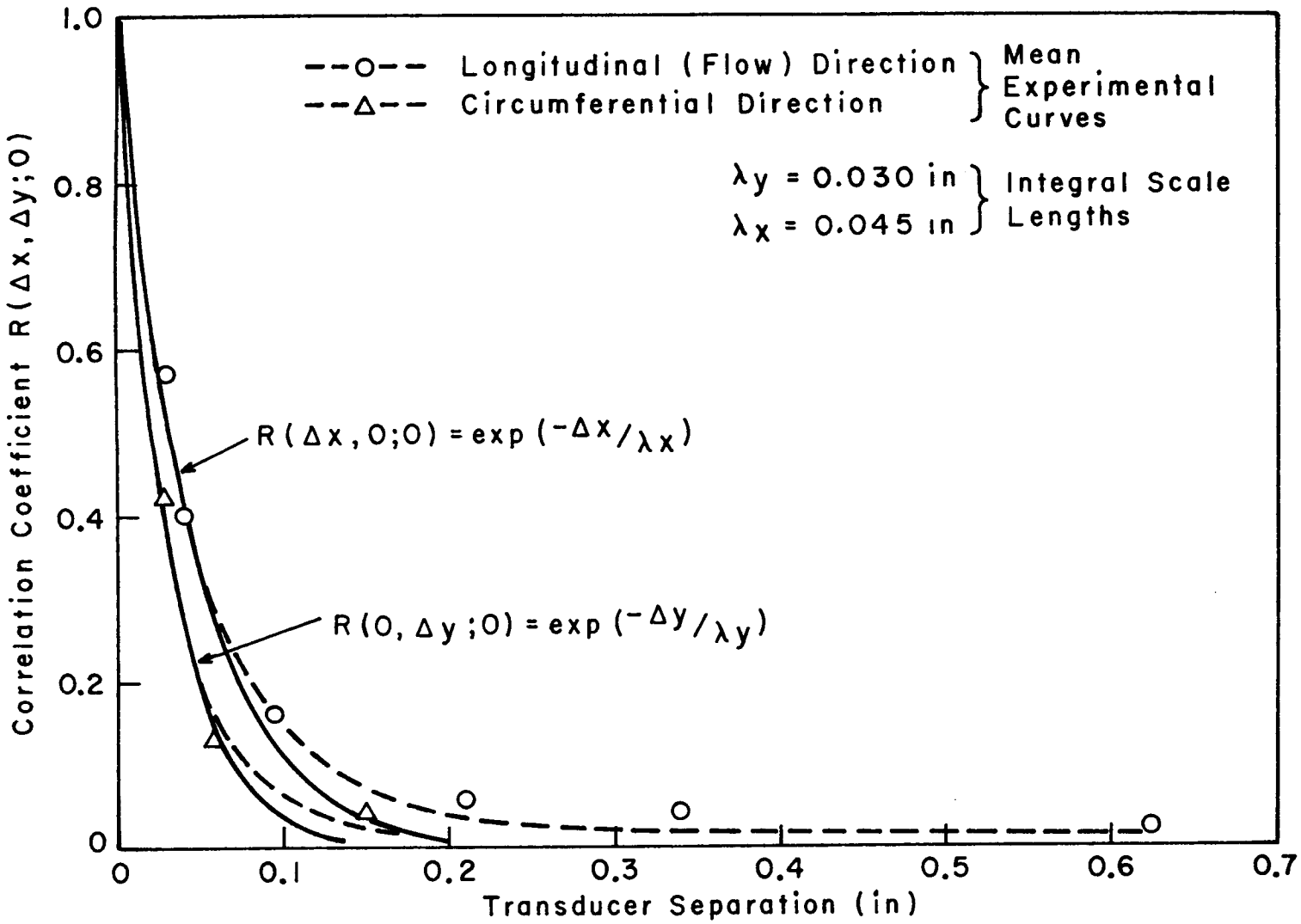

FIGURE 16. COMPARISON OF BROAD-BAND SPACE CORRELATIONS IN LONGITUDINAL AND CIRCUMFERENTIAL DIRECTIONS. (FLOW VELOCITY = 193 in/sec).

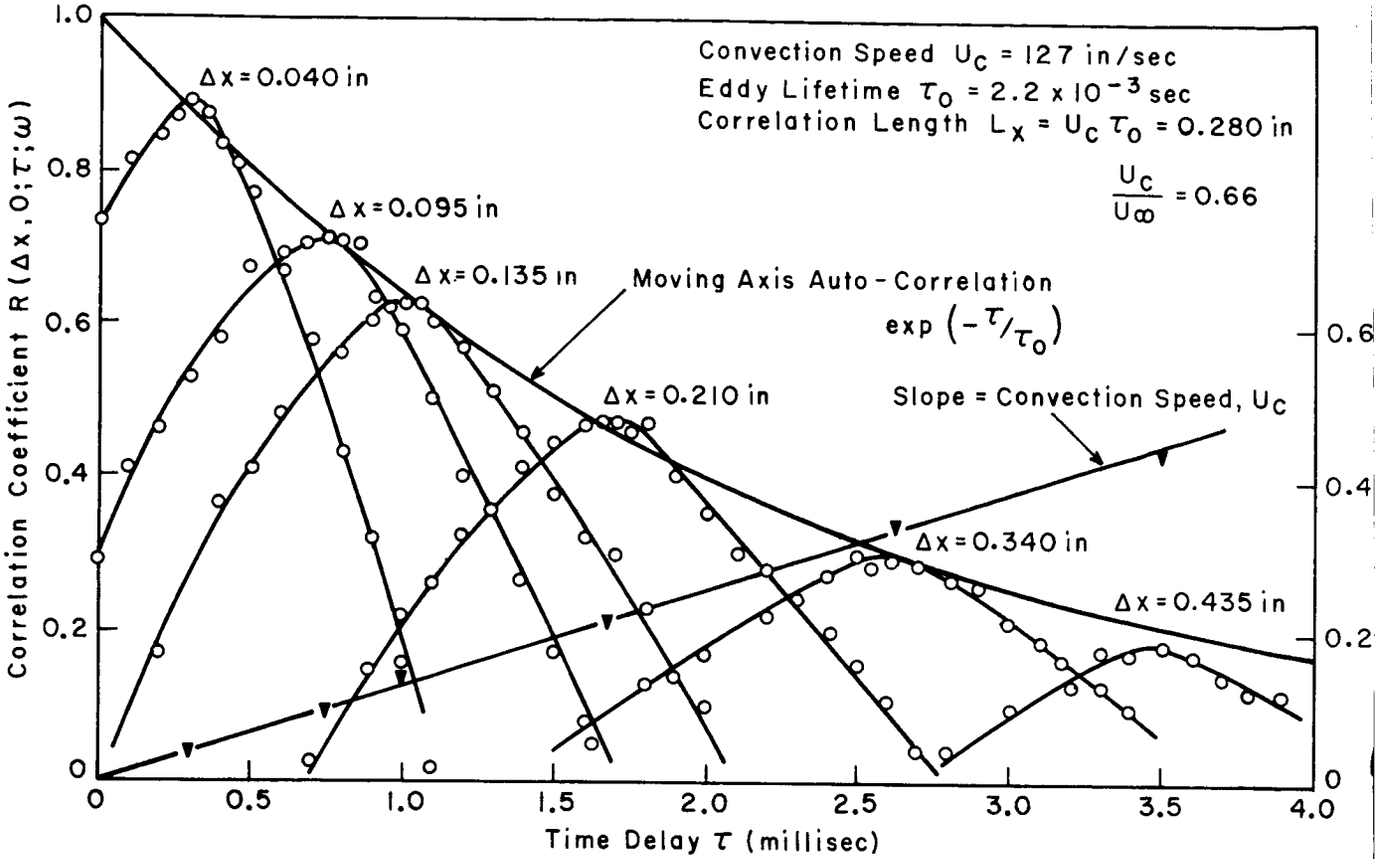

(a) Centre Band Frequency = 250 cps

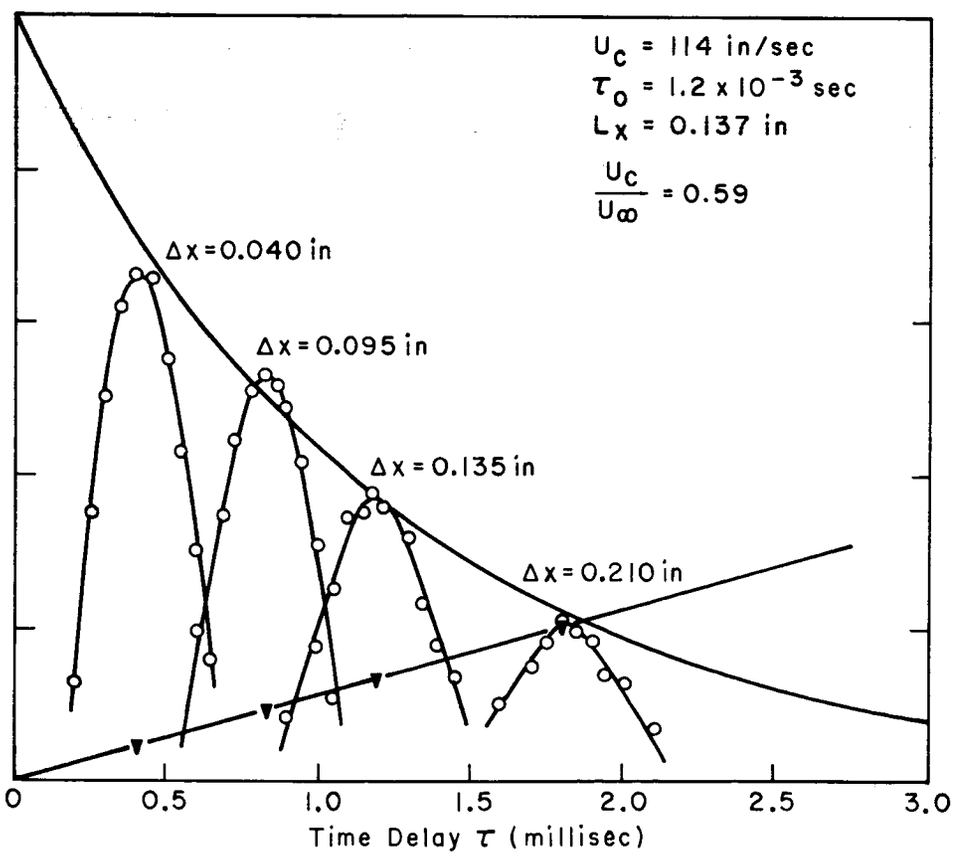

(c) Centre Band Frequency = 1000 cps

FIGURE 17. NARROW-BAND SPACE-TIME CORRELATIONS IN LONGITUDI

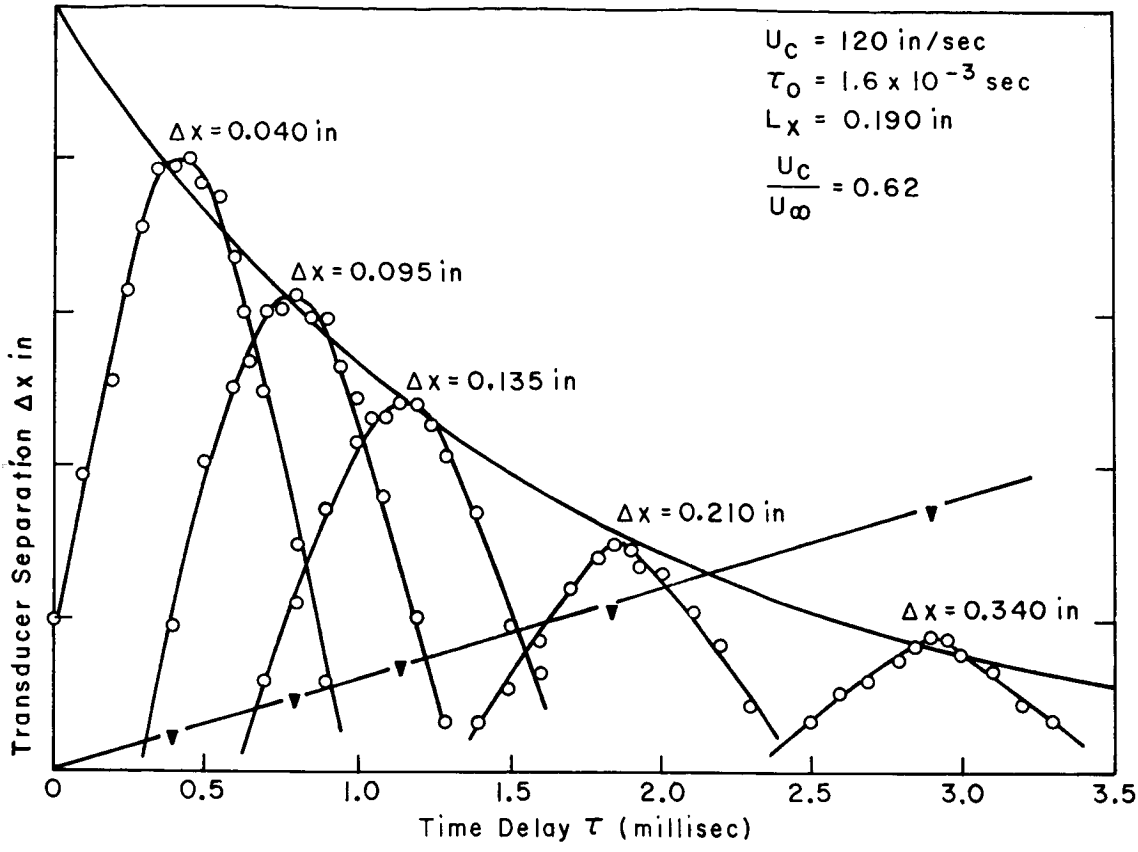

(b) Centre Band Frequency = 500 cps

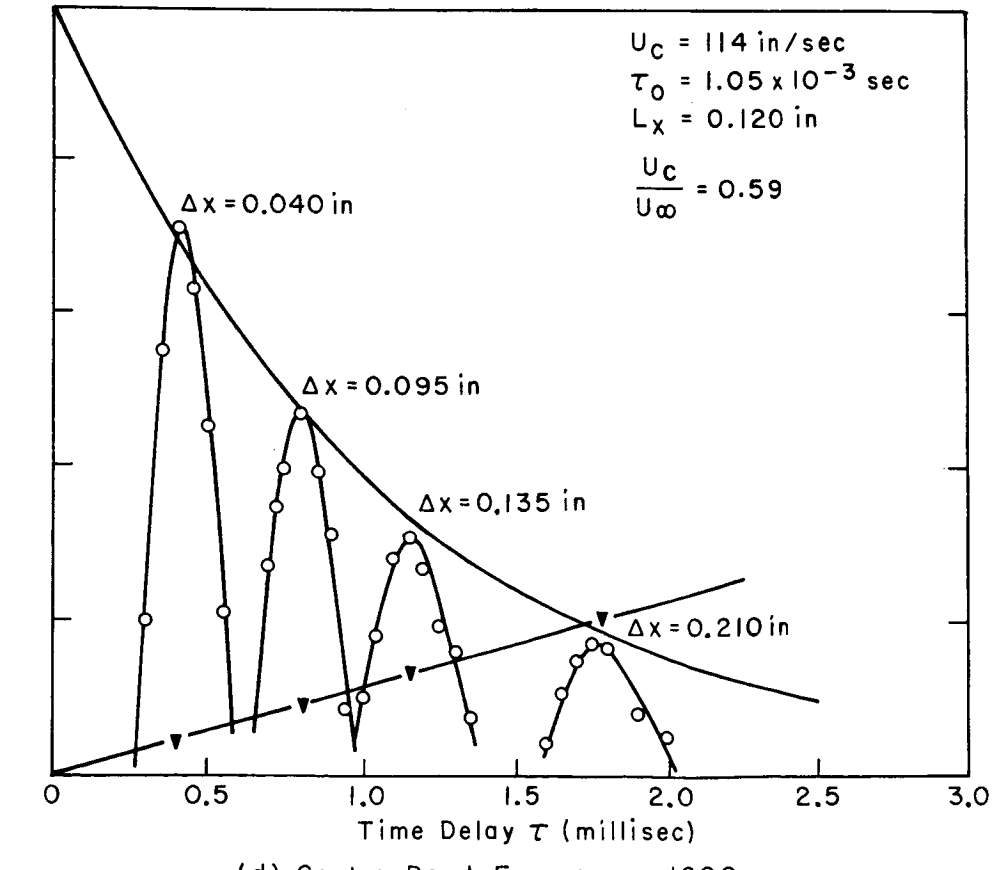

(d) Centre Band Frequency = 1600 cps

NAL DIRECTION. FLOW VELOCITY, U_∞ = 193 in/sec

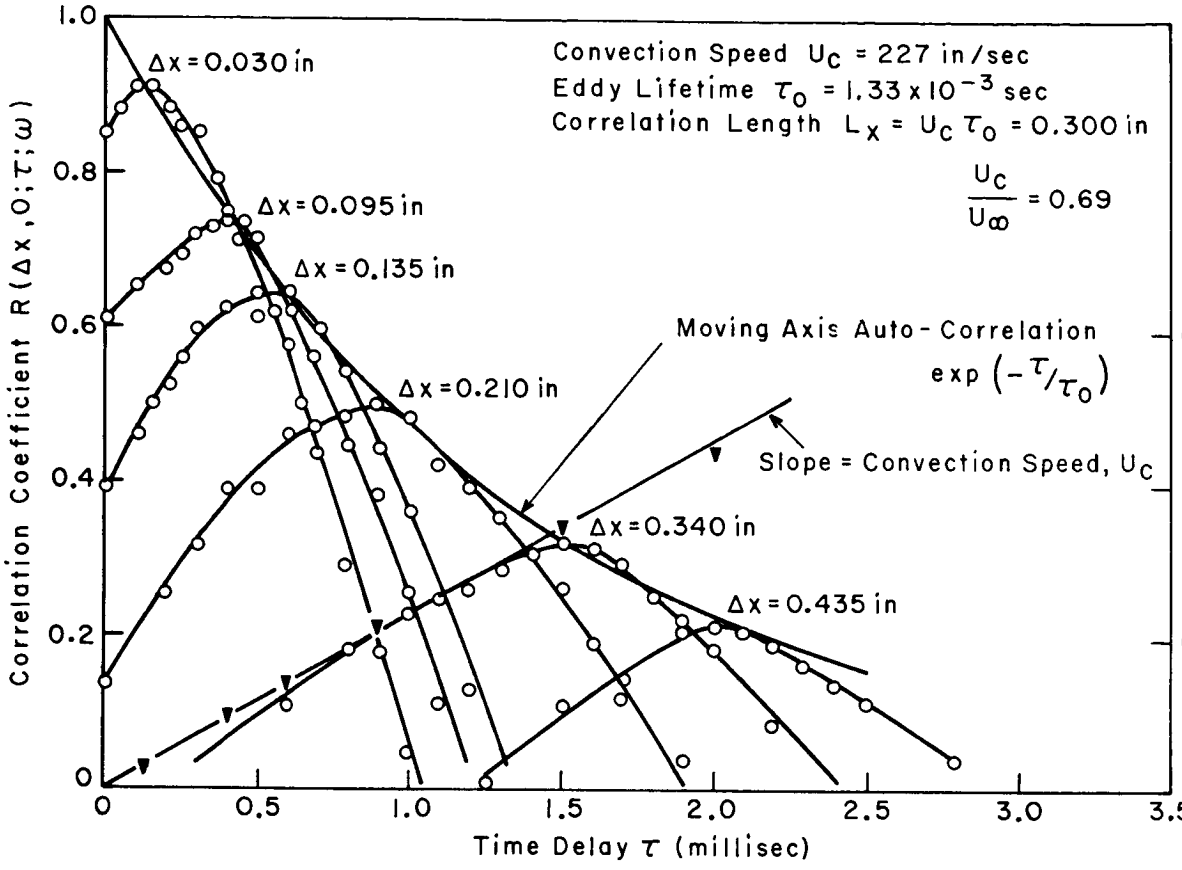

(a) Centre Band Frequency = 250 cps

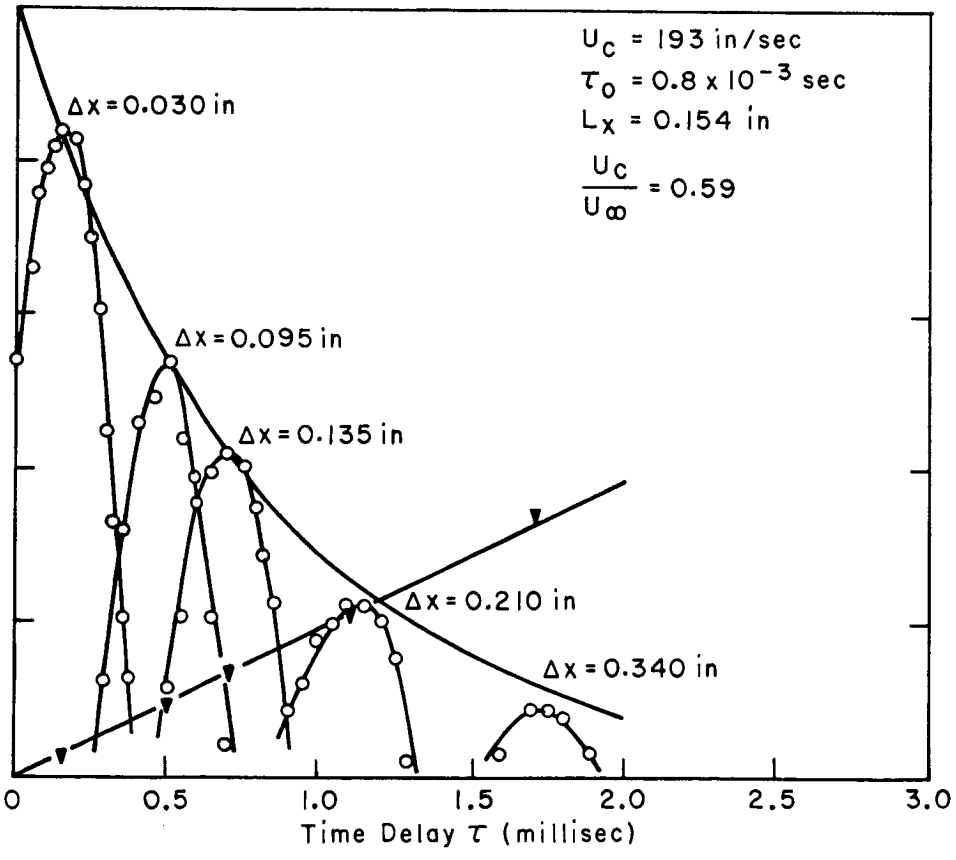

(c) Centre Band Frequency = 1000 cps

FIGURE 18. NARROW-BAND SPACE-TIME CORRELATIONS IN LONG

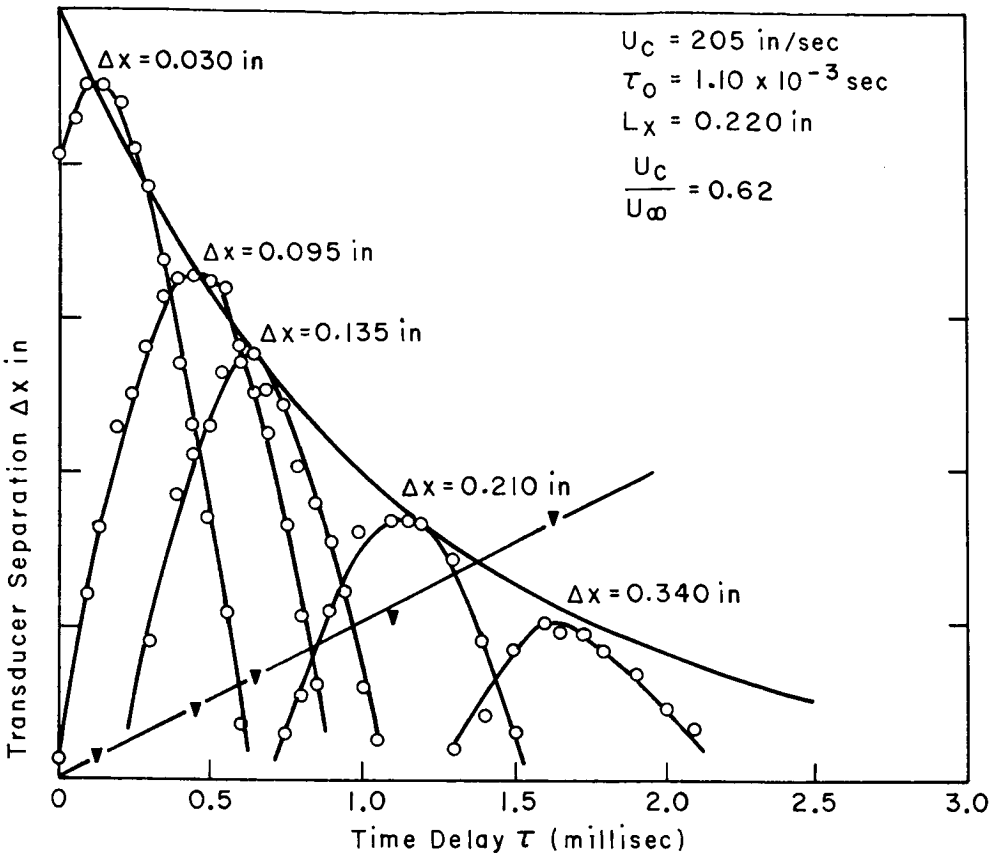

(b) Centre Band Frequency = 500 cps

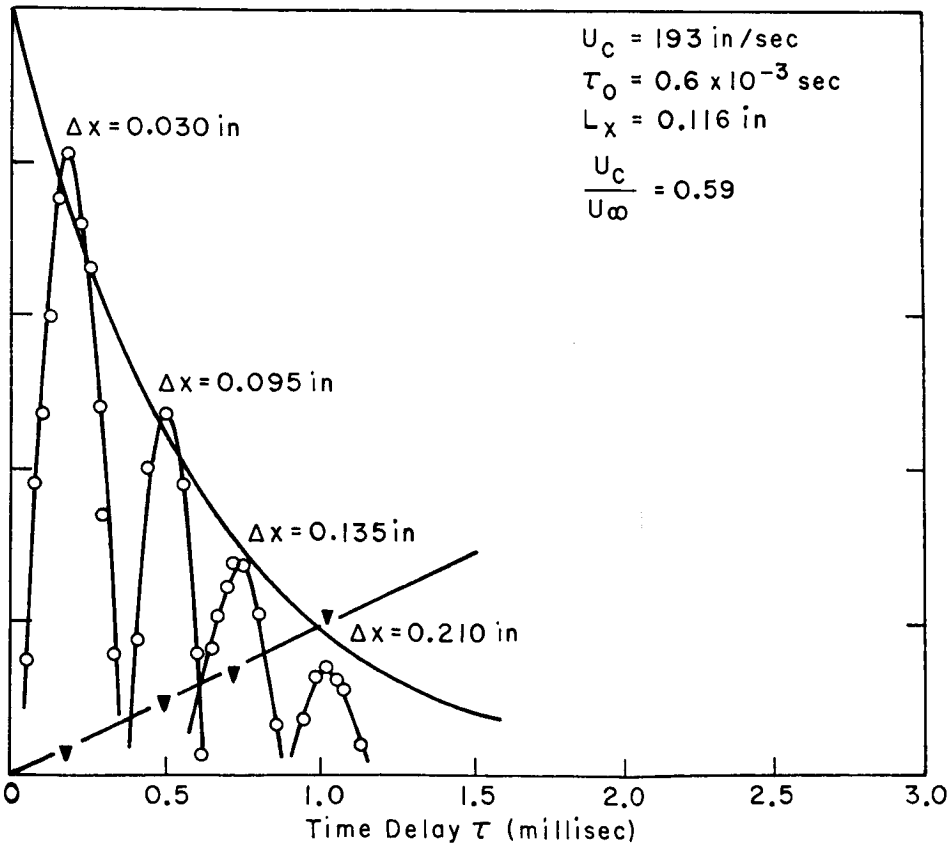

(d) Centre Band Frequency = 1600 cps

ITUDINAL DIRECTION. FLOW VELOCITY, U_∞ = 330 in/sec.

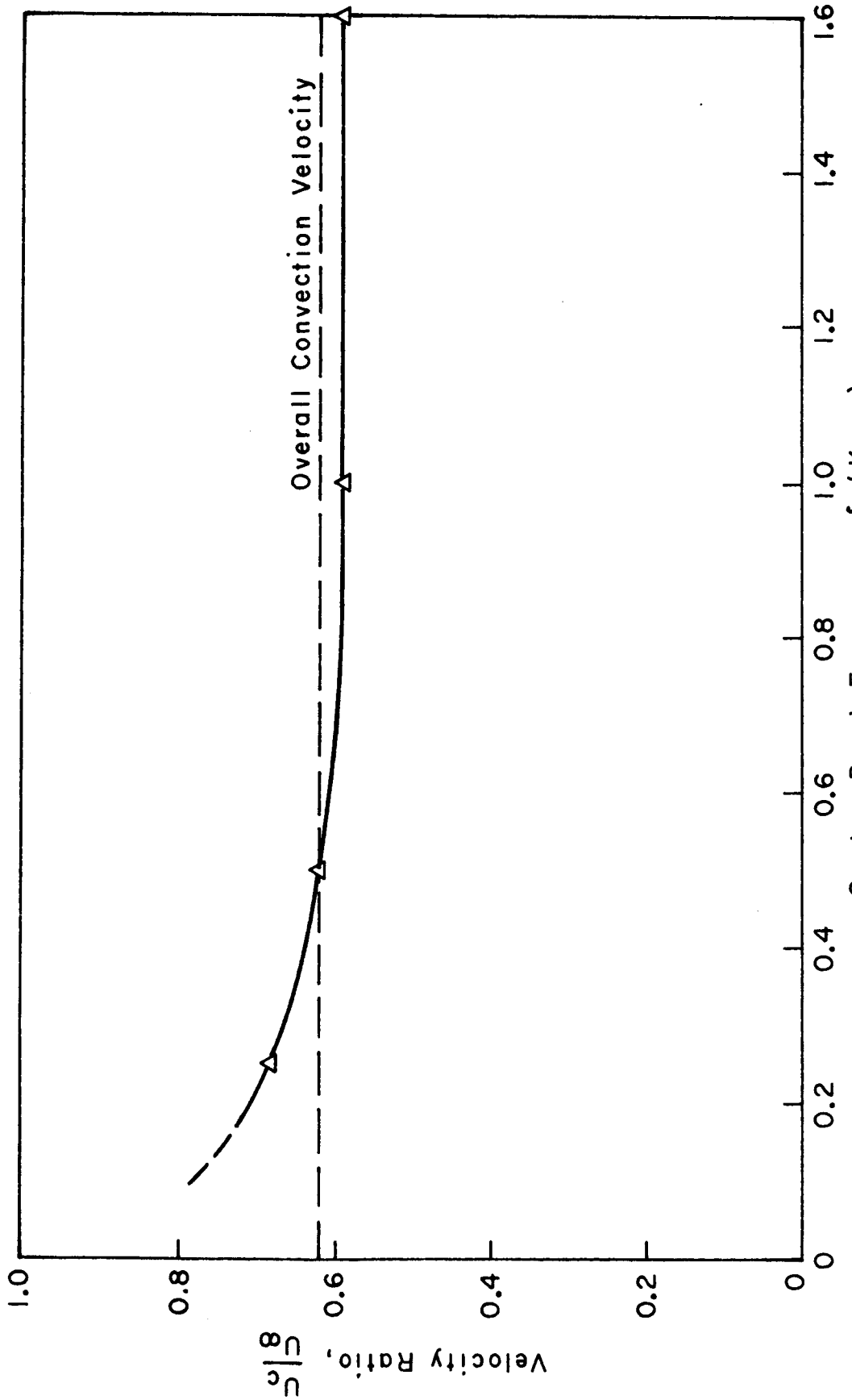

FIGURE 19. VARIATION OF CONVECTION VELOCITY WITH NARROW BAND CENTRE FREQUENCY.

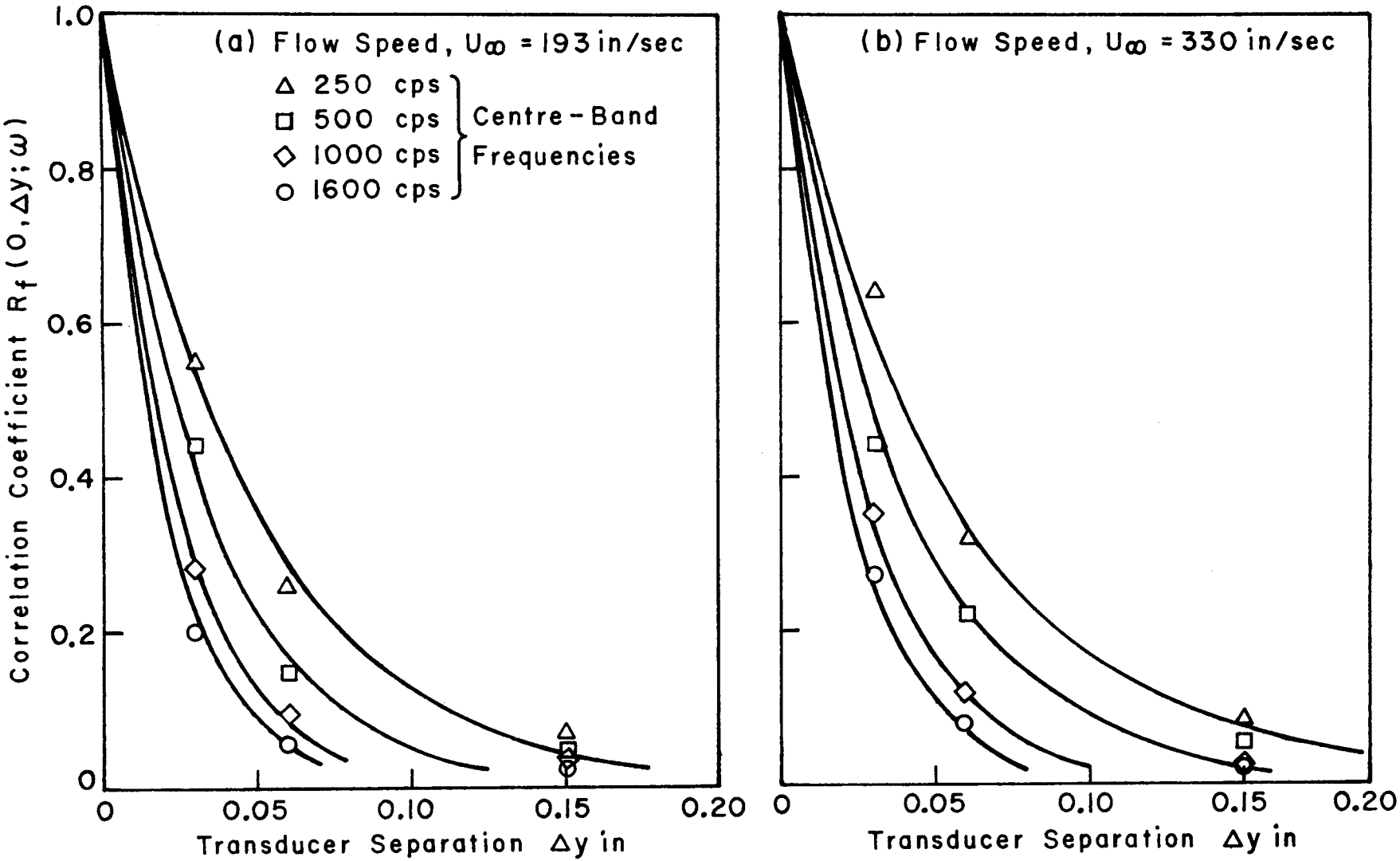

FIGURE 20. NARROW BAND SPACE CORRELATIONS IN THE CIRCUMFERENTIAL DIRECTION.

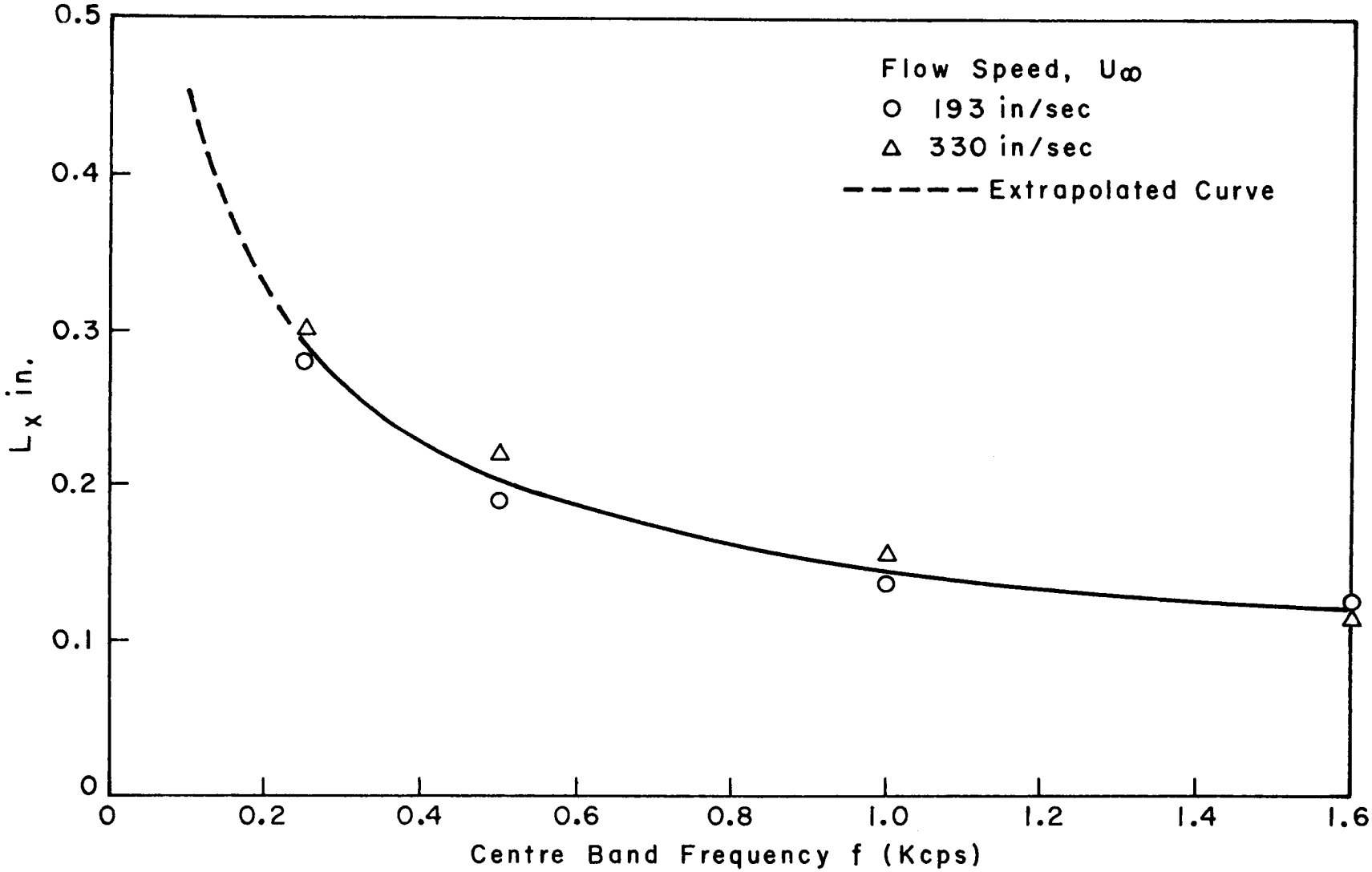

FIGURE 21. VARIATION OF LONGITUDINAL CORRELATION LENGTH L_x WITH FREQUENCY.

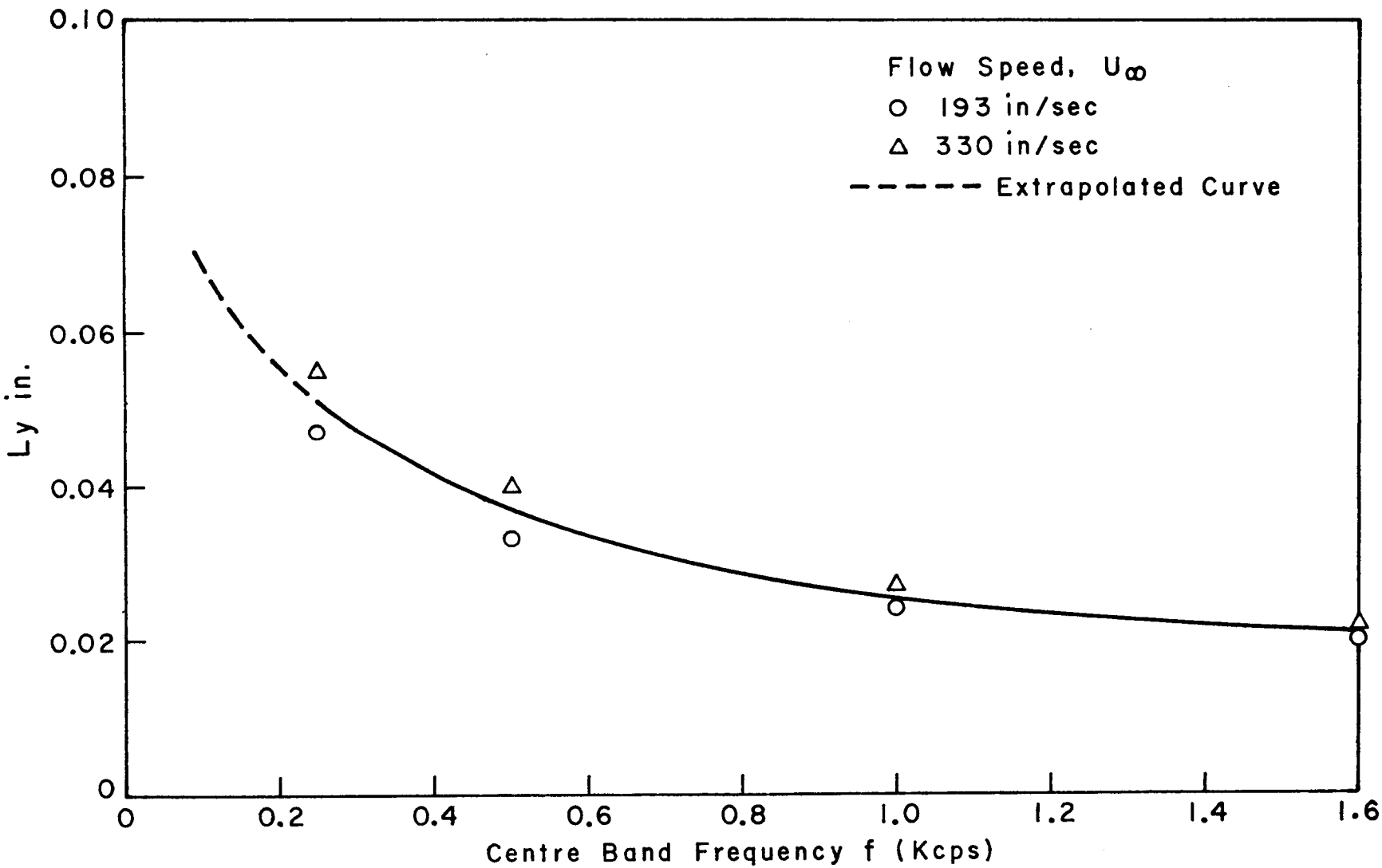

FIGURE 22. VARIATION OF CIRCUMFERENTIAL CORRELATION LENGTH Ly WITH FREQUENCY.

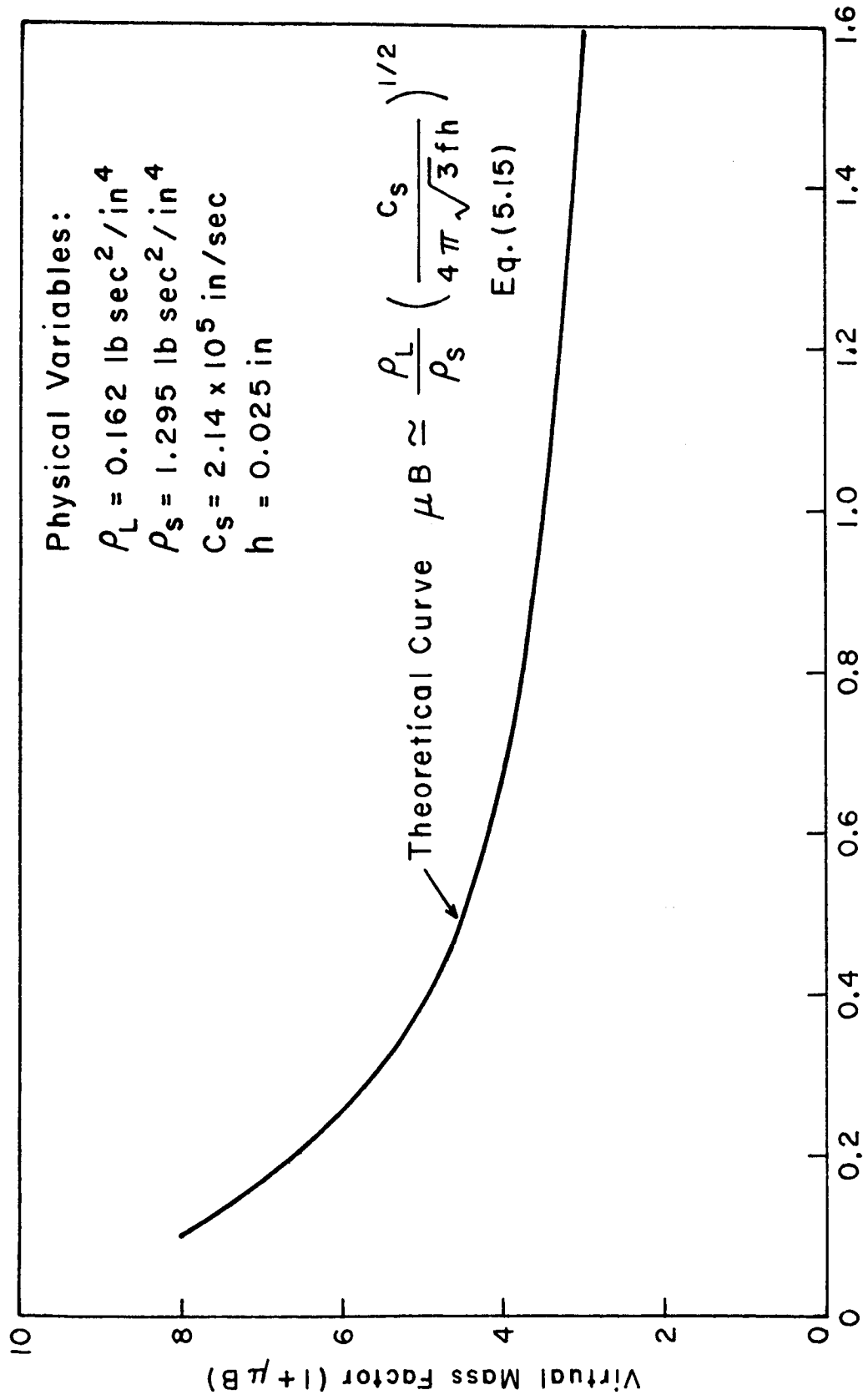

FIGURE 23. CALCULATED VARIATION OF VIRTUAL MASS FACTOR WITH FREQUENCY FOR FLEXURAL WAVES IN A WATER-LOADED FLAT PLATE.

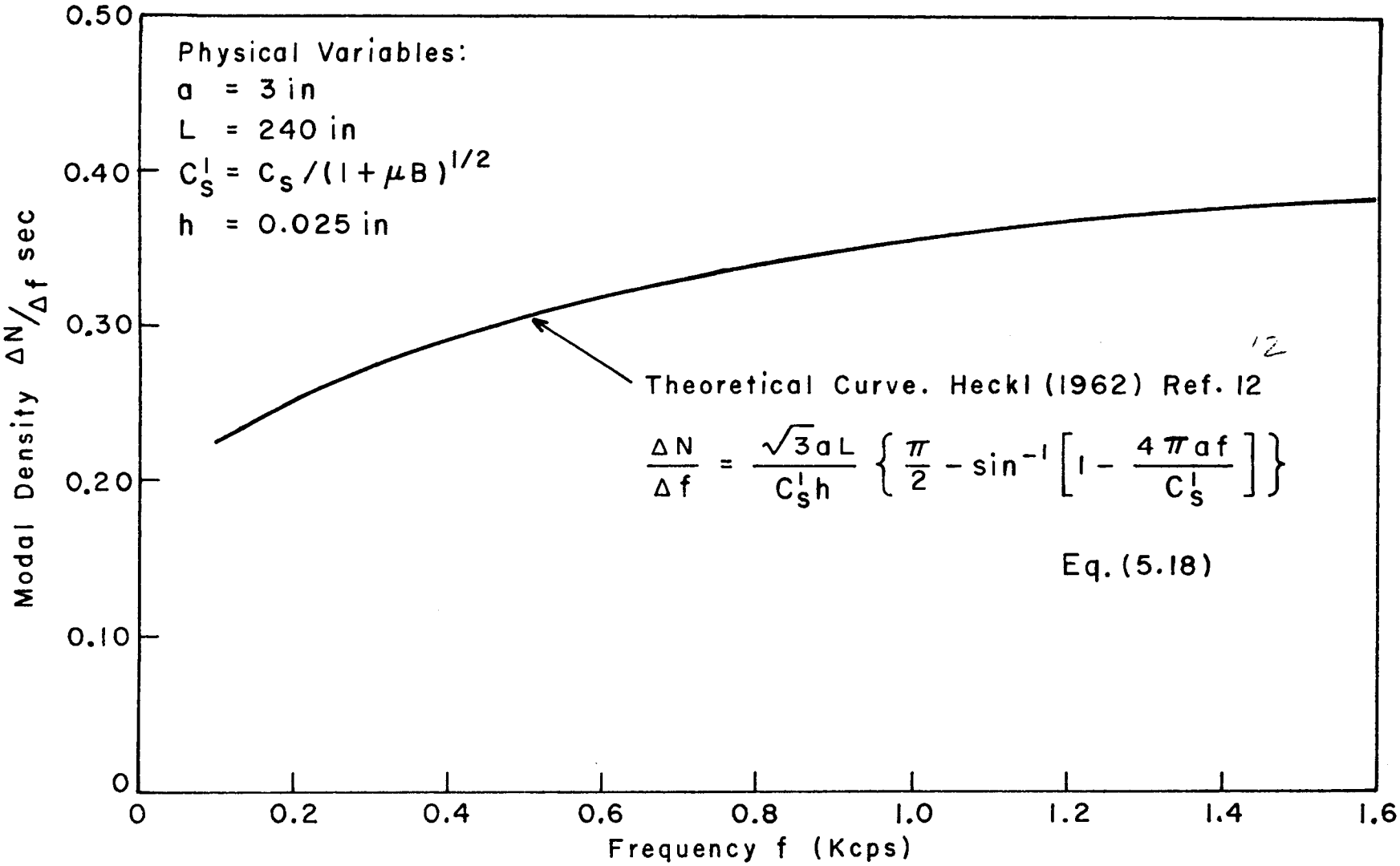

FIGURE 24. CALCULATED VARIATION OF MODAL DENSITY WITH FREQUENCY FOR GIVEN WATER-LOADED THIN-WALLED CYLINDRICAL SHELL.

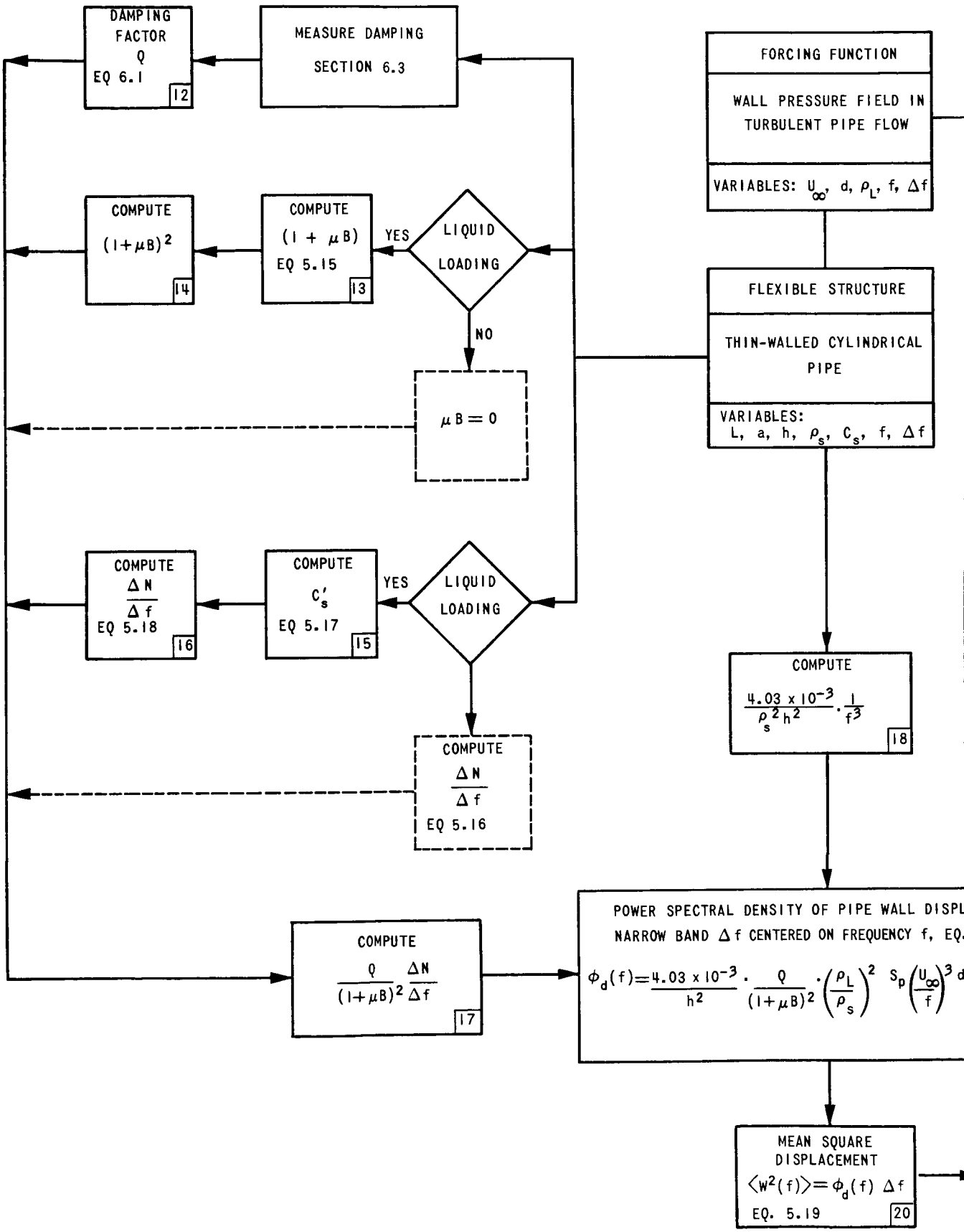

FIG. 25 COMPUTATIONAL CHART SHOWING STEP-

VIBRATIONAL RESPONSE OF A THIN-WA

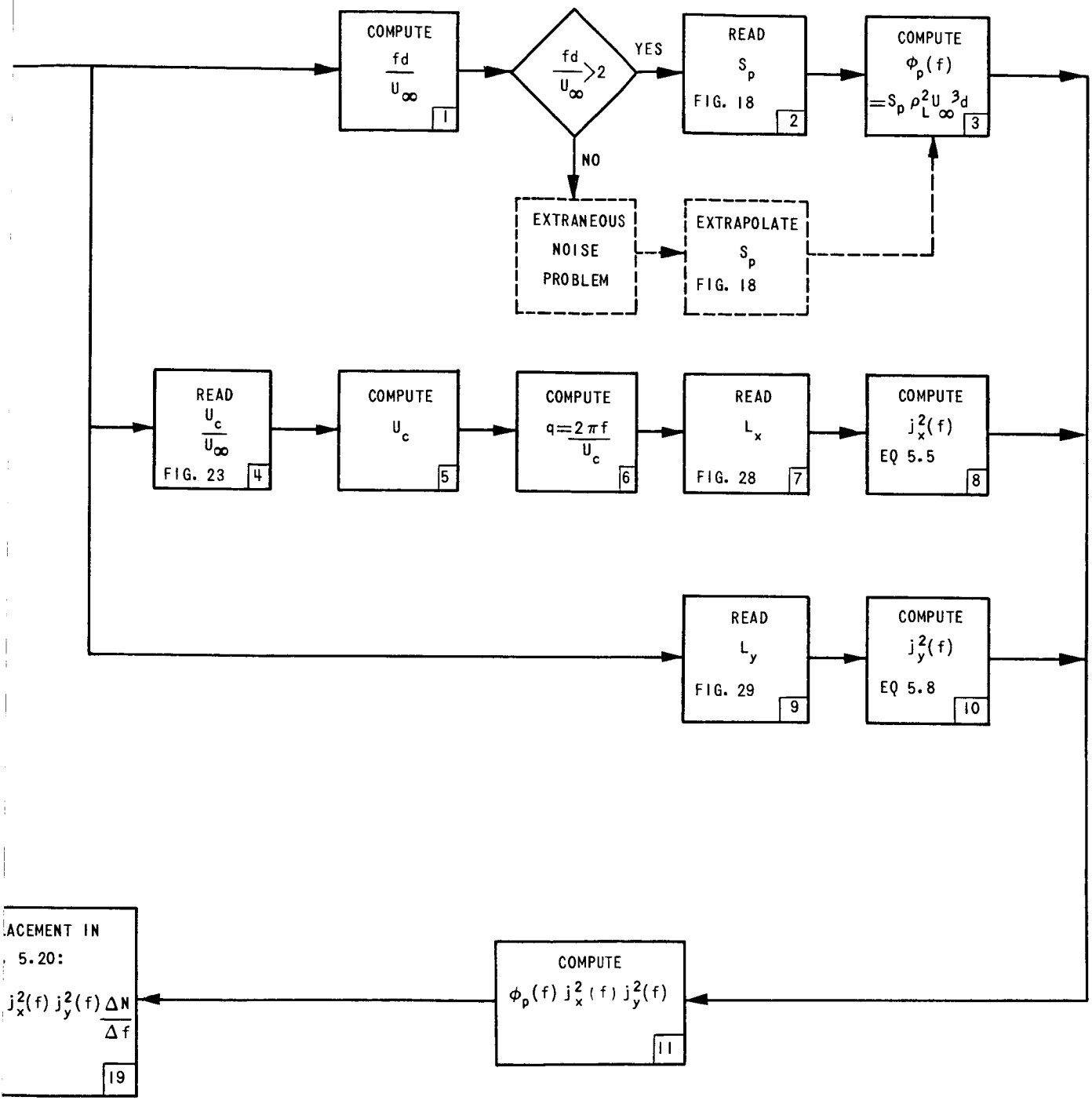

BY-STEP PROCEDURE FOR CALCULATING THE
LED PIPE TO TURBULENT FLOW EXCITATION .

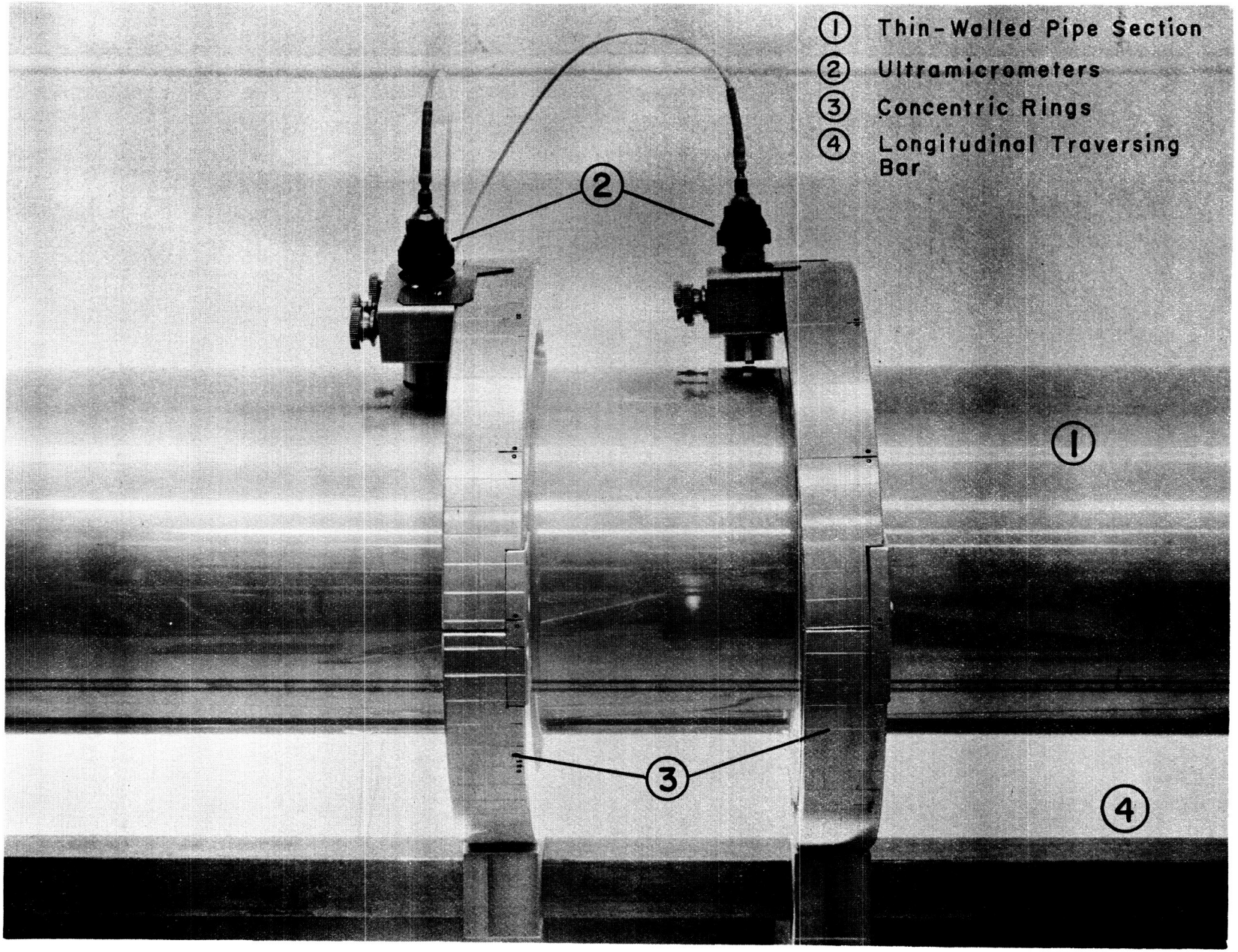

FIGURE 26. TRAVERSING SYSTEM FOR ULTRAMICROMETERS.

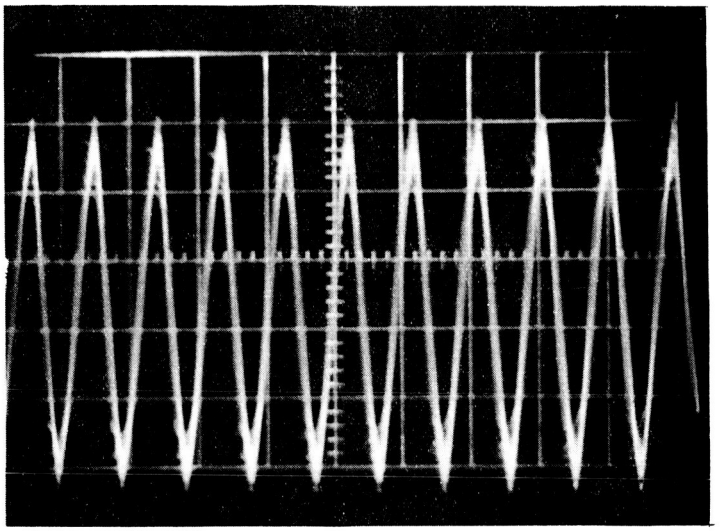

(a) Frequency of Pipe Vibration

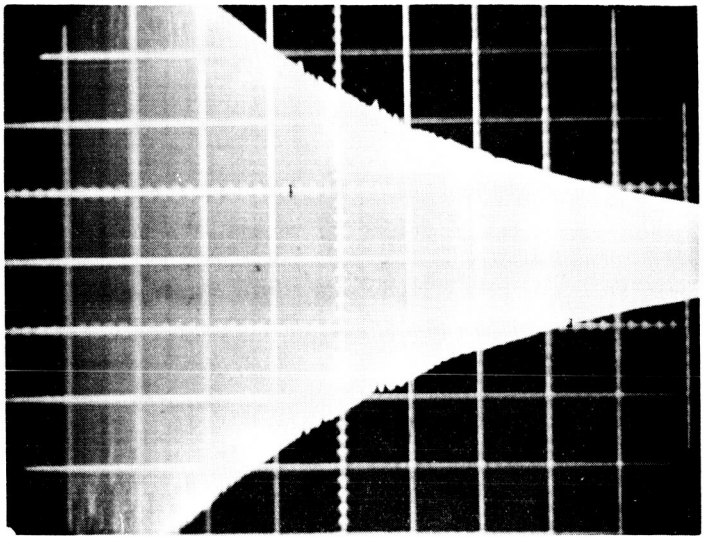

(b) Amplitude Decay Curve

FIGURE 27. MEASUREMENT OF THE DAMPING FACTOR

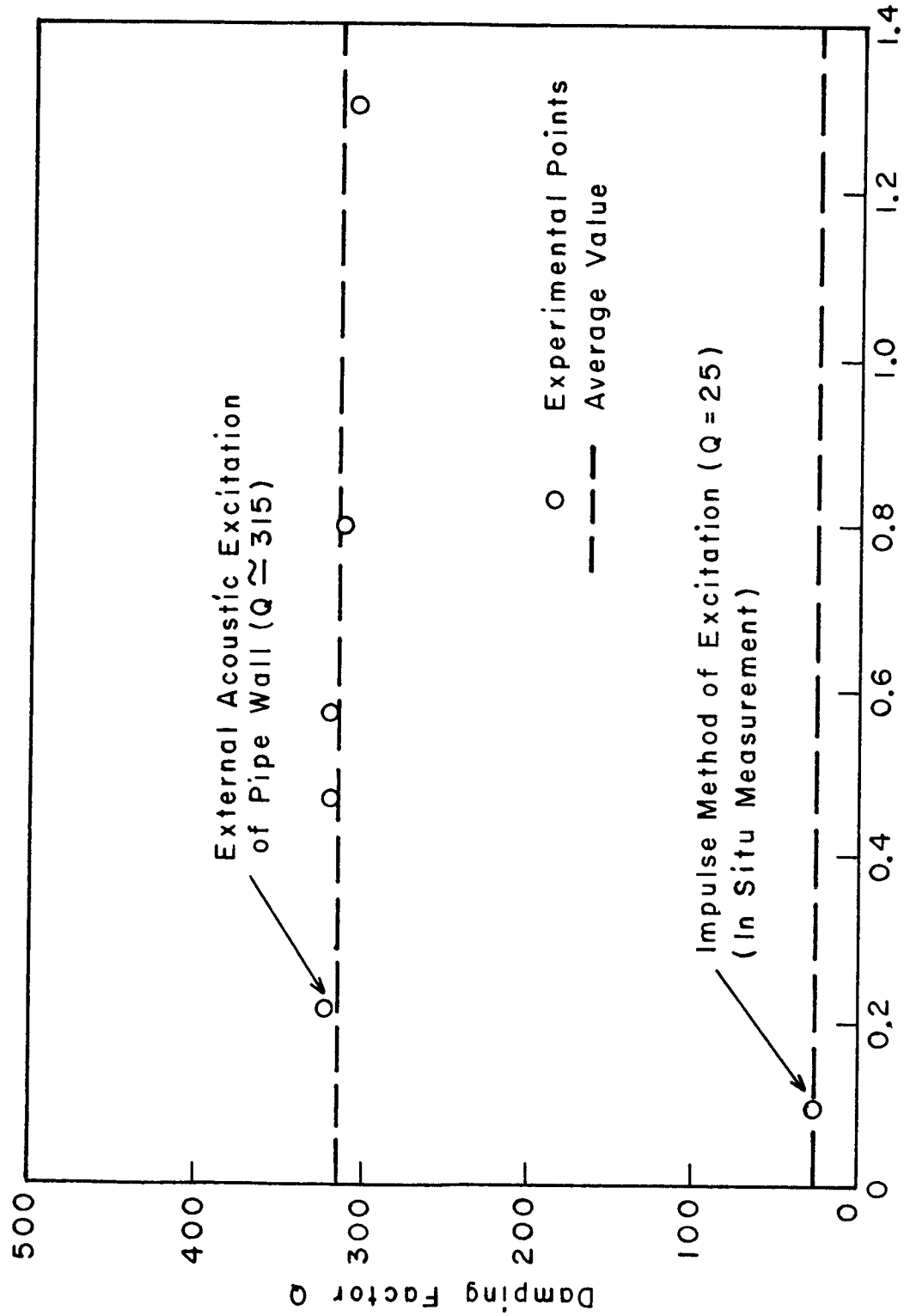

FIGURE 28. MEASUREMENT OF THE DAMPING FACTOR OF THE WATER-FILLED CYLINDRICAL SHELL.

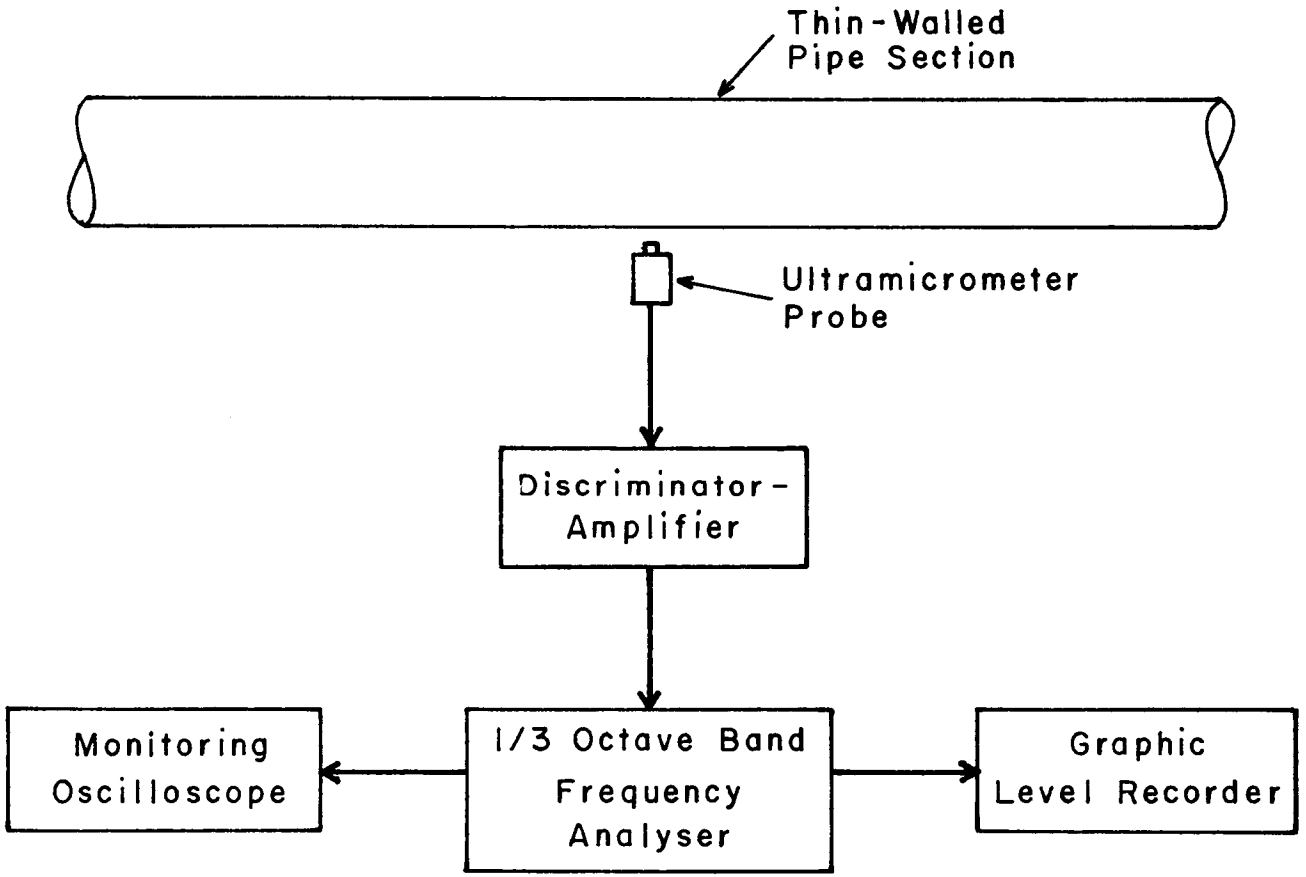

FIGURE 29. BLOCK DIAGRAM OF EQUIPMENT USED FOR RECORDING AND ANALYZING THE PIPE WALL DISPLACEMENT SPECTRA.

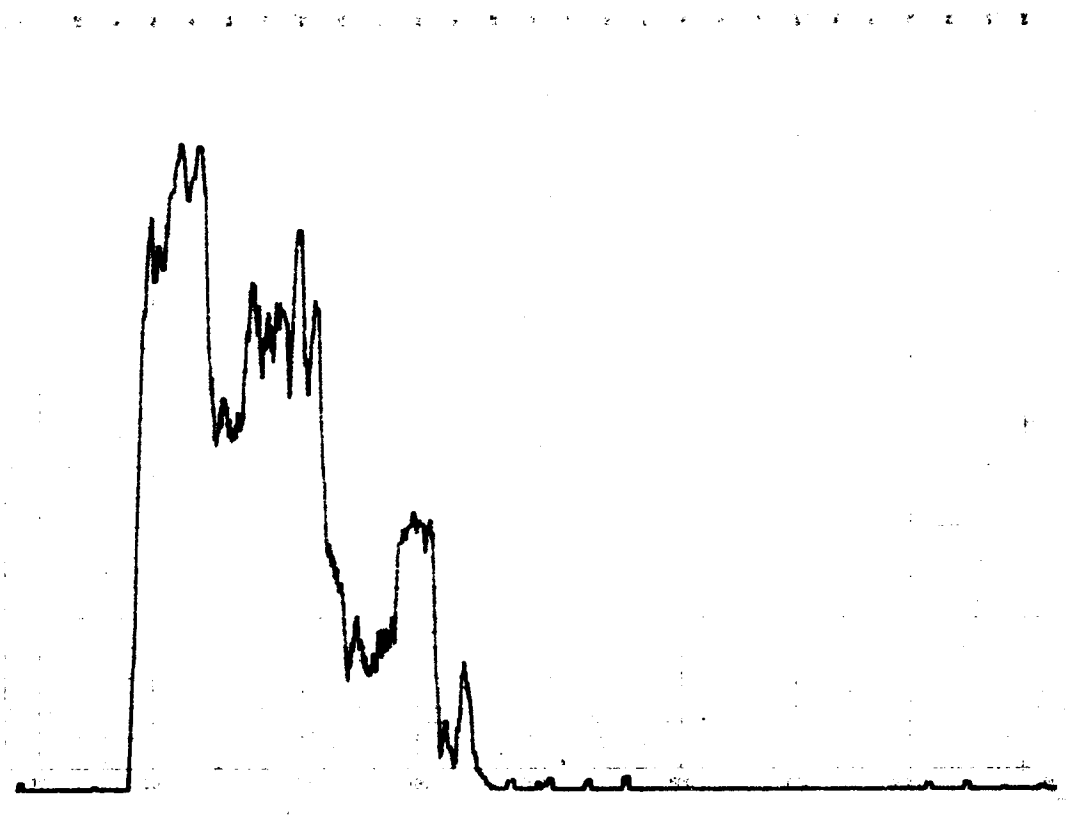

FIGURE 30. BACKGROUND NOISE LEVEL SPECTRUM.
(NO FLOW CONDITION)

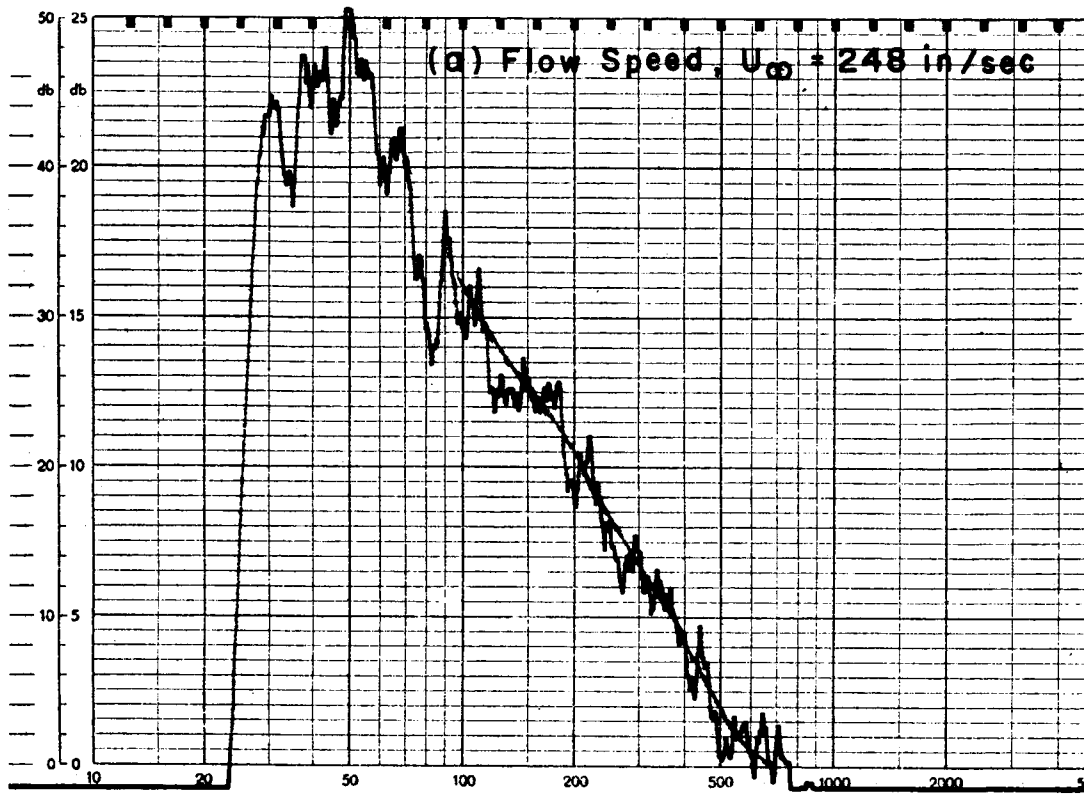

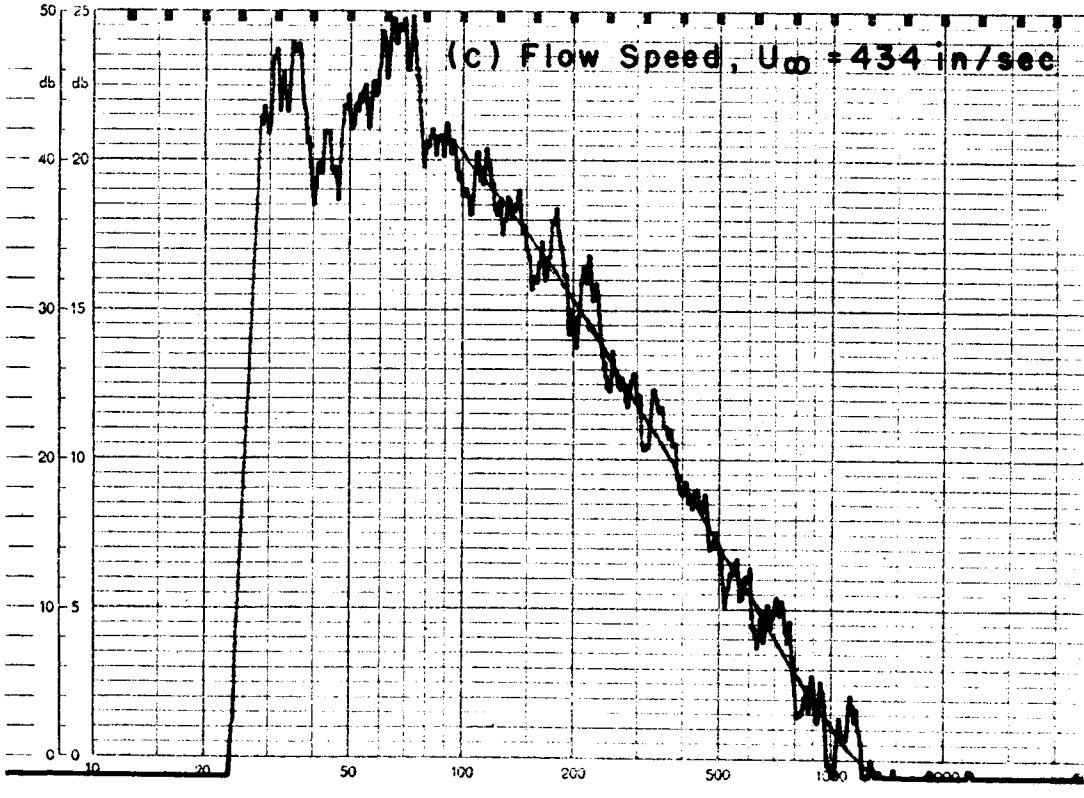

FIGURE 31. TYPICAL RECORDS OF
(PAPER SPEED, 3 mm/

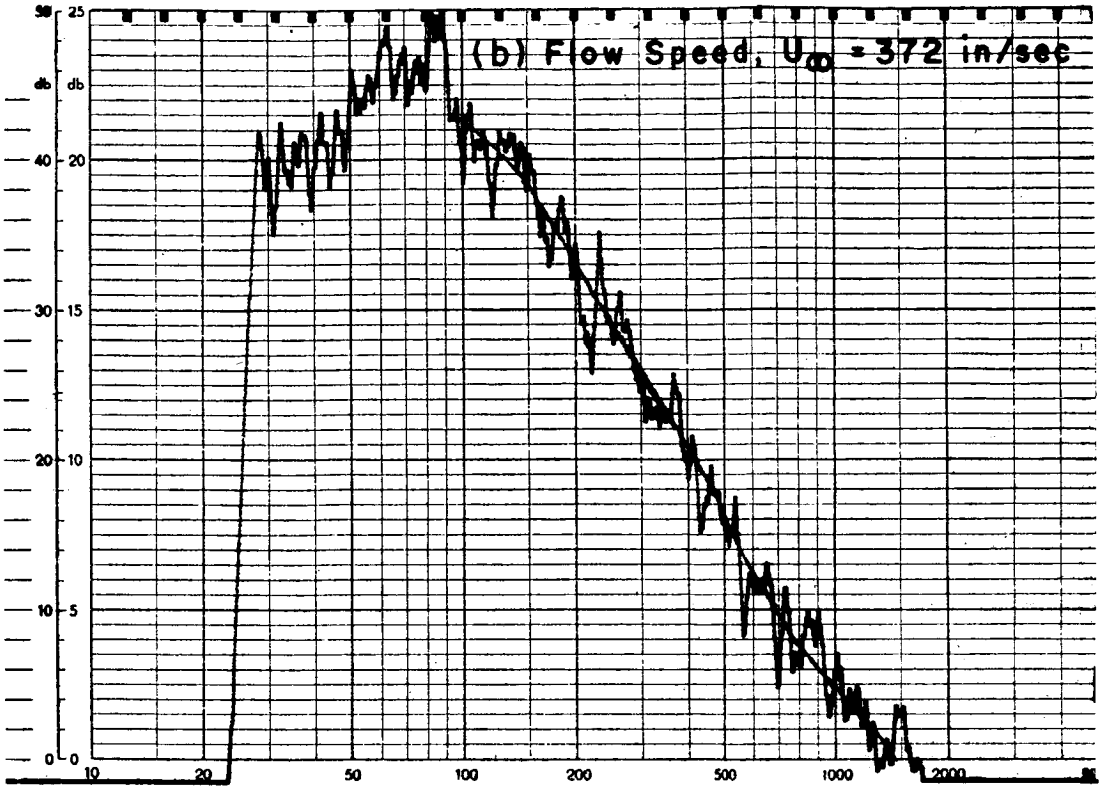

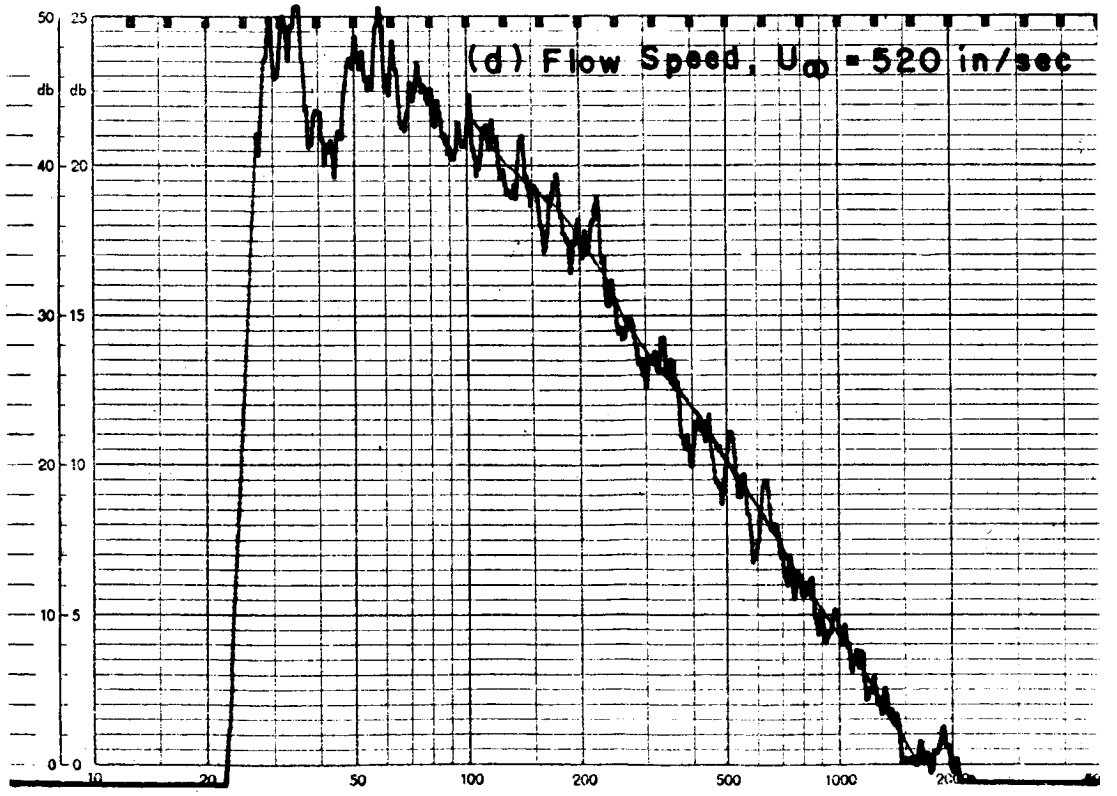

PIPE WALL DISPLACEMENT SPECTRA.
sec, WRITING SPEED, 80 mm/sec)

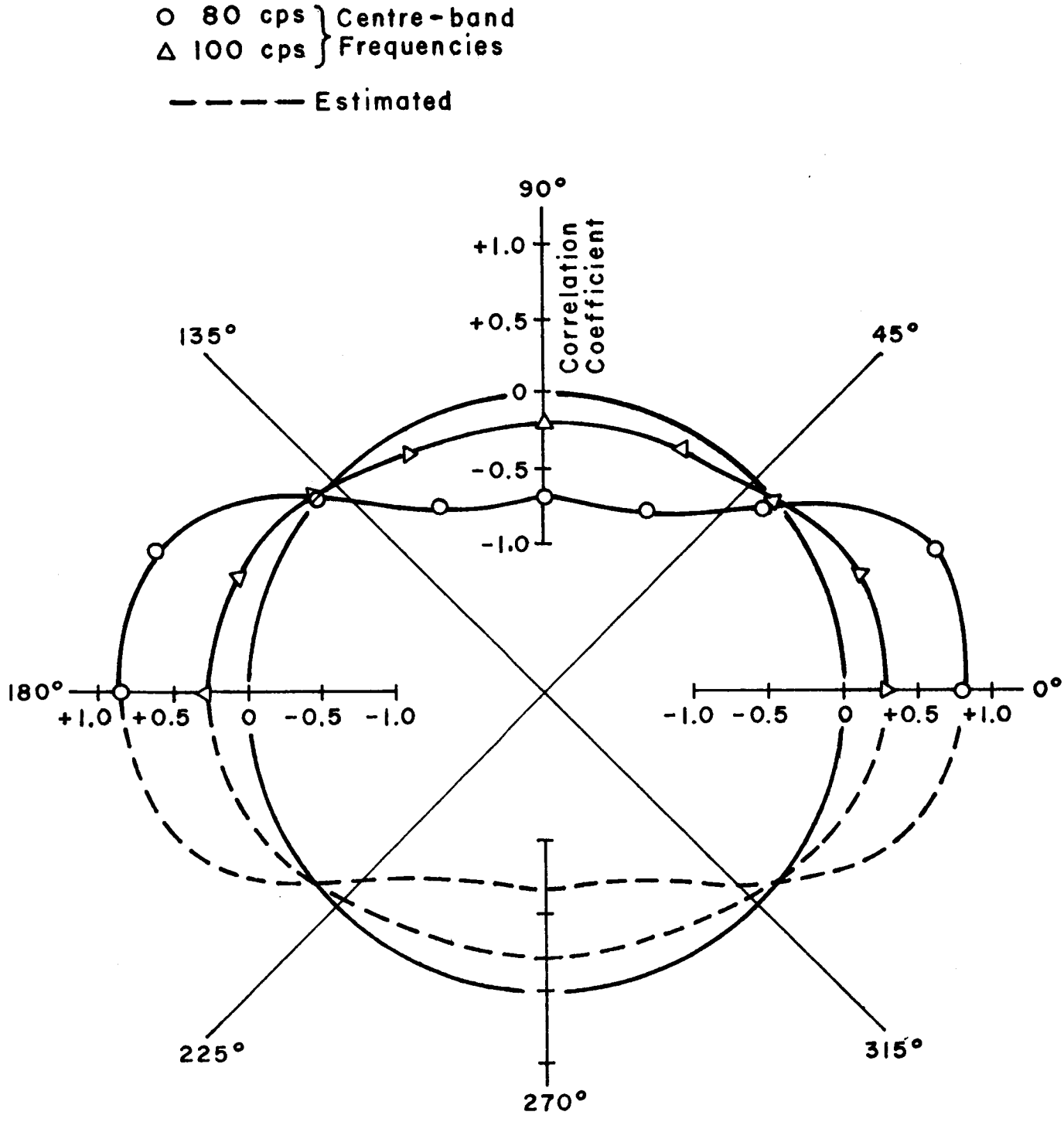

FIGURE 32. NARROW BAND CIRCUMFERENTIAL SPACE CORRELATIONS.
(FLOW SPEED, U_∞ = 434 in/sec)

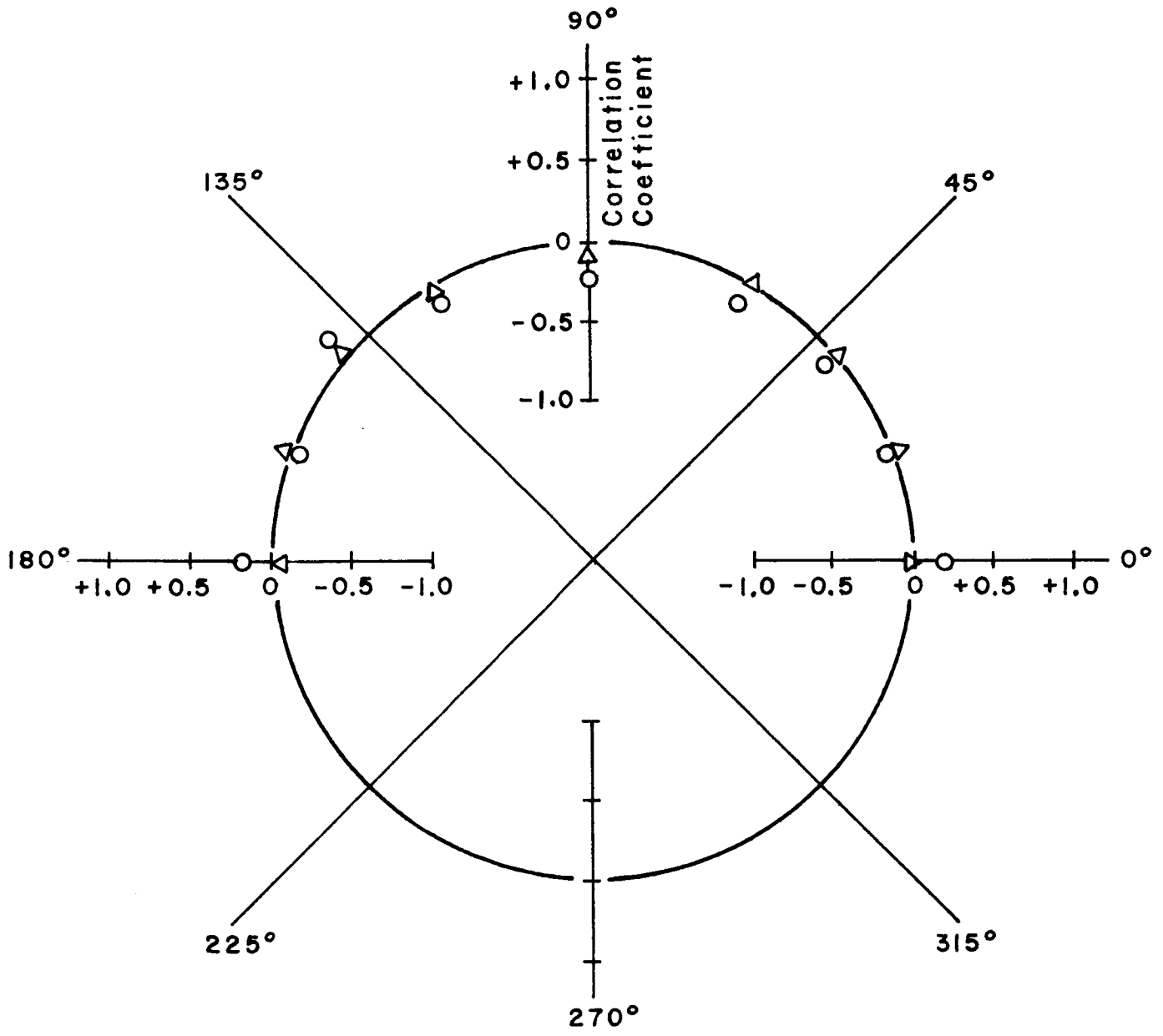

FIGURE 33. NARROW BAND CIRCUMFERENTIAL SPACE CORRELATIONS.
(FLOW SPEED, U_∞ = 434 in/sec)

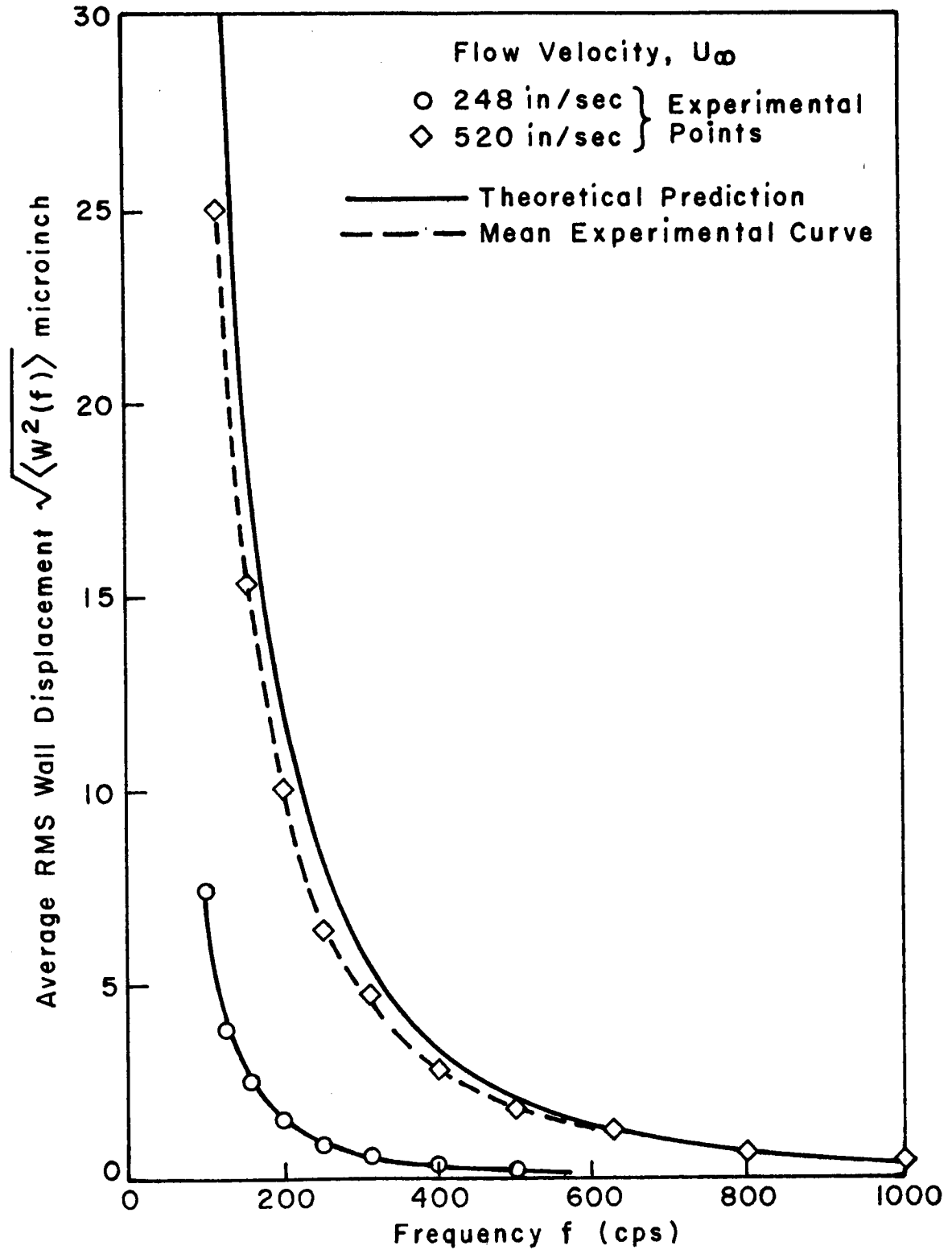

FIGURE 34. COMPARISON OF MEASURED RMS DISPLACEMENTS WITH PREDICTED VALUES AT TWO FLOW SPEEDS.

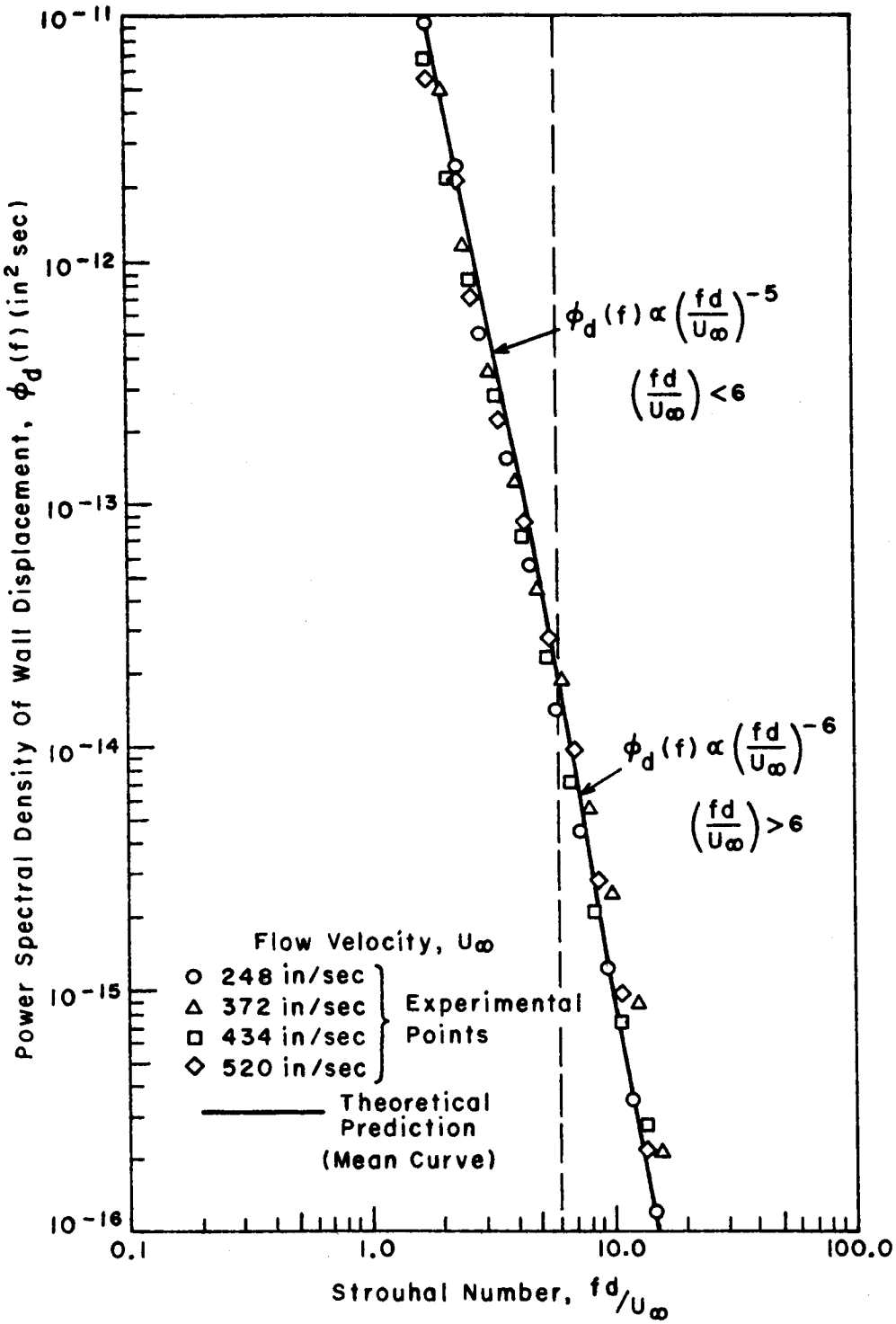

FIGURE 35. COMPARISON BETWEEN MEASURED AND PREDICTED POWER SPECTRAL DENSITY OF PIPE WALL DISPLACEMENT.

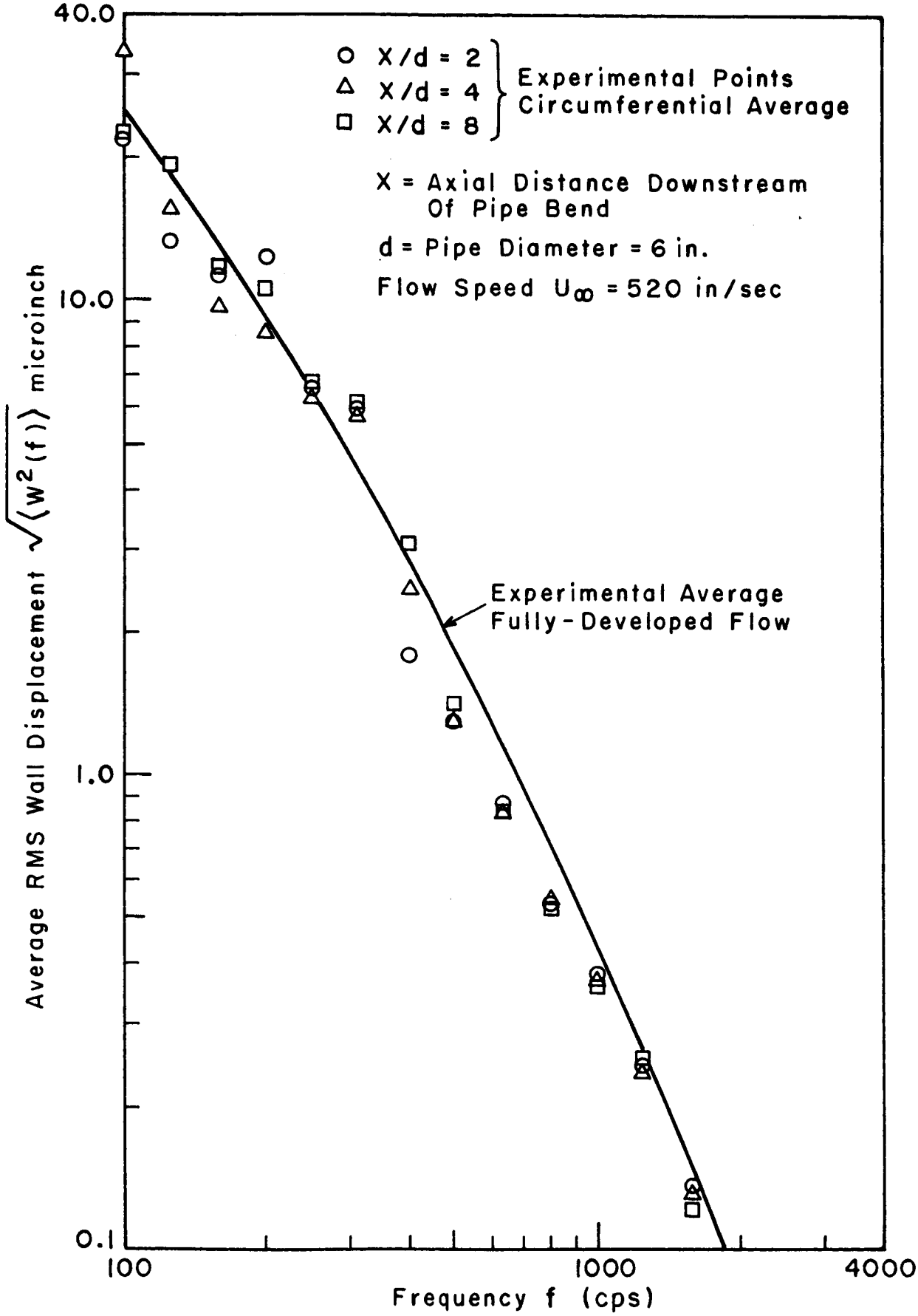

FIGURE 36. EXPERIMENTAL DATA FOR DISPLACEMENT OF PIPE WALL COUPLED DOWNSTREAM OF 90° RIGID PIPE BEND.

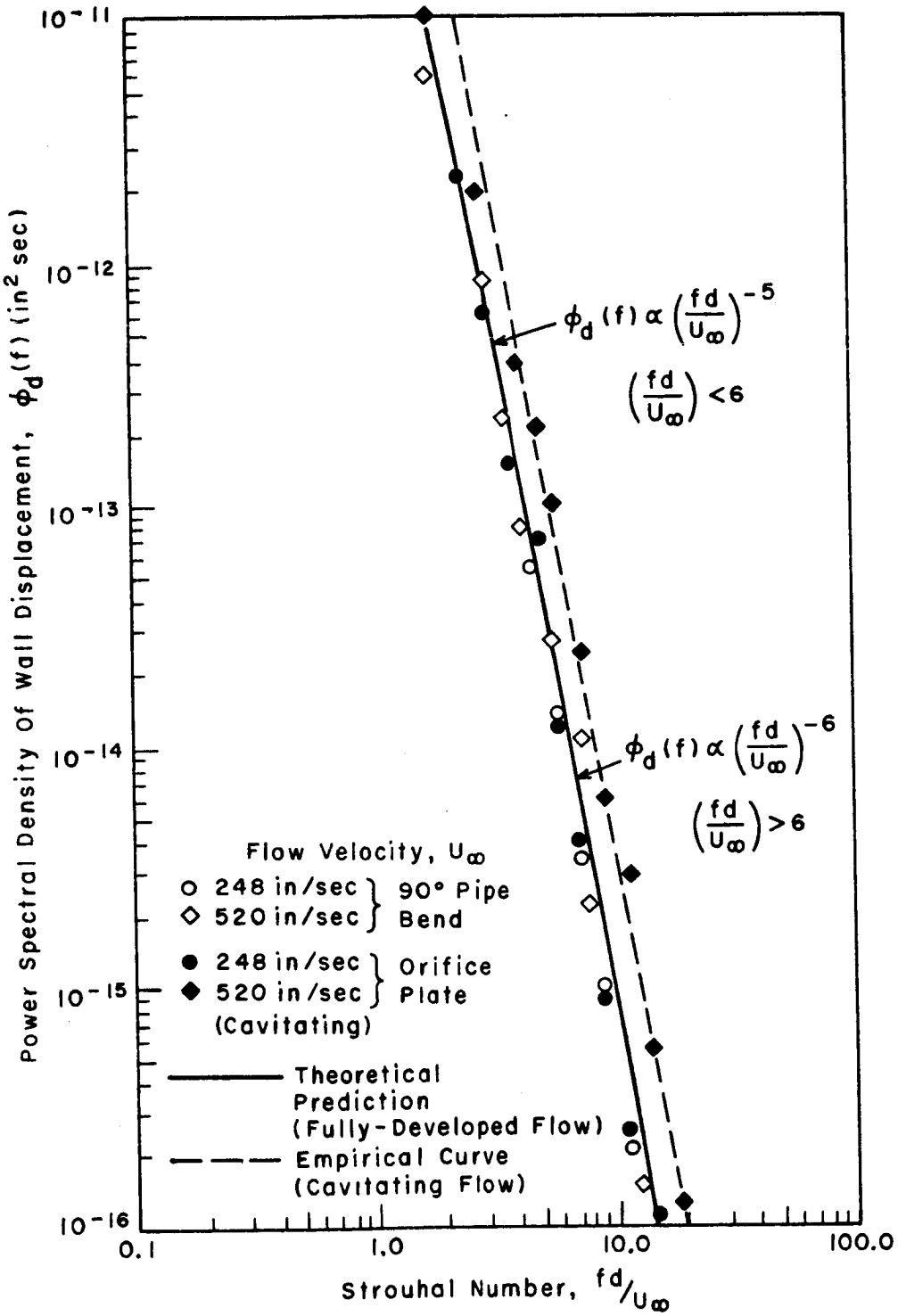

FIGURE 37. COMPARISON BETWEEN PIPE WALL RESPONSE DATA FOR VARYING FLOW CONDITIONS.